CORNER EFFECTS IN DEEP EXCAVATIONS

by

Mert Güner

B.S., Civil Engineering, Boğaziçi University, 2016

Submitted to the Institute for Graduate Studies in
Science and Engineering in partial fulfillment of
the requirements for the degree of
Master of Science

Graduate Program in Civil Engineering

Boğaziçi University

2019

ACKNOWLEDGEMENTS

First of all, my sincere appreciation and gratitude goes to my supervisor Assoc. Prof. Özer Çinicioğlu for his valuable help in instructing, sharing of knowledge, guiding and supporting me throughout my study.

I place on record, my sincere gratitude to member of the thesis committee, Prof. Erol Güler and Assist. Prof. Berrak Teymur for their efficient comments.

I also thank my friends Cem Şentay, Ahmet Talha Gezgin, İhsan Serdaroğlu, Emirhan Sancak, Uğur Can Erginağ, Adil Ayar and Muhittin Tan for their help and patience during my study.

Above all, I would like to thank my family for their support and great patience at all times. My mother and my sister have given me their endless support throughout the thesis, as always they do.

Finally, I would like to express my gratitude to Bilimsel Araştırma Projeleri (BAP) for supporting my research through Project code 12580.

ABSTRACT

CORNER EFFECTS IN DEEP EXCAVATIONS

The precise calculation of the anchorage free length used in retaining structures plays a crucial role in the design of such structures. The most important factors to be considered while determining the free length of the anchorages are the slip surfaces and their respective outer boundaries. The reason for that is to reach the calculated anchorage capacities, the roots of the anchorages must be installed in inert soil. There are a lot of factors which influence the outer boundaries of the slip surfaces. The corners in retaining structures are one of the most important of these factors. Models based on plain-strain are not adequate to determine possible active slip surfaces at the corners or at locations close to the corner. Taking this inadequacy into consideration, the effects of corners in retaining structures on active slip surfaces are researched. In this context, how corners between two adjacent retaining walls, the distance from the said corner and the variation of internal friction angle and dilatation angle depending on the relative density affect the outer boundary of the slip surface is researched. For this research, numerical models are created by using a finite element modelling program called Plaxis 3D. But before that, to determine the parameters of the models and verify the accuracy of the models, small-scale retaining wall models carried out within the scope of TUBITAK Project No:114M329 are modelled using Plaxis 3D. The results from the small-scale retaining wall models and the results of their respective numerical models are compared and it is seen that the predetermined parameters match with the results obtained from the numerical model test. Lastly, verified model specifications are used in creating the necessary models and the effects of the variables influencing the outer boundary of the slip surface are shown.

ÖZET

DERİN KAZILARDA KÖŞE ETKİLERİ

İstinat yapılarında kullanılan ankrajların boylarının doğru şekilde hesaplanabilmesi istinat yapılarının tasarımında önemli rol oynamaktadır. Ankraj boylarının belirlenmesi sırasında dikkat edilmesi gereken en önemli etkenlerden biri de aktif kayma yüzeyleri ve aktif kayma yüzeyi dış sınırlarıdır. Bunun nedeni ankraj kapasitesinin hesaplanan değerlere ulaşılması için ankraj köklerinin hareketsiz zemine yerleştirilmesi gerekliliğidir. Aktif kayma yüzeylerinin dış sınırını etkileyen bir çok faktör bulunmaktadır. İksa yapılarının köşe bölgeleri bu faktörlerin en önemlilerinden biridir. Düzlem şekil değiştirme şartları göz önüne alınarak yapılan modellemeler, iksa yapılarının köşe bölgelerinde oluşması muhtemel aktif kayma yüzeylerinin doğru tanımlanmasına yeterli gelmemektedir. Bu yetersizlik göz önüne alınarak, iksa yapılarındaki köşe bölgelerinin aktif kayma kaması üzerindeki etkisi araştırılmıştır. Bu kapsamda, komşu iksa duvarlarının oluşturduğu köşelerin açılarının, köşeden olan uzaklığın ve kohezyonsuz zeminin sıkılığından kaynaklı olarak değişen içsel sürtünme açısı ve dilatasyon açısının aktif kayma yüzeyi dış sınırı üzerindeki etkileri araştırılmıştır. Bu çalışmalar doğrultusunda, sonlu elemanlar yöntemi paket programı Plaxis 3D kullanılarak çeşitli nümerik modeller oluşturulmuştur. Bunun öncesinde, oluşturulan modellere ait parametrelerin belirlenebilmesi ve modellerin doğruluğunun tespit edilmesi gerekmiştir. Bu amaç doğrultusunda, nümerik modellerin doğrulanması için TUBITAK Proje No:114M329 kapsamında yapılan küçük ölçekli istinat duvarı modeli deneyleri Plaxis 3D programında modellenmiştir. Küçük ölçekli istinat duvarı modelinin fiziksel ve nümerik model sonuçları karşılaştırılmış ve belirlenen parametrelerin kullanıldığı nümerik modellerin test sonuçlarıyla uyumlu sonuçlar verdiği gözlemlenmiştir. Son adım olarak doğruluğu ortaya konmuş model özellikleri baz alınarak gerekli modeller oluşturulmuş ve aktif kayma yüzeyi dış sınırına etki edecek değişkenlerin etkileri ortaya konulmuştur.

TABLE OF CONTENTS

LIST OF FIGURES

LIST OF TABLES

LIST OF SYMBOLS

A_ψ	is constant value
c	Cohesion
C	is a coefficient with the dimension of length
C_u	Uniformity Coefficient
C_c	Coefficient of Gradation
d	The equivalent thickness
D_{50}	Median particle size
D_r	The relative density
E_1	Young's modulus in first axial direction
E_{50}^{ref}	Secant stiffness in standard drained triaxial test
E_{oed}^{ref}	Tangent stiffness for primary oedometer loading
E_{ur}^{ref}	Unloading/ reloading stiffness
e	Void ratio
e_{max}	Maximum void ratio
e_{min}	Minimum void ratio
G_{12}	In-plane shear modulus
G_s	Specific gravity
I_D	is the relative density
I_R	is the relative density index
m	is a power controlling the stress dependency of stiffness
m_ψ	Density-based dilatancy constant
N_{60}	Corrected N values
$p^{'}$	Confining pressure
$p_p^{'}$	The mean effective stress at peak shear strength
P	The reaction force due to the friction between the soil and the wall
p_A	is the reference stress
p_c	is location of the intersection with the p axis
p_{ref}	is the reference pressure

r	is a line fitting parameter
r_{tx}	Dilatancy effect on friction for axisymmetric conditions
r_{ps}	Dilatancy effect on friction for plane strain conditions
R	is line-fitting parameter
R	The reaction force on the slip plane
R_{ave}	Average roundness
R_f	is the failure ratio
R_{inter}	is interface strength reduction factor
S_{ave}	Average sphericity
T	is the tensile strength of the material
q	is the deviatoric stress
q^*	is a stress invariant
Q	is line-fitting parameter
W	The self-weight
α	Angle with the wall for active condition
α_s	is the shape factor
α_ψ	Stress-based dilatancy constant
β	Angle with the wall for passive condition
γ	The unit weight
γ_{sat}	Saturated unit weight
γ_{unsat}	Unsaturated unit weight
γ_s	Total deviatoric strains
ε_1	Principle strain
ε_v	Volumetric strain
ε_q	Shear strain
$\varepsilon_q^{p-shear}$	Deviatoric plastic strain
φ	Internal friction angle
$\varphi_c^{'}$	Effective critical state friction angle
$\varphi_p^{'}$	Effective peak friction angle
$\sigma_{mp}^{'}$	is the mean effective stress

$\sigma_{mp}^{'}$	is the mean effective stress at peak shear strength
υ_{12}	Poisson's ratio
ψ	Dilatancy angle
ψ_p	Peak angle of dilation

LIST OF ACRONYMS/ABBREVIATIONS

3D	Three Dimensional
FEM	Finite Element Method
HS	Hardening Soil Model
PIV	Particle Image Velocimetry Method

1. INTRODUCTION

The investigation and determination of active slip surfaces which occur due to translation and/or rotation created by the soil mass behind the designed retaining structure is very crucial for the design of this structure. There have been a lot of researches in this area until today (Coulomb, 1776; Rankine, 1857; Terzaghi, 1943; Fang and Ishibashi, 1986; Tsagareli, 1967; Toyosawa *et al.*, 2006). The slip surfaces tend to occur as wide bands, therefore the anchorages for the retaining structures must be installed in the outer boundary of these slip surfaces or simply, in the stabile soil mass.

The purpose of this thesis is the determination of the changes in the outer boundary of the slip surface in cohesionless soils due to corner angles, distance from the corner and the relative density of the soil, subsequently the peak friction angle and dilatation angle. In this work, the wall was not allowed to rotate and the outer boundary of the slip surface created solely by translation was tried to be determined. This helps the determination of the anchorage depths needed to ensure the stability of the retaining structure translating due to the loads created by the soil.

For this purpose, numerical deep excavation models with different corner angles were created using a finite element model program, namely Plaxis 3D. To ensure the created models to function correctly and determination of important soil parameters, verification models were created beforehand. Physical models (small-scale retaining wall models carried out within the scope of TUBITAK Project No. 114M329.) were modelled in Plaxis 3D numerically and the results obtained from finite element analysis were compared for verification. Then, the models were checked if they worked properly with the correct parameters. Finally, numerical models were created and the changes in the outer boundary of the slip surface in cohesionless soils due to corner angles, distance from the corner and the relative density of the soil, subsequently the peak friction angle and dilatation angle are determined.

2. LITERATURE REVIEW

2.1. Active Slip Plane Geometry

Active slip planes, also referred as failure planes, failure surfaces, slip surfaces, shear surfaces or shear planes, are basically assumed as straight lines. The theories of Coulomb (1776) and Rankine (1857) based on limit equilibrium have this assumption in common. There are similar theories on this subject proposed by (Coulomb, 1776; Rankine, 1857; Terzaghi, 1943; Fang and Ishibashi, 1986; Tsagareli, 1967; Toyosawa *et al.*, 2006)

For an active slip plane to form, the retaining structure must undergo a certain amount of horizontal displacement. The amount of the required horizontal displacement varies in between soil types. The required amount of horizontal displacements are given in the table below (Coduto, 2001) Table 2.1.

Table 2.1. Horizontal movement required to reach the active failure condition (Coduto, 2001).

Soil Type	Horizontal Movement Required to Reach the Active Condition
Dense sand	0.001H
Loose sand	0.004H
Stiff clay	0.010H
Solf clay	0.020H
H = Wall height	

2.1.1. Coulomb Theory (1776)

The first theory for the prediction of earth pressure coefficients were made by Coulomb (1776). Considering the soil-wall friction angle as the main variable, he proposed a mathematical and geometrical solution for the calculation of the earth pressure magnitudes and the location of the failure surface. Failure, in this case, was seen as a plane strain problem. The only backside of this theory was that the failure surface is assumed to be planar.

In Coulomb's theory, the main actors in equilibrium are the self-weight (W), the reaction force (P) due to the friction between the soil and the wall and the reaction on the slip plane (R) Figure 2.1. The magnitude of the reaction force can be determined from the triangle of forces, because self-weight and the directions of the forces are known.

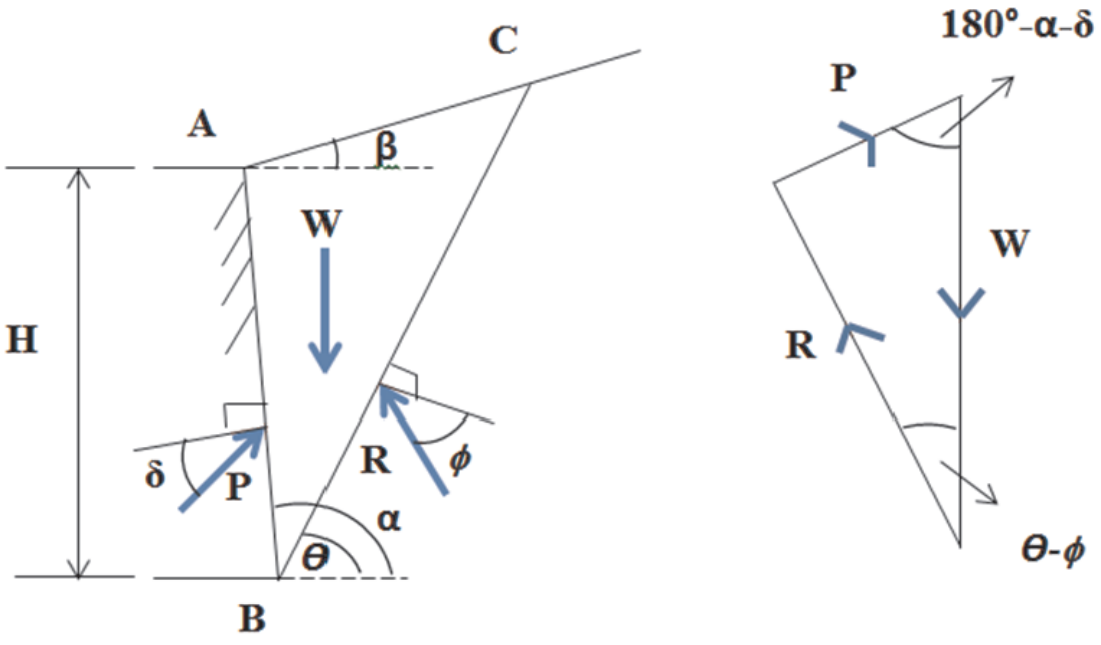

Figure 2.1. Active Case with c=0, Coulomb Theory (Craig, 2004).

In this theory, the point of application is not specifically given, but is assumed to act at a distance of a third of the height above the base of the wall (Craig, 2004).

Despite the only concern in this study is to be the active failure planes, it is also important to note that both active and passive failure planes are curved near the bottom of the wall. In the active case, this curve at the end is so small that it can be neglected as shown in the Figure 2.2.

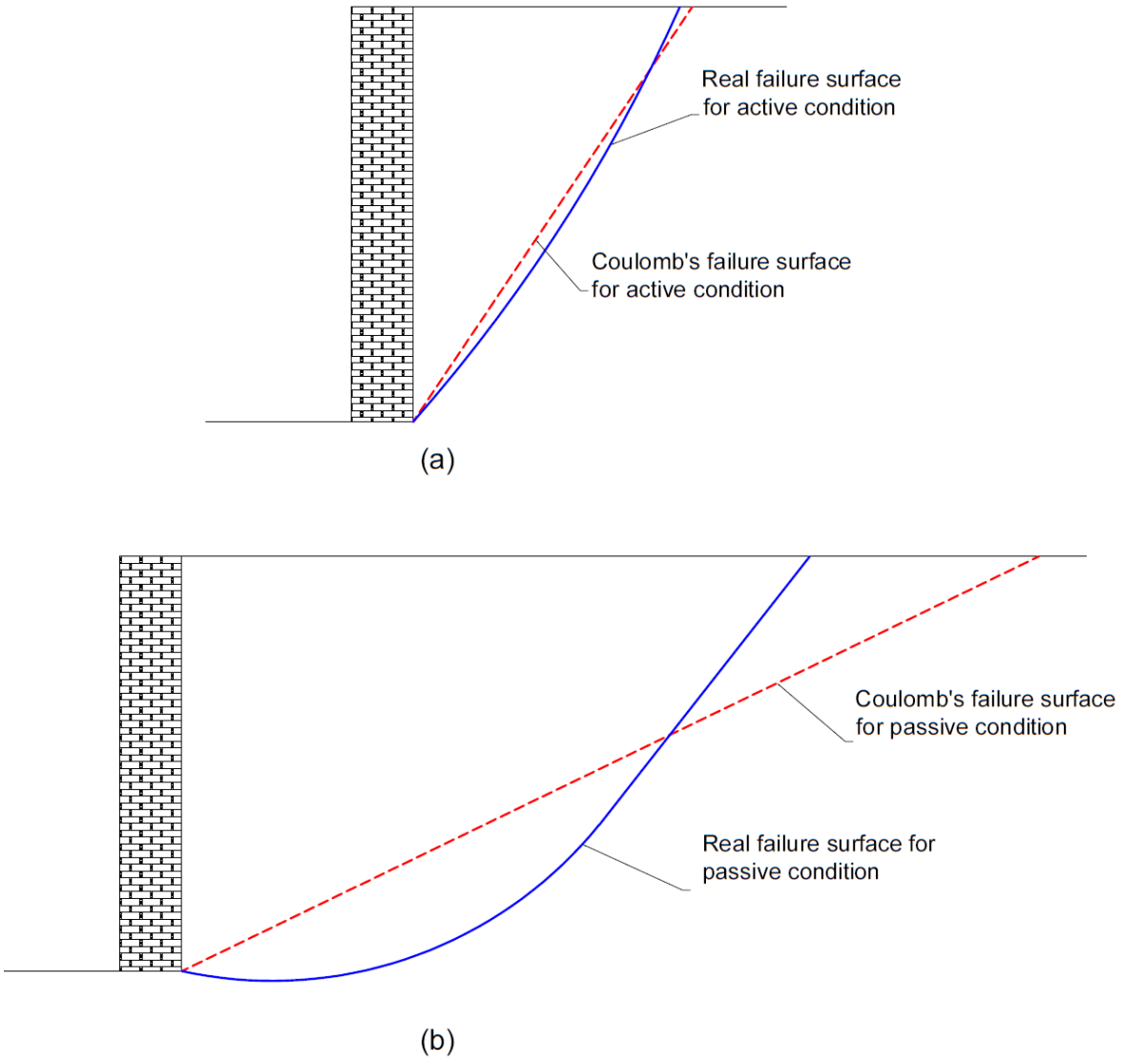

Figure 2.2. Real Failure Surfaces and Coulomb's Failure Surfaces: (a) Active Condition and (b) Passive Condition.

2.1.2. Rankine Theory (1857)

Making the same assumptions as Coulomb (1776), Rankine (1857) came up with a new way to determine lateral earth pressures. He considered the soil to be in a state of plastic equilibrium. The thing that makes Rankine's theory different are the lack of interface wall friction and soil cohesion. In a Rankine limit state, there are only two directions for the slip planes, as shown in the Figure 2.3.

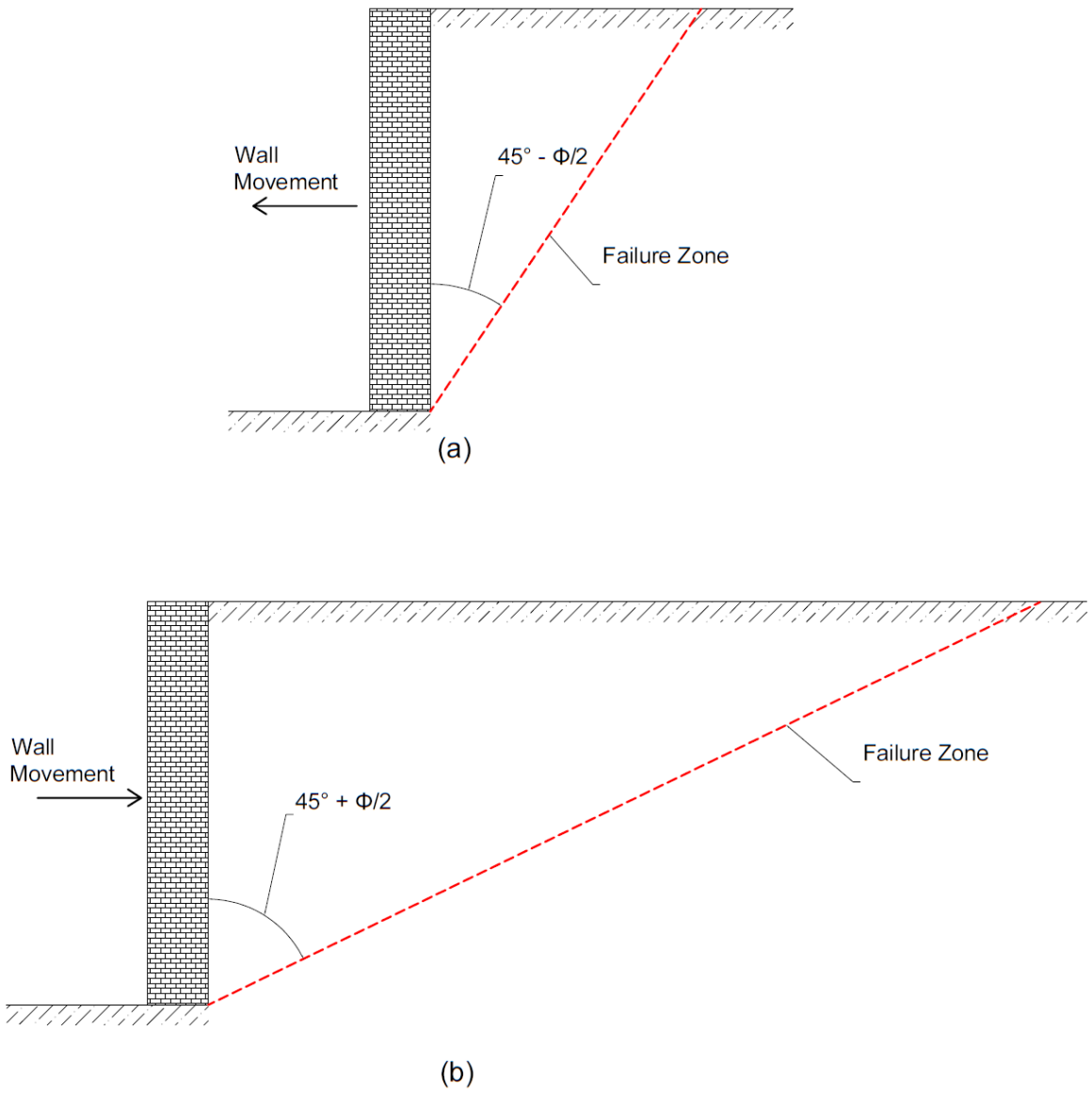

Figure 2.3. Rankine Failure Zones: (a) Active Condition and (b) Passive Condition.

Failure occurs with only two soil friction angles, respectively for active and passive limit states. On the failure surfaces, the soil is assumed to be reached the Mohr-Coulomb failure criterion. The formed failure wedges are determined by the two soil friction angles, shown in Figure 2.4.

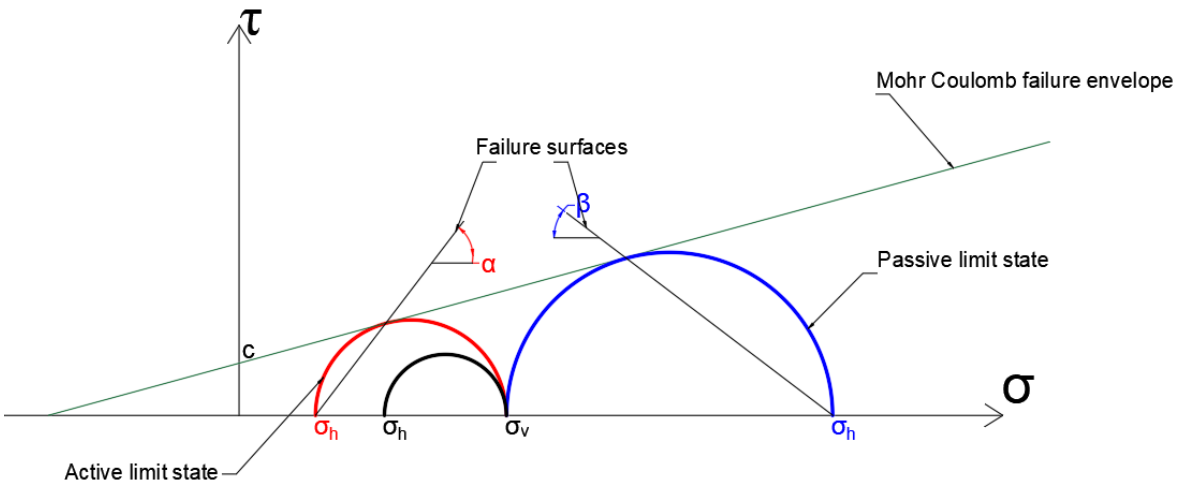

Figure 2.4. Mohr-Coulomb Failure Criterion for Active and Passive Cases.

After the geometrical procedure shown in the Figure above, the wedge angles for both the active and passive slip planes can be calculated using only the soil friction angle, given in Equation 2.1 and Equation 2.2.

$$\alpha = \frac{\pi}{4} - \frac{\varphi}{2} \tag{2.1}$$

$$\beta = \frac{\pi}{4} + \frac{\varphi}{2} \tag{2.2}$$

2.1.3. Tsagareli (1967)

The characterization of the slip surface with fixed walls is very important for the sake of this research. Z. V. Tsagareli (1967) conducted many researches on this area

to define a mathematical formulation for the slip surface function. To determine the characterization of the slip surface, experiments were conducted using parallel motion of the wall model by 2-4 cm with walls of height H = 2, 2.5, 3, 3.5 and 4 m.

For a sand with internal friction angle $\varphi = 37°$, an experimental curve of the slip surface was plotted using the results from the experiments Figure 2.5.

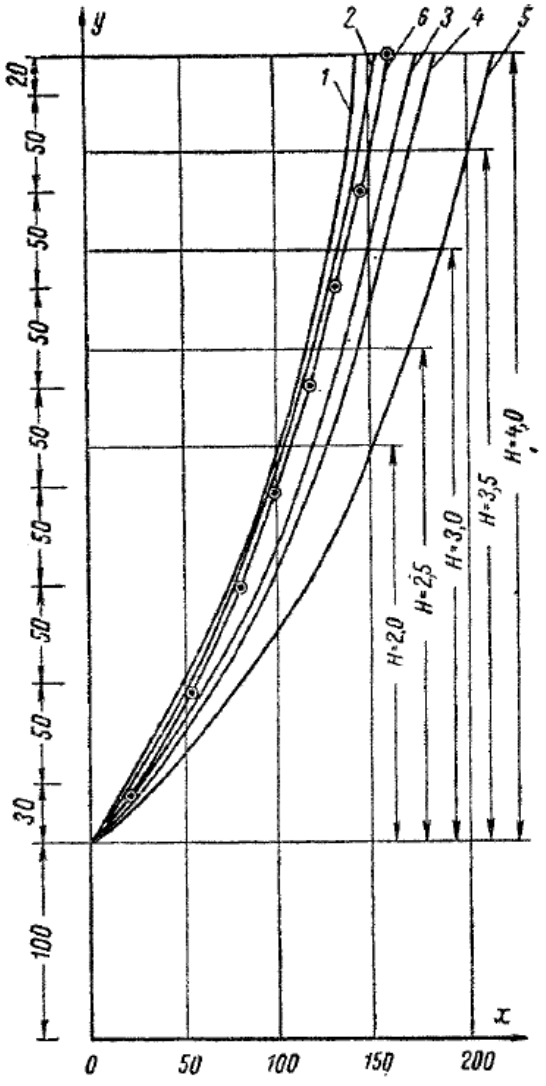

Figure 2.5. Slip Surfaces Plotted from Equation 2.3 and Experimental Data. 1) $\varphi = 40°$; 2) $\varphi = 37°$; 3) $\varphi = 32°$; 4) $\varphi = 30°$; 5) $\varphi = 25°$; Experimental Curves for $\varphi = 37°$ (Tsagereli, 1965).

From Figure 2.5, a simple power function denoting the curve of the slip surface can be obtained.

$$Y = C(3.6\varphi + 0.5)^{\frac{x}{C}} \tag{2.3}$$

where,

- The unit of the internal friction angle is in radians.
- C is a coefficient with the dimension of length.

2.2. Dilatancy

Dilatancy is a widely known phenomenon in soil mechanics, which defines the volume change in compacted granular soils during shearing as a result of the grains without any freedom to move starting to slide over each other. Until today, many researches have worked on the dilatancy phenomenon (Reynolds, 1885, dilatancy is also known as Reynolds dilatancy; Taylor, 1948; Rowe, 1962; Bolton, 1986; Vaid and Sasitharan, 1993; Schanz and Vermeer, 1996; Chakraborty and Salgado, 2010; Cinicioglu and Abadkon, 2014). Theoretically, dilatancy is simply explained as the volume change during shearing. The dilatancy angle can be calculated as

$$\psi = sin^{-1}(\frac{d\varepsilon_v}{d\varepsilon_q}) \tag{2.4}$$

In this equation, ψ is the dilatancy angle, $d\varepsilon_v$ is defined as the volumetric strain change and $d\varepsilon_q$ is the shear strain change.

2.2.1. Bolton's Theory (1986)

The main focus of Bolton's (1986) experiments are to understand the effects of compaction and confining pressure on peak angles of dilation (ψ_p) and shearing resistance ($\varphi_p^{'}$). He suggested an empirical equation which utilizes the mean effective

stress at peak shear strength ($p_p^{'}$) as the quantity expressing confining pressure, after collecting data from 17 different sand samples from the literature.

Bolton (1986) uses a simplified version of Rowe's stress-dilatancy relationship for plane-strain shearing to come up with a correlation between $\varphi_p^{'}$ and ψ_p, as shown in the Equation 2.5 below.

$$\varphi_p^{'} = \varphi_c^{'} + r\psi_p \tag{2.5}$$

where,

- r is a line fitting parameter, suggested 0.8 by Bolton (1986).
- $\varphi_c^{'}$ is the critical state friction angle.
- ψ_p is peak angles of dilation.
- $\varphi_p^{'}$ is the peak friction angle.

By using the data from plain-strain tests, Bolton researched the effects of variables like relative density and mean effective stress on the angle of dilatancy for sands.

For plain-strain tests:

$$\varphi_{max}^{'} - \varphi_{critical}^{'} = 0.8\psi = 5I_R \tag{2.6}$$

For triaxial tests:

$$\varphi_{max}^{'} - \varphi_{critical}^{'} = 0.8\psi = 3I_R \tag{2.7}$$

where I_R is the relative density index.

$$I_R = I_D(Q - \ln p_p^{'}) - R \tag{2.8}$$

where,

- I_D is the relative density, ranging from 0 to 1.
- Q and R are line-fitting parameters, depending on soil characteristics, Q=10 and R=1.

Bolton recommended $(-\frac{d\varepsilon_v}{d\varepsilon_1})_{max}$ to be a measure of dilatancy rate in triaxial test and he proposed the following equation for plain-strain and triaxial tests.

$$(-\frac{d\varepsilon_v}{d\varepsilon_1})_{max} = 0.3I_R \tag{2.9}$$

where,

- $d\varepsilon_v$ is the volumetric strain increment.
- $d\varepsilon_1$ is the principal strain increment.

2.2.2. Chakraborty and Salgado Equation (2010)

Chakraborty and Salgado (2010) used the test results of plain-strain compression and triaxial compression tests data to research a relationship between peak friction angle, dilatancy angle and critical state friction angle. The most important part of these tests are that they are conducted for low confining pressures, in comparison to Bolton (1986). Three ranges for the confinement pressures are determined. These are:

- $p^{'} < 50\,kPa$
- $50\,kPa < p^{'} < 100\,kPa$
- $100\,kPa < p^{'}$

Five different types of specimens with differing relative densities were used. These specimens are classified in the following manner:

- Very loose (0-15%)
- Loose (15-35%)
- Medium (35-65%)
- Dense (65-85%)
- Very dense (85-100%)

From these specimens, Touyora sand gave the most complete data for the research. After their research, they create the following equation as similar to Bolton's equation (1986).

$$\varphi_p = \varphi_c + A_\psi I_R \tag{2.10}$$

- φ_p is the peak state friction angle.
- φ_c is the critical state friction angle.
- A_ψ is constant value.
- I_R is the relative dilatancy index for both plane-strain and triaxial tests.

From the numerous plain-strain compression and triaxial test results, Chakraborty and Salgado (2010) showed the relationship between $(\varphi_p - \varphi_c)$ and I_D and I_R in the following Figure 2.6 and Figure 2.7. As can be seen from the figures, both the triaxial data points and the plain-strain data points lie approximately at the same locations. This proves that for both of the cases, the contribution of dilatancy to shear strength is similar. $A_\psi = 3.8$ can be used for both plain-strain and triaxial test conditions. Therefore Equation 2.11 can be also written as

$$\frac{\varphi_p - \varphi_c}{3.8} + I_D \ln \frac{100\sigma'_{mp}}{p_A} = I_D Q - R \tag{2.11}$$

- σ'_{mp} is the mean effective stress at peak shear strength.
- p_A is the reference stress = 100 kPa.

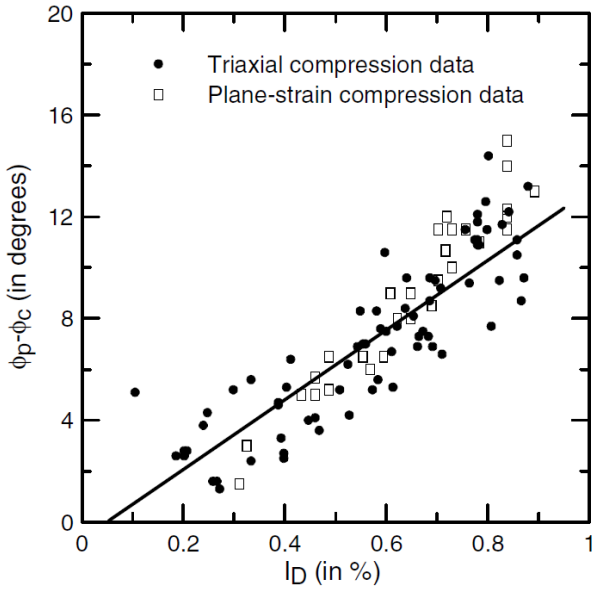

Figure 2.6. Triaxial and Plane-strain Compression Data Points for Toyoura Sand for Determining A_ψ with $(\varphi_p - \varphi_c)$ vs I_D Curve. (Chakraborty and Salgado, 2010).

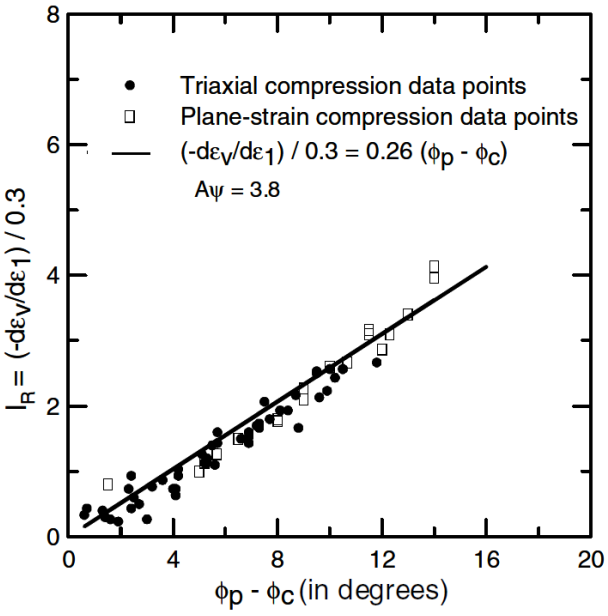

Figure 2.7. Triaxial and Plane-strain Compression Data Points for Toyoura Sand for Determining A_ψ with $(\varphi_p - \varphi_c)$ vs I_R Curve. (Chakraborty and Salgado, 2010).

The effects of the variation of the parameters Q and R were also observed by Chakraborty and Salgado (2010). In these tests, R was set to 1 and the values of Q varied. The change of Q was observed in relation with the initial confinement stress. This relation can be seen in the Figure 2.8 and Figure 2.9:

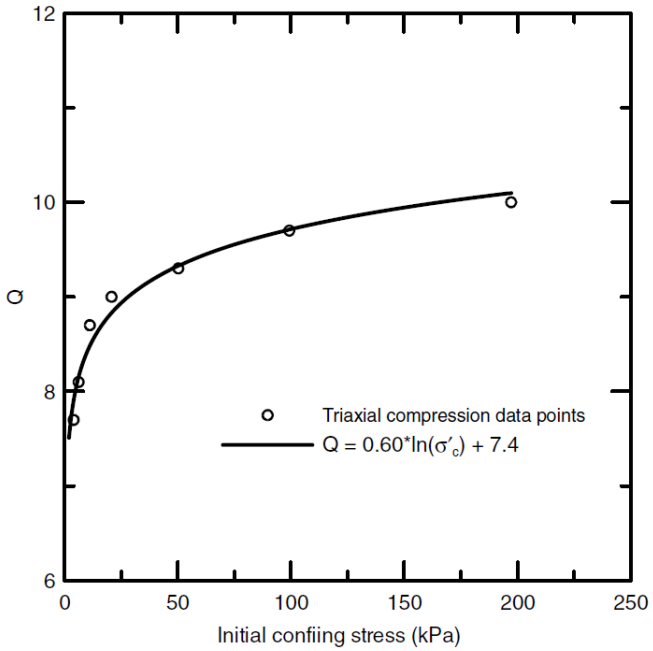

Figure 2.8. Variation of Q Values with Increasing Effective Confining Stress for Triaxial Compression (R = 1). (Chakraborty and Salgado, 2010).

Based on these test and observation results, simple equations for Q in both triaxial compression and plain-strain compression was proposed.

For plain-strain compression:

$$Q = 7.1 + 0.75 \ln \sigma_c^{'} \tag{2.12}$$

For triaxial compression:

$$Q = 7.4 + 0.60 \ln \sigma_c^{'} \tag{2.13}$$

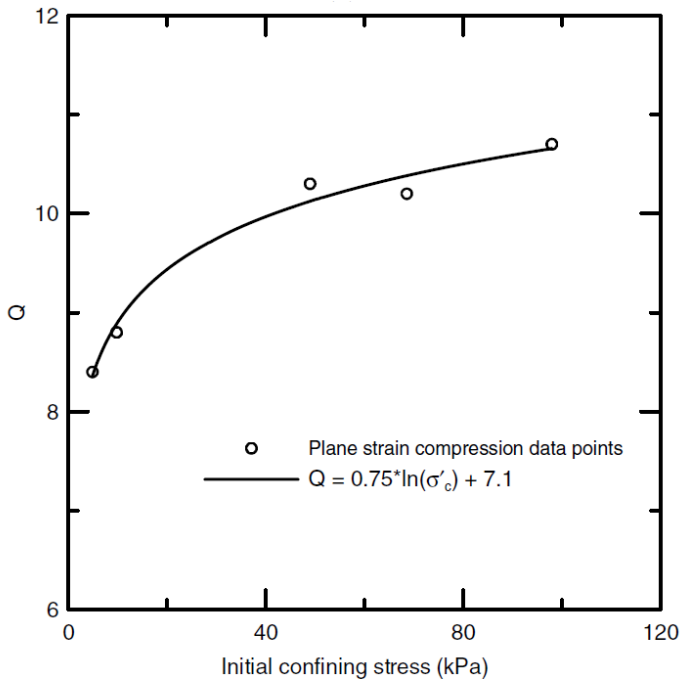

Figure 2.9. Variation of Q Values with Increasing Effective Confining Stress for Plane-strain Compression (R = 1). (Chakraborty and Salgado, 2010).

Combining Equation 2.11 with Equation 2.12 and Equation 2.13 yields in a formula, with which the peak friction angle and dilatancy angle can be calculated.

For plain-strain compression:

$$\frac{\varphi_p - \varphi_c}{3.8} + I_D \ln \frac{100\sigma'_{mp}}{p_A} = I_D(7.1 + 0.75 \ln \sigma'_c) - R \tag{2.14}$$

For triaxial compression:

$$\frac{\varphi_p - \varphi_c}{3.8} + I_D \ln \frac{100\sigma'_{mp}}{p_A} = I_D(7.4 + 0.60 \ln \sigma'_c) - R \tag{2.15}$$

2.3. FEM

The finite element method, FEM, is a widely used numerical analysis technique. This technique can be implemented to numerous engineering problems to obtain approximate solutions. The technique was original developed to be used in the aerospace industry, but since then it has been used in the general field of continuum mechanics. The most important aspects of this method, which makes it so popular in the engineering schools and industry is the diversity and the flexibility of the method as an analysis tool.

As the engineering industry develops and the problems become more and more complex, approximate numerical solutions are more preferable to exact closed-form solutions. The reason for the complexity of the problems comes from the fact that the problem in question has a feature which is irregular or "arbitrary". Although analytical solutions to these types of problems rarely exist, these are the most common types of problems in the engineering applications. Simplifying such problems by eliminating certain uncertainties and irregularities may make it solvable, yet such simplifications usually result in inaccuracies or wrong answers.

Over the years, several numerical methods have been found Figure 2.10. One of these methods is the finite difference method. Finite difference method utilizes difference equations written for an array of grid points. This method can be seen as a crude and unrefined predecessor of finite element method. Finite difference method gives a pointwise approximation to the equations of the problem, whereas finite element method gives a piecewise approximation to the equations of the problem. Another difference between these two methods is that finite difference method sees the problem as an assemblage of points, whereas the finite elements method sees the problem as a sum of many interconnected subregions or elements.

The finite element method works in many steps. The first of these steps is to divide the continuum or the solution region into fine elements. This process is also called Discretising the Continuum. The most commonly used geometrical shape for

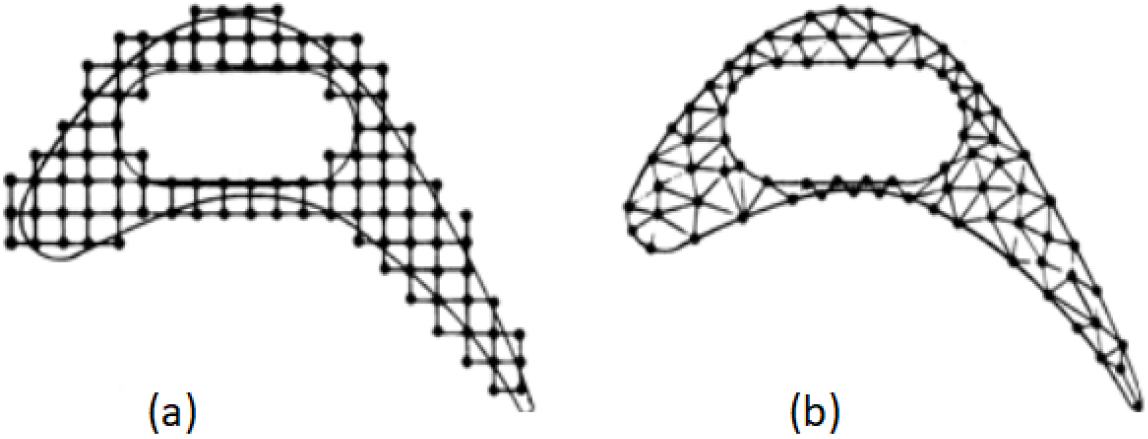

Figure 2.10. (a) Finite Difference and (b) Finite Element Discretizations of a Turbine Blade Profile (Huebner, 2001).

these small elements are the triangles. Triangles are the simplest linear closed shapes one can create.

Next step in the process is the selecting of the Interpolation Functions. This means assigning nodes to the elements created in the previous step and then choosing the interpolation function to define the changes of the field variable over the element. Also, on these nodes, the functions of the main problem are defined in terms of the values of the field variables. The most commonly used types of interpolation functions are polynomials, since they are easy to integrate and differentiate. The degree of the polynomial depends on many things, such as the number of assigned to an element, the nature and number of unknowns at each node and certain continuity requirements. Other types of interpolation function include scalars, vectors or high-order tensors.

The third step of the process helps with finding the Element Properties. After establishing a model, the matrix equations expressing the properties of the individual elements are determined. Three approaches may be used for this process, the direct approach, the variational approach or the weighted residuals approach. The direct approach is only usable, if the origins of the element properties are traceable by means

of stiffness method or structural analysis. The variational approach involves extremizing a functional like the potential energy, the complementary energy etc. Variational approach can be used in both the simple and complex element shapes, whereas direct approach can also work with simple methods. Weighted residual approach is the most versatile of the batch. This approach begins with the governing equation of the problem and continues to solve the problem depending on the various boundary conditions. The advantage of this approach is that it makes it possible to use finite elements method in problems where there are no available functional.

In the next step, the element properties are assembled to obtain the System Equations. This step is necessary to find the properties of the overall system. To this end, the matrix equations expressing the properties of the individual elements are combined into the matrix equations of the entire system. The matrix equations of the system are similar to those of the elements, but they contain more terms.

Next, the Boundary Conditions are imposed. Whether it is a mass of soil, or a beam in a structure, every model must have boundary conditions. This step is necessary for the solution of the system equations.

After imposing the boundary condition, the system equations are solved. Many times, this is not the final step, and the solutions of the system equations are used to calculate other important parameters for the problem.

Range of Applications:

There are three categories, divided according to the nature of the problem, which can be solved by the application of finite element method:

- Equilibrium or Time-Independent Problems
- Eigenvalue Problems
- Propagation Problems

The majority of the Equilibrium Problems in solid mechanics require mainly the computation of displacement or stress distribution for a given mechanical or thermal loading. In the case of fluid mechanics, the searched parameters are the pressure, velocity and density distributions under steady-state conditions. It is imperative for the problem to be in steady state condition, otherwise it would have been a propagation problem.

The Eigenvalue Problems are used to determine the natural frequencies and mode shapes of solids and fluids. In civil engineering, eigenvalue solutions are mainly used in the area of structural and earthquake engineering, for the calculation of mode shapes and natural periods of the structures.

Lastly, Propagation Problems are used when time is also a variable. These types of problems can be either Equilibrium or Eigenvalue problems, with the addition of the dependency on the change of time.

3. STATEMENT OF THE PROBLEM

Retaining structures are one of the most important geotechnical structures built especially in metropolises and cities where there are dense settlements. As in every constructed structure, internal forces in the design of the shoring systems are carried out using the loads acting on the structure. The loads and stresses on the shoring systems are mainly influenced by the ground behind the structure. The position and geometry of the failure zones which will be formed in the ground is of great importance for the calculation of the soil stresses acting on the shoring systems, because the soil between the failure zone and the shoring system is responsible for the stresses acting on the structure. In addition to that, in order to determine the free length of the anchors used for the shoring systems, the positions of the slip bands are of great importance. The anchor roots must be at the outside of the active failure zone, because anchor roots that are inside the active failure zone can be dislodged with the sliding soil.

A lot of research is involved in determining the locations of the failure zone, but most of these studies are only valid for the shoring system and retaining structures where the plane strain condition are faced. However, in the corners of the shoring system and the retaining structures in deep excavations Figure 3.1, the plane strain conditions are not valid so the three-dimensional conditions should be considered in the problem. Numerical methods are the best method for determining the failure zone in shoring systems and retaining structures where a three-dimensional stress environment is applicable. Therefore, Plaxis 3D numerical modelling program was used in this study to solve these problems.

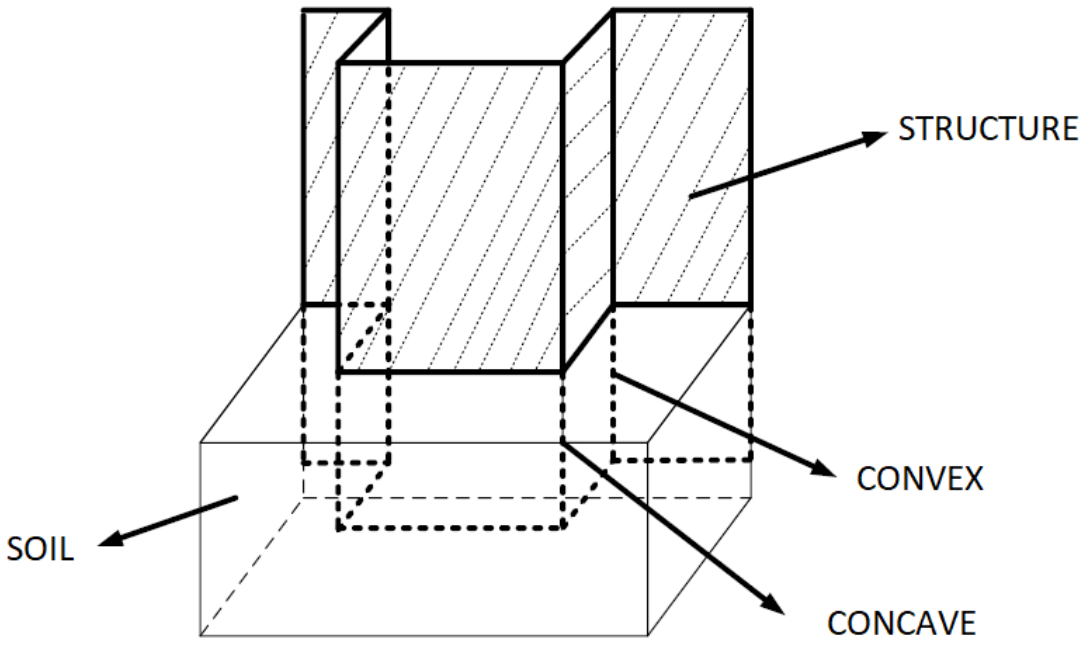

Figure 3.1. Convex and Concave Corners due to Excavation Geometry.

4. NUMERICAL MODEL AND ITS VERIFICATION

4.1. Plaxis and FEM

Plaxis 3D is a numerical analysis program and it is developed for analysis of deformation, stability and groundwater flow in geotechnical engineering (Plaxis 3D manual, 2018). Real situations such as deep excavation in the field can be easily modelled with the help of its user-friendly user interface. It uses the finite element method (FEM). The finite element method is a numerical technique for solving physical problems such as structural or fluid behaviour, wave propagation, etc. In that numerical technique, the whole model divides into smaller parts which are called finite elements. In these finite elements, differential equations are approximately solved. Then, the whole problem can be solved by bringing together solutions of these finite elements. In general, these finite elements have a quadrilateral shape. However, in Plaxis the finite elements are triangular. The triangular finite elements are composed of the stress points and the nodes. In the stress points, the stresses and strains are determined. In the nodes, the displacements are determined.

4.2. Constitutive Model (Hardening Soil Model)

Empirical results show that at the first stages of loading, deformation in soils starts. The widely used elasto-perfect models fall short in showing this phenomenon in a constitutive model. Models implementing a hardening law after initial yielding are required to model such behavior. The hardening of soils was first researched by Schanz and Vermeer (1999). There are two main parts of this hardening model, namely deviatoric and volumetric hardenings. Nonlinear elastic behavior is also used in this model.

The model has three yield surfaces, deviatoric (shear), volumetric (cap) and tension cut off. These surfaces and hardening characteristics are shown in Figure 4.1.

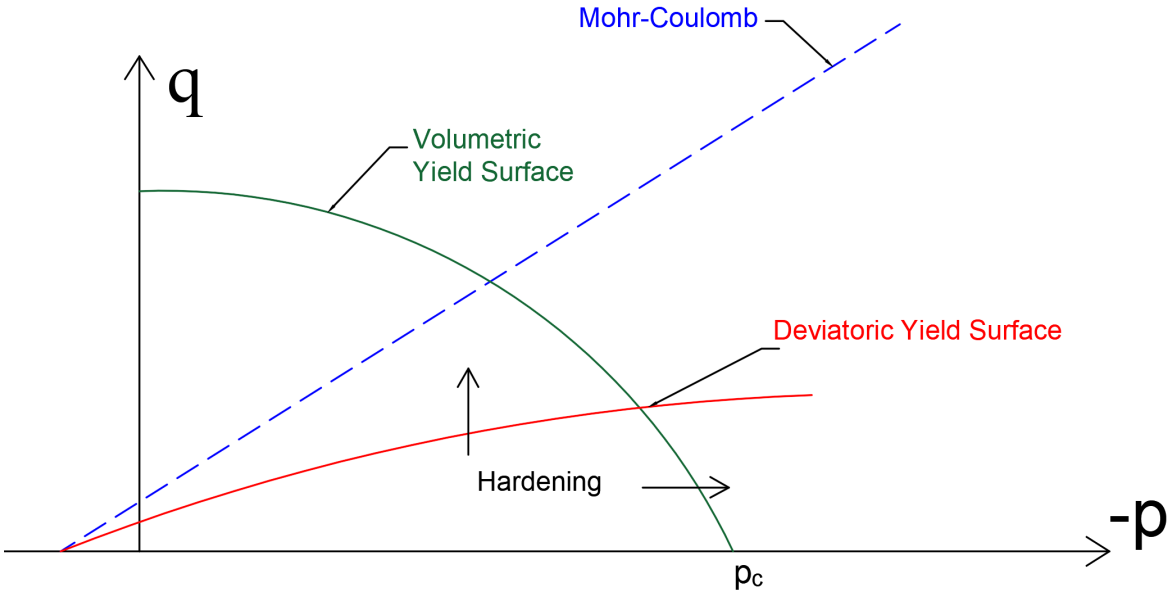

Figure 4.1. The Yield Surfaces of the Hardening Soil Model.

4.2.1. Deviatoric Hardening Mechanism

The hardening model is based on the deviatoric mechanism, which is defined by the Mohr-Coulomb properties and reaches to the failure at Mohr-Coulomb yield surface at its ultimate state. The curve of the yield surface of the deviatoric mechanism is defined as

$$F_s = \frac{q}{E_i(1 - q/q_a)} - \frac{q}{E_{ur}} - \varepsilon_q^{p-shear} = 0 \tag{4.1}$$

where,

- q is the deviatoric stress.
- $\varepsilon_q^{p-shear}$ is the deviatoric plastic strain.

q_a is defined as;

$$q_a = \frac{q_f}{R_f},\ q_f = (c\cot\varphi + \sigma_1)\frac{2\sin\varphi}{1-\sin\varphi} \tag{4.2}$$

where,

- R_f is the failure ratio with a default value 0.9.
- φ is the friction angle.
- c is cohesion.

E_{ur} is the elastic modulus in unloading and reloading, defined as

$$E_{ur} = E_{ur}^{ref}\Big(\frac{c\cos\varphi + \sigma_1\sin\varphi}{c\cot\varphi + p_{ref}\sin\varphi}\Big)^m \tag{4.3}$$

where,

- E_{ur}^{ref} is the reference elastic modulus at a stress level, p_{ref}.
- p_{ref} is a reference pressure.
- m is a power controlling the stress dependency of the elastic modulus, $0.5 < m < 1.0$.

E_i controls the slope of the hyperbolic curve and is equal to

$$E_i = \frac{2E_{50}}{2-R_f},\ E_{50} = E_{50}^{ref}\Big(\frac{c\cos\varphi + \sigma_1\sin\varphi}{c\cot\varphi + p_{ref}\sin\varphi}\Big)^m \tag{4.4}$$

4.2.2. Volumetric Hardening Mechanism

Volumetric mechanism (cap) simulates the compaction of the material and closes the elastic domain on the hydrostatic axis. The cap has an elliptical shape defined as;

$$F_c = \left(\frac{q^*}{\alpha_s}\right)^2 + p^2 - p_c^2 = 0 \tag{4.5}$$

where,

- p_c is the location of the intersection with the p axis.
- α_s is the shape factor.

q^* is a stress invariant and is defined as

$$q^* = \frac{q}{f(\theta)},\ f(\theta) = \frac{3 - \sin\varphi}{2(\sqrt{3}\cos\theta - \sin\theta\sin\alpha)} \tag{4.6}$$

4.2.3. Tension Cut off

In this model, tension cut of mechanism takes the tensile strength of the material into consideration. The mechanism has no hardening and the equation for tension cut off is

$$F_T = \sigma_1 - T = 0 \tag{4.7}$$

where,

- T is the tensile strength of the material.

4.3. Verification

4.3.1. Physical Model

The physical model is small-scale retaining wall models carried out within the scope of TUBITAK Project No. 114M329. The test setup consists of a frame of 15 cm

X 30 cm X 20 cm as shown Figure 4.2. The front and back surfaces of the model box are covered with plexiglass material in order to monitor the movement of the ground placed in the model box. The retaining wall is modelled in such a way that it is moved in the outwards horizontal direction by rotating a sleeve wheel. Wall motion is recorded with the digital sensor and wall movement is determined. One side of the model box is rigid and the other side has a movable aluminum plate representing the retaining wall. The movement of the floor with the wall displacement is recorded with a digital camera that can shoot with 0.5 s interval. In all tests, recordings are made with fixed camera-model distance and focus range. Subsequent records can be analyzed with the help of the PIV program.

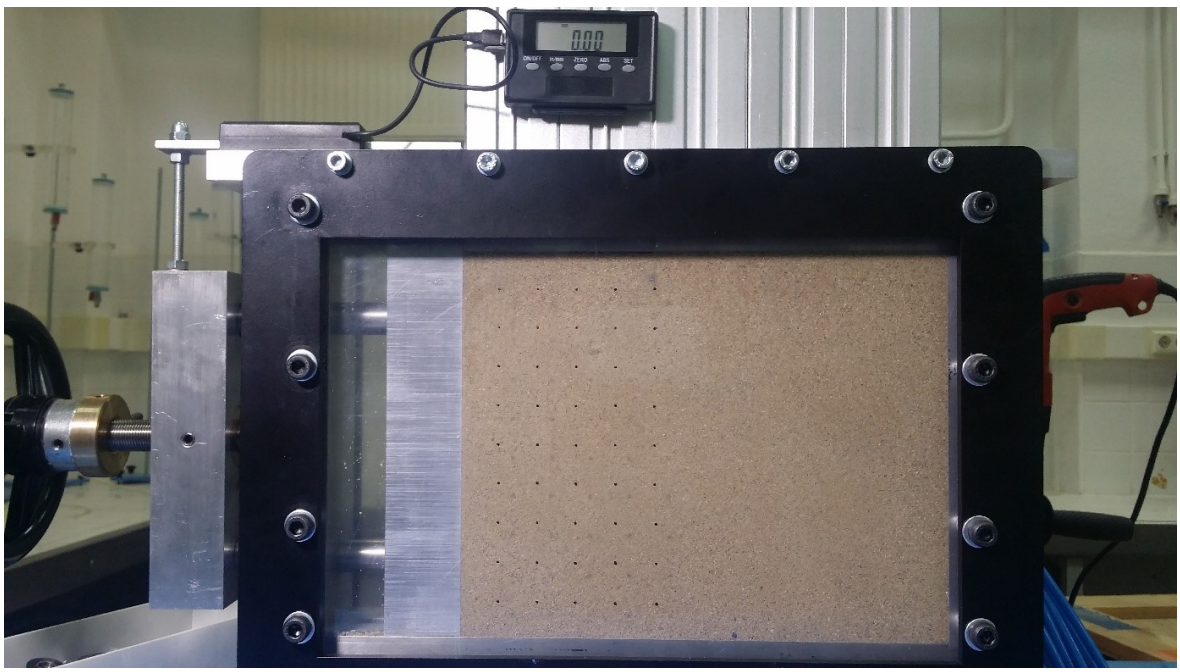

Figure 4.2. Small-scale Retaining Wall Model.

4.3.2. PIV

Particle Image Velocimetry method is used in the experimental part of the study to determine failure surfaces. The PIV method is used in physical model experiments to be performed under plane-strain deformation conditions to follow the evolution of the failure surface from photographs taken through the transparent plexiglass sidewalls.

The PIV method is a method of flow measurement that does not interfere with the flow and is a method used for examining the flow in many branches. White *et al.* (2003) made some changes in PIV technique and made it suitable for the studies in the geotechnical field. Thus, it has become possible to define and evaluate the deformations of soils (White *et al.*, 2001; Niedostatkiewicz *et al.*., 2011; Lesniewska and Wood, 2009; Lesniewska *et al.*, 2012; Soltanbeigi *et al.*, 2015).

PIV determines a reference image in a photo frame. It then follows the displacements from the reference point as a result of the wall offset. In order to determine the displacements, consecutively taken photographs are used. The displacements resulting from the comparison of photographs are expressed by colour scale (White *et al.*, 2003). Since the displacements in the parts are high along the failure surface, the image is at a darker colour scale than the other regions of the photographic frame, and so the failure surface plane is determined. Figure 4.3 shows the variation between the reference image and the following sequential image. Figure 4.4 shows the failure surface geometry obtained as a result of PIV analysis.

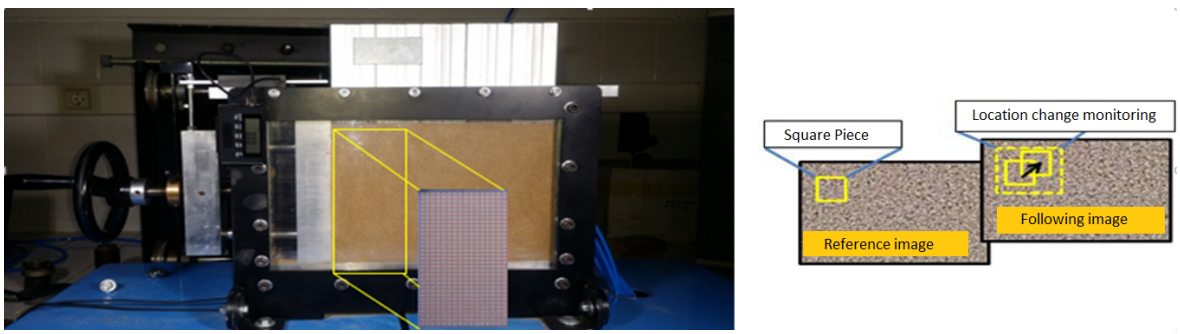

Figure 4.3. Selection of the Area to be Examined in PIV Analysis.

4.3.3. Results from Physical Model

The photographs taken during the physical experiments are examined in a computer environment with the help of PIV program. As a result of the investigations on the physical modal tests, the formed failure surfaces of the samples are determined. The results obtained from the physical models in Sile sand samples with four different

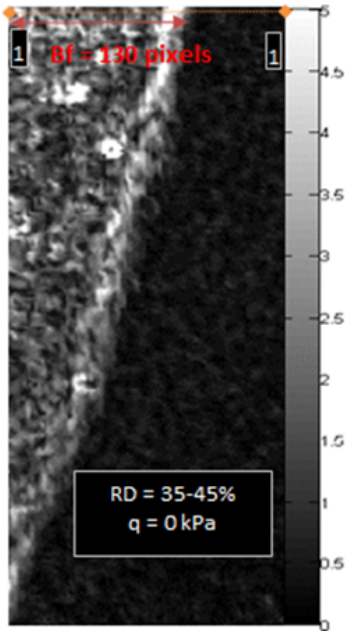

Figure 4.4. Failure Surface Obtained by PIV Analysis.

relative density are given in the Figure 4.5 and these results are used in the validation of this study.

4.3.4. Verification Model

The results of the analyses using the Plaxis 3D program vary according to the parameters used during the creation of the models. For this reason, it is aimed to verify the parameters to be used before modelling the numerical model. For this purpose, small-scale retaining wall models made within the scope of TUBITAK Project No. 114M329 are modelled numerically and the results are compared.

4.3.4.1. Definition and Assumptions of Verification Model. The graphical illustration of verification model is shown in Figure 4.6. The first goal of the model is to verify soil parameters and determine the interface (R_{inter}) coefficient between soil and walls. The second goal of the model is to show the influence of the interface coefficient at the failure surface.

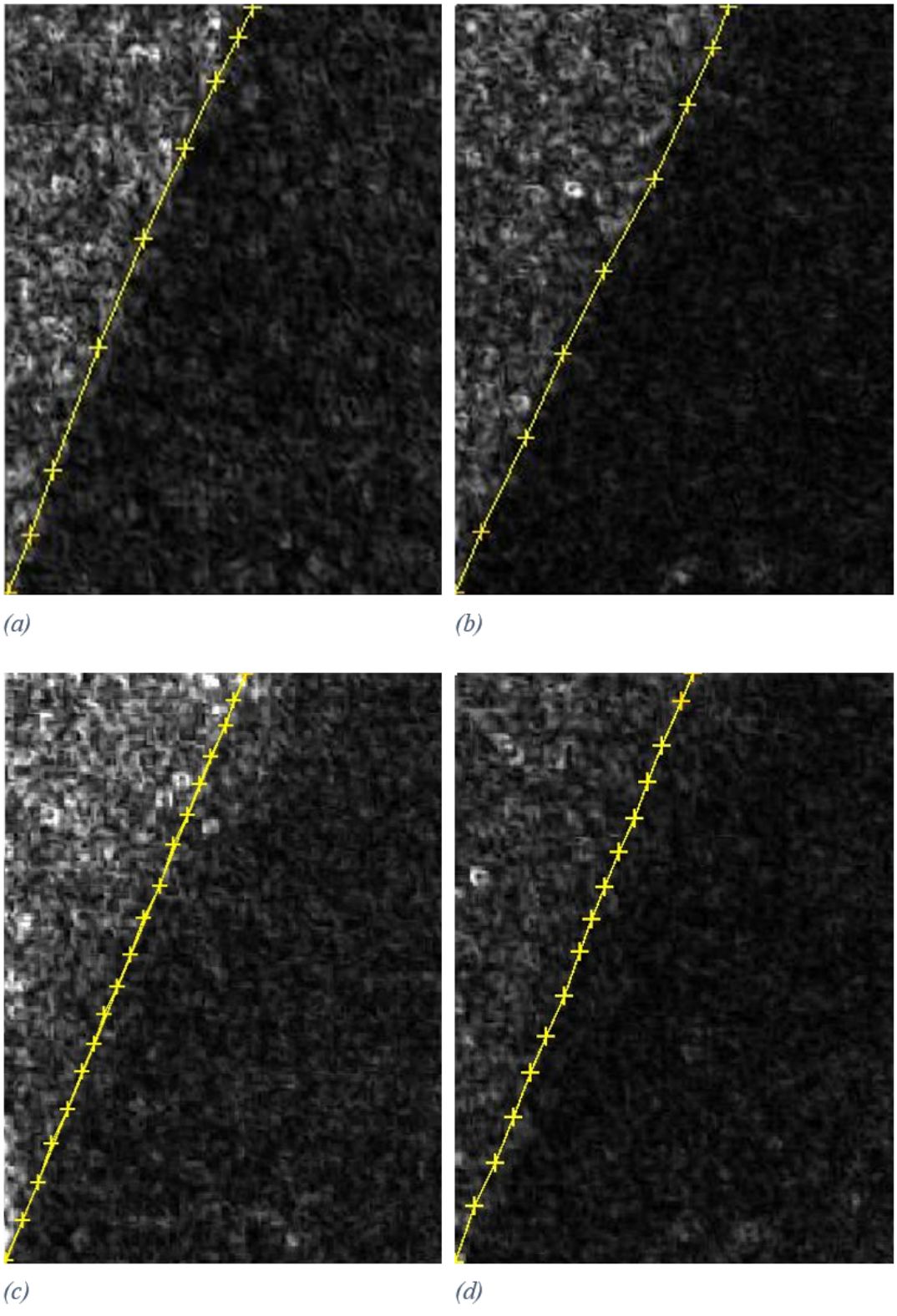

Figure 4.5. Results of the Physical model. (a) Soil 1 (b) Soil 2 (c) Soil 3 (d) Soil 4.

Assumptions made for verification model are summarized below. If required, detailed explanations regarding the assumptions stated below will be given later.

- The geometry of the small box is 30 cm length, 15 cm width and 20 cm height.
- Hardening Soil is used as a constitutive model to provide precise soil behaviour.
- It is assumed that soil strength parameters do not change with depth.
- All the walls are represented with rigid plate elements and only one wall can move. The other walls are fixed.
- 0.1 cm displacement (0.005H) is defined on the moving wall to create active failure surface.
- Free connections are defined between the moving wall and the other walls.

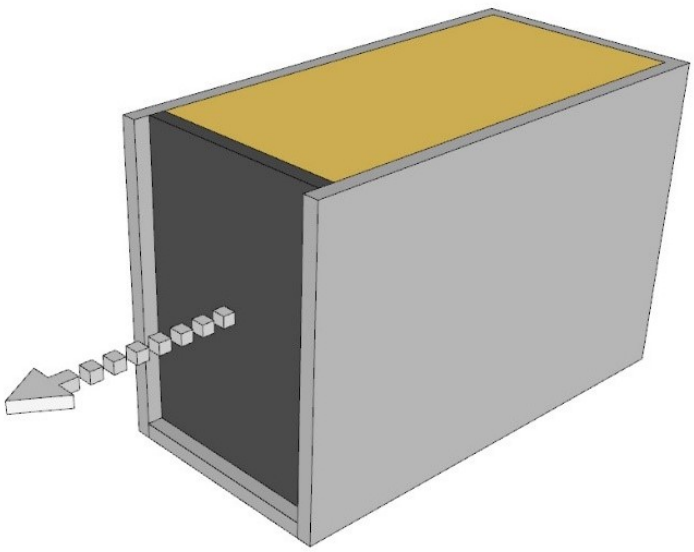

Figure 4.6. Graphical Illustration of Small Scale Retaining Wall Models Made Within the Scope of TUBITAK Project No. 114M329.

4.3.4.2. Data Input in Plaxis 3D. Project Properties: Project properties window is the first step to create a new project. There are two tabsheets in "Project properties" window of Plaxis 3D. They are named as "Project" and "Model".

In the Project tabsheet Figure 4.7, there are five boxes called as "Title", "Directory", "File name", "Comments" and "Company logo". Title of the project is written

in “Title” box. “Directory” box shows the address where the project is saved. “File name” box displays the name of the project after saving the project. “Comment” box can be used to enter an extra comment about the project if it is needed and the last box in the Project tabsheet is “Company” box where the company loga can be loaded. In the Model tabsheet Figure 4.8 , there are four boxes called as “Type”, “Units”,

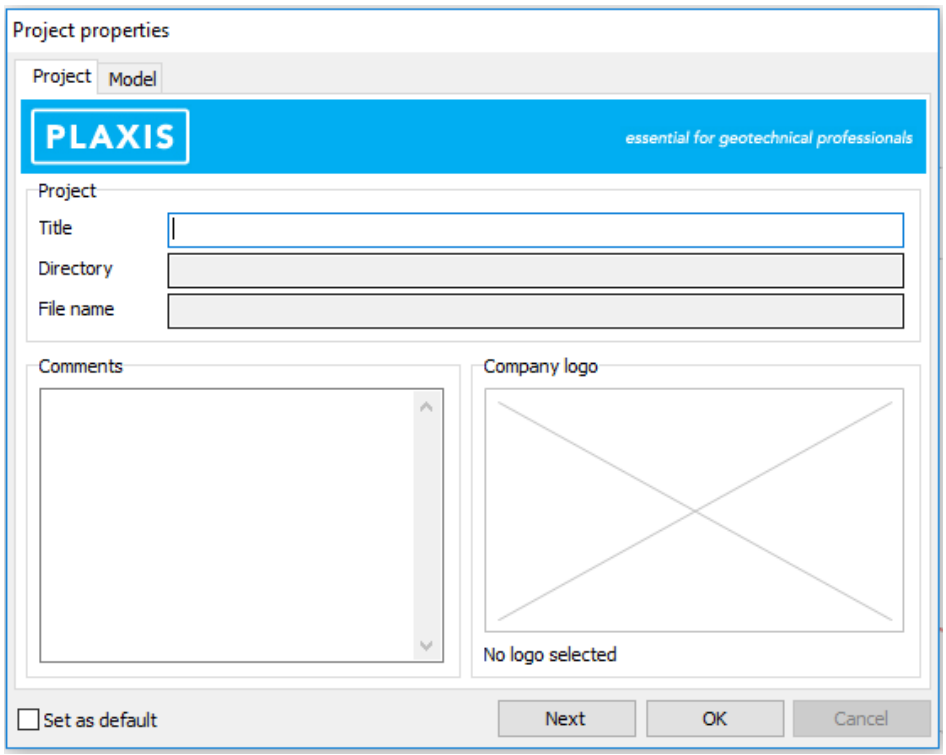

Figure 4.7. Project Properties Window (Project Tabsheet).

“General” and “Contour”. In the “Type” box, model and elements type is shown and it is not allowed to change. In the “Units” box, basic units (length, force and time) are shown and their units can be changed. “General” box shows earth gravity, the direction of gravity and magnitude of water unit weight. In the last box which called as “Contour”, there are four input boxes which are used to define the outer boundary of the drawing. For the verification model and the numerical model of this study, the boundary is defined as shown in Table 4.1 and Table 4.2.

Material Sets: In this study, two different types of materials are used to create Plaxis 3D models. The first material is a plate element which represents walls and base

Table 4.1. Contour of the Verification Model.

x_{min} (cm)	0
x_{max} (cm)	100
y_{min} (cm)	0
y_{max} (cm)	75

Table 4.2. Contour of the Numerical Model.

x_{min} (m)	0
x_{max} (m)	300
y_{min} (m)	0
y_{max} (m)	300

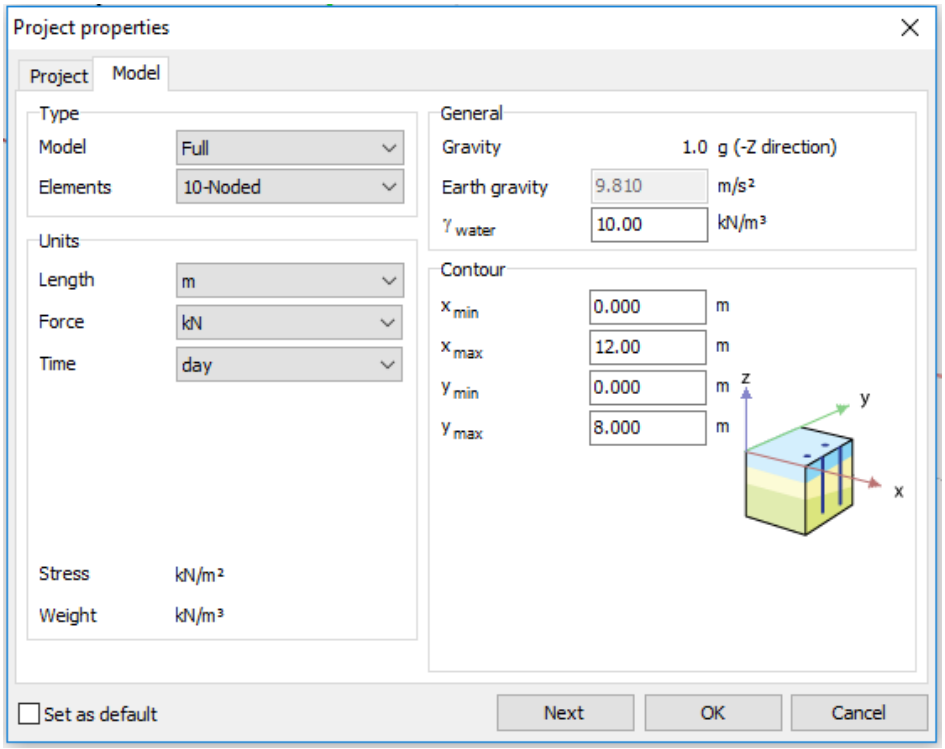

Figure 4.8. Project Properties Window (Model Tabsheet)

of 3D models, and the second material is a soil which represents soil material of 3D models.

Plates are a two-dimensional structural elements which have significant bending stiffness. In this study, all the walls and base of the models are rigid since prescribed displacements are defined. Therefore, the properties of the plates do not change results. Typical plate parameters are used in all models as given Table 4.3. The unit weight of the plate is used as 8 kN/m^3 instead of 24 kN/m^3 because of overlapping with the soil. Therefore, the unit weight of plate element entered in Plaxis is the unit weight of the soil subtracted from the unit weight of the plate element.

The results of the analyses vary according to the parameters used during the creation of the models. It is very important to select correct soil and interface parameters for the analysis. To verify the parameters, it must be comparable with some research. Therefore, soil parameters of small-scale retaining wall models made within the scope

Table 4.3. Plate Element Material Properties.

Plate Element Material Properties			
	Name	**Unit**	**Value**
Title for a data set	Identification	-	Wall
The material type for plates	Material type	-	Elastic
The equivalent thickness	d	m	0.2
The unit weight	γ	kN/m3	8
Isotropic	Isotropic	-	Yes
Young's modulus in first axial direction	E1	(kN/m2)	3.00E+07
Poisson's ratio	v12	-	0.2
In-plane shear modulus	G12	(kN/m2)	1.25E+07

of TUBITAK Project No. 114M329 were used and the soil properties shown in Table 4.4 and Table 4.5 are taken into consideration.

Four soil data sets are used in Plaxis 3D models as the given Table 4.6. As shown in Table 4.6 Hardening soil model (HS) is used. Hardening soil model (HS) is an advanced model which is an elasto-plastic type of hyperbolic model, formulated in the framework of shear hardening plasticity. In addition to that, the model includes compression hardening to simulate irreversible compaction of soil under primary compression (Plaxis 3D manual, 2018). All models are considered not to have groundwater so the type of drainage is taken as drained. There is no information about elastic modulus at given tables about Sile sand. Hence, elastic modules should be theoretically calculated with the help of the relative density of the soils. In this calculation, the following equations are used.

$$D_r(\%) \approx 100\left(\frac{N_{60}}{60}\right)^{0.5} \tag{4.8}$$

Table 4.4. Soil Properties of Sile Sand.

Property	Value
Classification	SP
Median particle size (D_{50})	0.71
Uniformity Coefficient (C_u)	2.80
Coefficient of Gradation (C_c)	1.12
Specific gravity (G_s)	2.61
Maximum Void Ratio (e_{max})	0.78
Minimum Void Ratio (e_{min})	0.52
Average Sphericity (S_{ave})	0.674
Average Roundness (R_{ave})	0.725
Stress-based dilatancy constant (α_ψ)	-0.098
Density-based dilatancy constant (m_ψ)	0.474
Dilatancy effect on friction for axisymmetric conditions (r_{tx})	0.59
Dilatancy effect on friction for plane strain conditions (r_{ps})	0.91
Line fitting parameter – Q	8.324
Line fitting parameter – R	0.514
Critical state friction angle (ϕ'_c) (°)	33.2

Table 4.5. Some Soil Properties of Sile Sand for Four Different Relative Density.

	Name	Unit	Soil 1	Soil 2	Soil 3	Soil 4
Relative density	RD	%	40	51	61	67
Void ratio	e	-	0.676	0.6474	0.6214	0.6058
The unit weight	γ	kN/m^3	15.27691	15.54213	15.79135	15.94476
Dilatancy angle	ψ	°	10.3	13.3	15.8	17.3

$$E_s(kN/m^2) = \begin{cases} 500N_{60}\ for\ silty\ and\ clayey\ sands \\ 500N_{60}\ for\ clean\ sands \\ 500N_{60}\ for\ over\ consolidated\ clean\ sands \end{cases} \tag{4.9}$$

In the equation of Jamilowski vd. (1998) Equation 4.8, N_{60} value should multiplied with 0.92 for course sands and 1.08 for fine sands. Sile sand is a fine grained sand so N_{60} values are multiplied with 1.08. Sile sand is a over consolidated clean sand so in the calculations $1500N_{60}$ is used for Kulhawy and Mayne (1990) Equation 4.9. Secant stiffness (E_{50}^{ref}) and tangent stiffness for primary oedometer loading (E_{ode}^{ref}) are accepted to be same with elastic modulus (E_s). As it is given default in Plaxis 3D, Unloading / reloading stiffness (E_{ur}^{ref}) is accepted as $E_{ur}^{ref} = 3E_{50}^{ref}$. Power for stress-level dependency of stiffness is used as default value 0.5. Sile sand is a clean sand therefore effective cohesion is zero. In the models for effective angle of internal friction, peak friction angle are used. To determine peak friction angles Equation 2.5 is used. In verification model for each dataset, four different interface strength reduction factor (R_{inter}) is defined as 0.5, 0.6, 0.7 and 0.8.

Creating Structure of Model: Small-scale retaining wall models made within the scope of TUBITAK Project No. 114M329 are modelled numerically according to physical model dimensions as shown in Table 4.7. In the verification model, the walls next to the movable wall and the base of the model are made 5 cm longer than the length in the physical model. This is because the moving wall moves outward to prevent the sand from spilling out. Plate elements are used to model the base and all the walls of the verification model. After that, positive and negative interface elements are defined on all plate elements. The reason for this is to create soil-structure interaction conditions and to define the connections between plate elements. Then, prescribed displacements are defined for the model base, moving and stationary walls. The model base and the stationary walls are fixed in the x, y, and z directions as in the actual physical model by the prescribed displacements. As shown Figure 4.9 the moving wall is fixed in the y and z directions and is allowed to move 0.10 cm out of the box in the x-direction same

Table 4.6. Properties of Sile Sand Samples.

Parameter			**Sile Sand Samples**			
			Soil 1	**Soil 2**	**Soil 3**	**Soil 4**
	Name	Unit	Value	Value	Value	Value
Material Model	-	-	HS	HS	HS	HS
Drainage Type	-	-	Drained	Drained	Drained	Drained
Unsaturated unit weight	γ_{unsat}	kN/m^3	15.28	15.54	15.79	15.94
Saturated unit weight	γ_{sat}	kN/m^3	15.28	15.54	15.79	15.94
Secant stiffness	E_{50}^{ref}	kN/m^2	13320	21653	30977	37371
Tangent stiffness	E_{ode}^{ref}	kN/m^2	13320	21653	30977	37371
Unloading / reloading stiffness	E_{ur}^{ref}	kN/m^2	39960	64960	92932	112113
Power for stress-level dependency of stiffness	m	-	0.5	0.5	0.5	0.5
Effective cohesion	c'_{ref}	kN/m^2	0	0	0	0
Effective angle of internal friction	Φ'	°	35.58	45.3	47.58	48.94
Dilatancy angle	ψ	°	10.3	13.3	15.8	17.3

as in the physical model.

Mesh Generation and Connections: After the model is geometrically modelled, it must be divided into finite elements to make the calculations. A composition of finite elements is called a mesh. Finite elements should be as frequent as possible to ensure accurate results in calculations (Plaxis 3D manual, 2018). However, as the frequency increases, the calculation times of the models are prolonged and the memory they occupy increases. In this study, element distribution is defined as very fine. The relative element sizes were taken as 0.5, and element dimension was taken as 3.466 which are the default value for very fine element distribution. In order for the movable wall to move smoothly, the connections between the movable wall and the other walls are defined as shown in the Figure 4.10. After that, In these connections, rotation 1, translation 1, 2 and 3 are defined as free.

Construction Stages: Staged construction, which is the last part of the modelling stage of the verification model, consists of 4 stages and the first of which is

Table 4.7. Dimensions of Physical Model.

Dimensions of physical model		
Name	Unit	Value
Width	cm	15
Length	cm	30
Height	cm	20

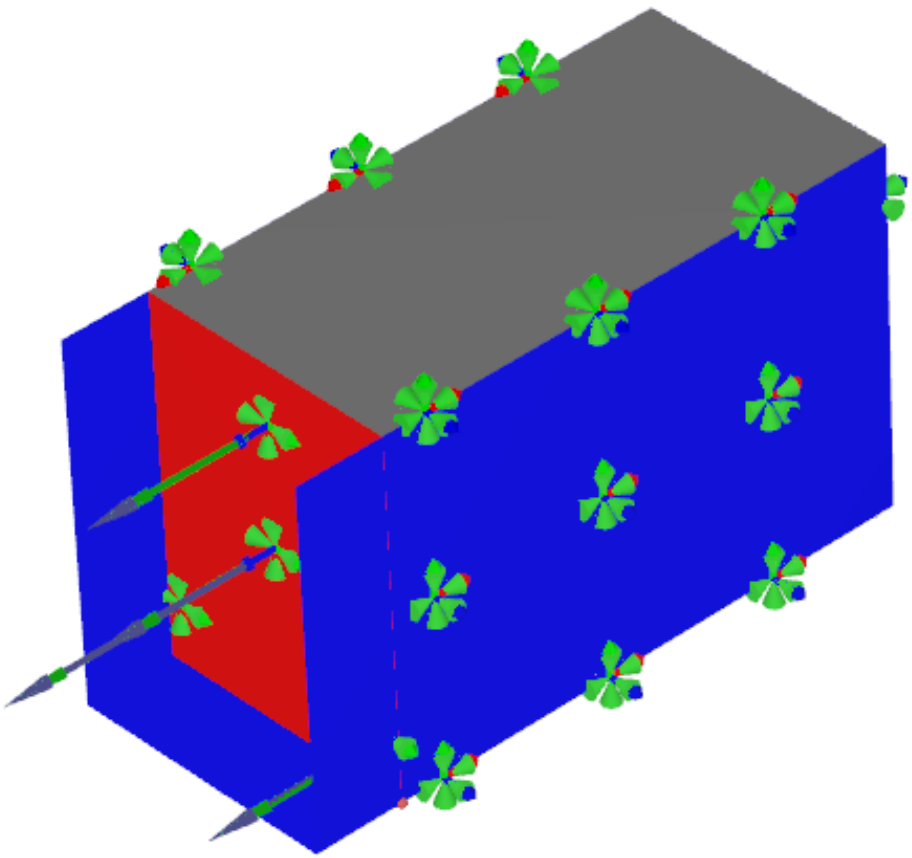

Figure 4.9. The Moving Wall in the Verification Model.

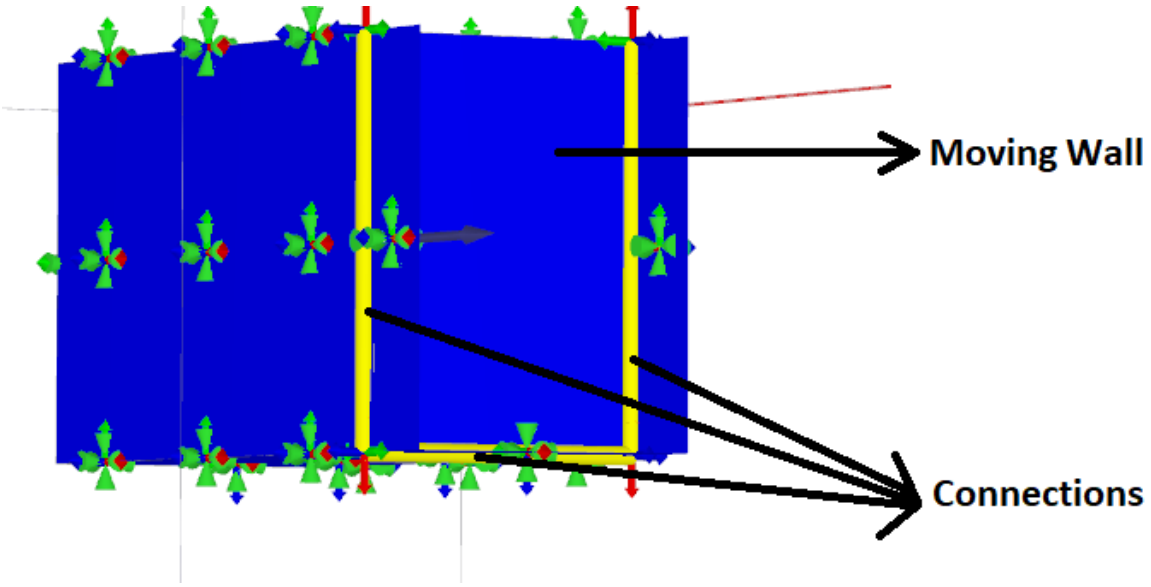

Figure 4.10. Connections of Verification Model.

the initial phase. The initial phase is the default part of stage construction and cannot be removed. In this calculation phase, the initial stress field for initial geometry configuration is calculated by means of gravity loading or K_0 procedure (Plaxis 3D manual, 2018). The next stage, Phase 1, all plate, interfaces, connections and prescribed displacements are activated and all prescribed displacements were fixed in all directions. In Phase 2, the soil around the verification model box is deactivated. In the final phase, Phase 3, 0.10 cm prescribed displacement is applied to the moving wall in negative x-direction and all stage construction stages are completed.

4.3.5. Results Obtained from Verification Model

After the analysis of the verification model, the results of the analysis are taken from Plaxis 3D output. For the determination of the failure surfaces the cross-sectional area is taken from the side walls of the verification model as in the physical model. Total deviatoric strains (γ_s) are examined in the sections taken. The reason for this is that the failure surface occurs where the maximum total deviatoric strain occurs (γ_s). The results are given in the Figure 4.11 to Figure 4.14.

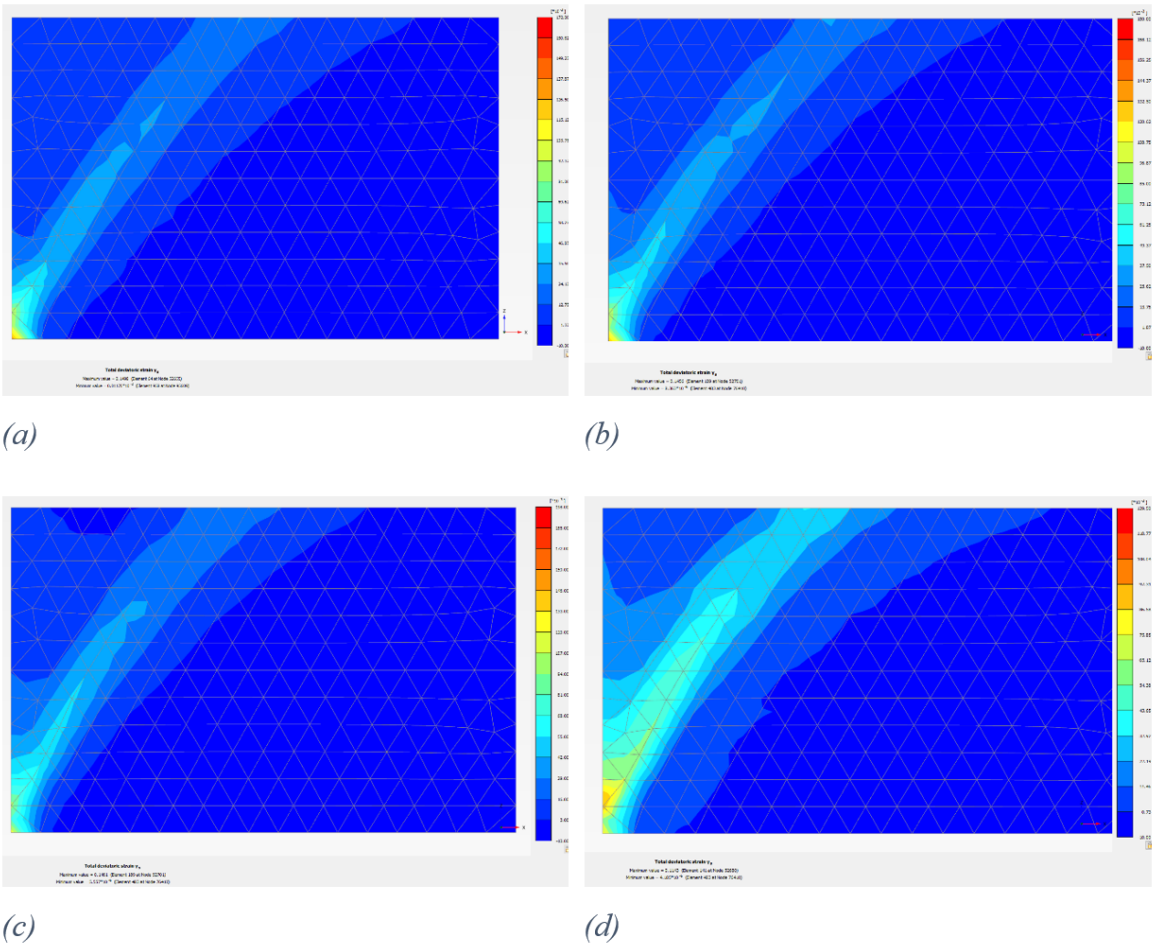

(a) *(b)*

(c) *(d)*

Figure 4.11. Total Deviatoric Strains (γ_s) for Soil 1. Interface Strength Reduction Factor (R_{inter}); (a) 0.5 (b) 0.6 (c) 0.7 (d) 0.8.

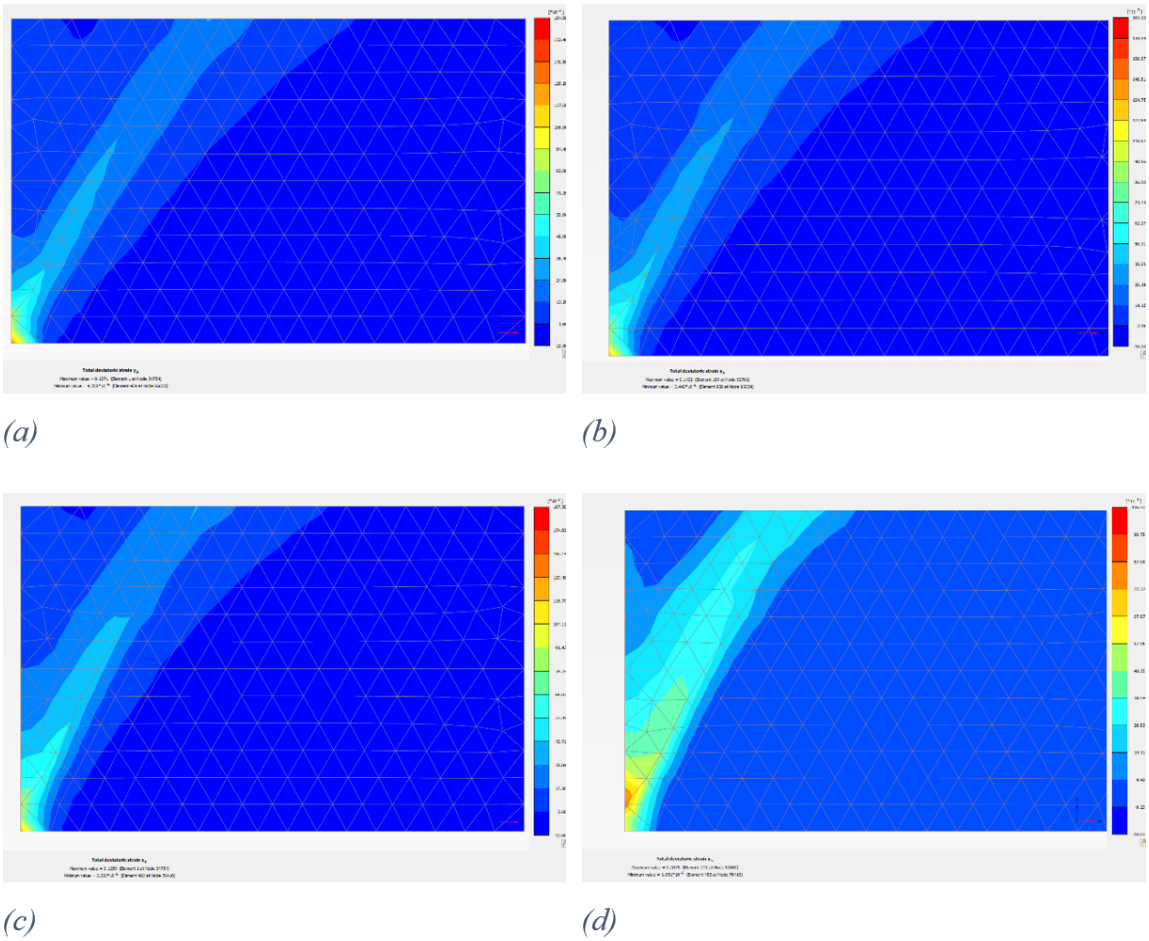

Figure 4.12. Total Deviatoric Strains (γ_s) for Soil 2. Interface Strength Reduction Factor (R_{inter}); (a) 0.5 (b) 0.6 (c) 0.7 (d) 0.8.

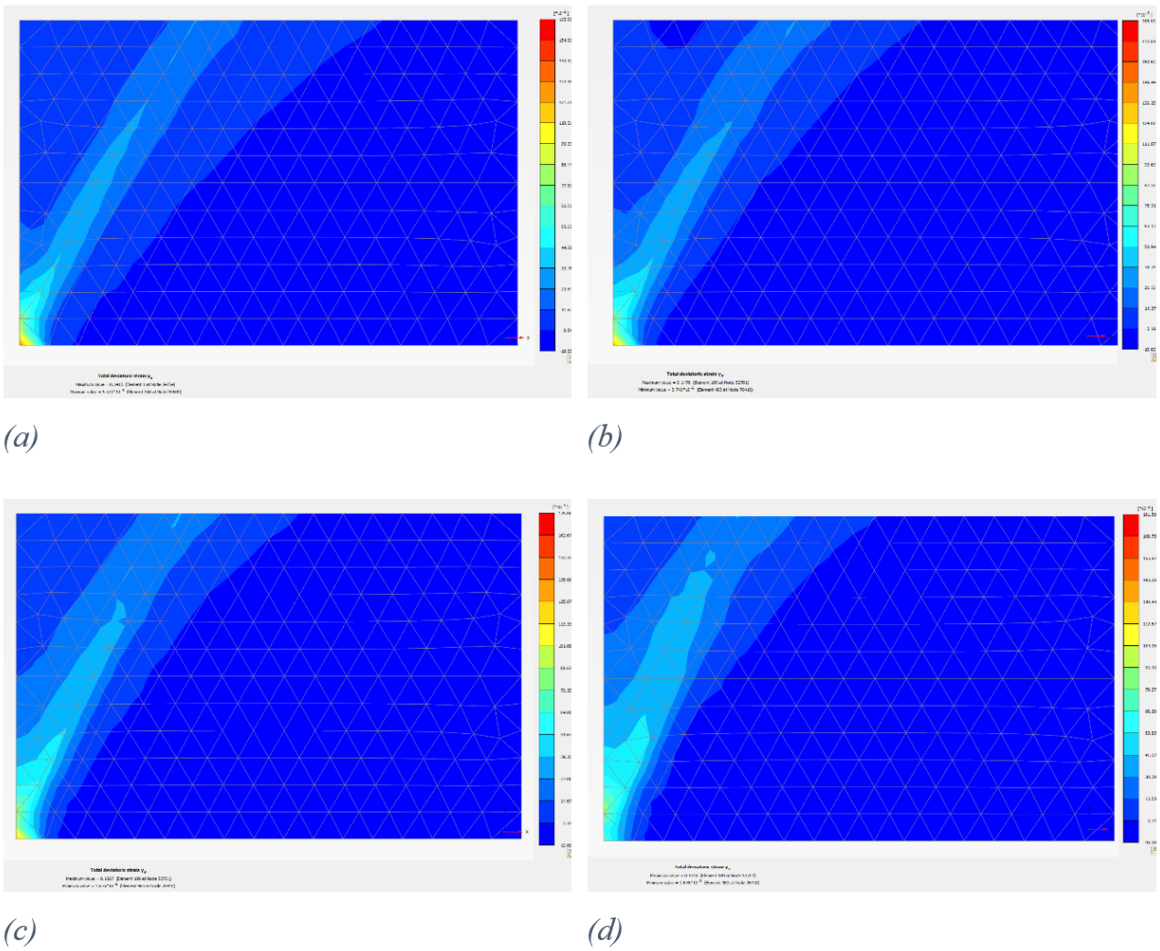

Figure 4.13. Total Deviatoric Strains (γ_s) for Soil 3. Interface Strength Reduction Factor (R_{inter}); (a) 0.5 (b) 0.6 (c) 0.7 (d) 0.8.

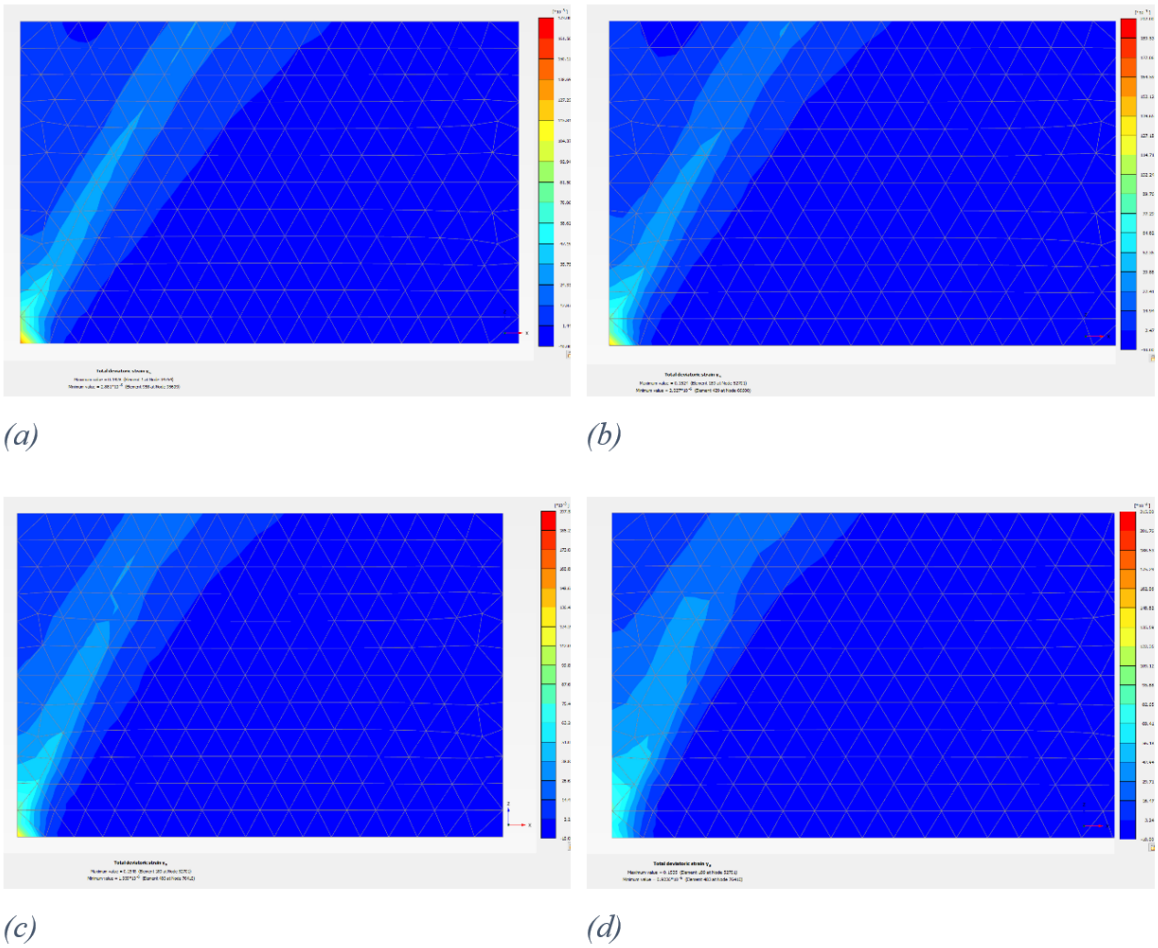

Figure 4.14. Total Deviatoric Strains (γ_s) for Soil 4. Interface Strength Reduction Factor (R_{inter}); (a) 0.5 (b) 0.6 (c) 0.7 (d) 0.8.

4.3.6. Comparisons and Discussions

In this section, the most proper interface strength reduction factor (R_{inter}) between wall and sand is tried to be determined. For this reason, the failure surface obtained from the physical models and the failure surface obtained from verification models by using different interface strength reduction factor (R_{inter}) are compared. After that, interface strength reduction factor (R_{inter}), which gives the closest results, is used as a valid coefficient in the numerical model of the study. Comparison of the results of the physical models with the results of the verification models is shown in the Figure 4.15 to Figure 4.18.

As shown in the Figure 4.15 to Figure 4.18, the comparison between the results of the physical models and the verification models show that the best results are obtained if the interface strength reduction factor (R_{inter}) is 0.7. Therefore, in all numerical model, the interface strength reduction factor (R_{inter}) is used as 0.7. The comparison of the results of the physical models and the verification models for four different sands with 0.7 the interface strength reduction factor (R_{inter}) is shown in Figure 4.19. In the light of these results, it is revealed that the parameters used for the modelling of the physical models were sufficiently accurate.

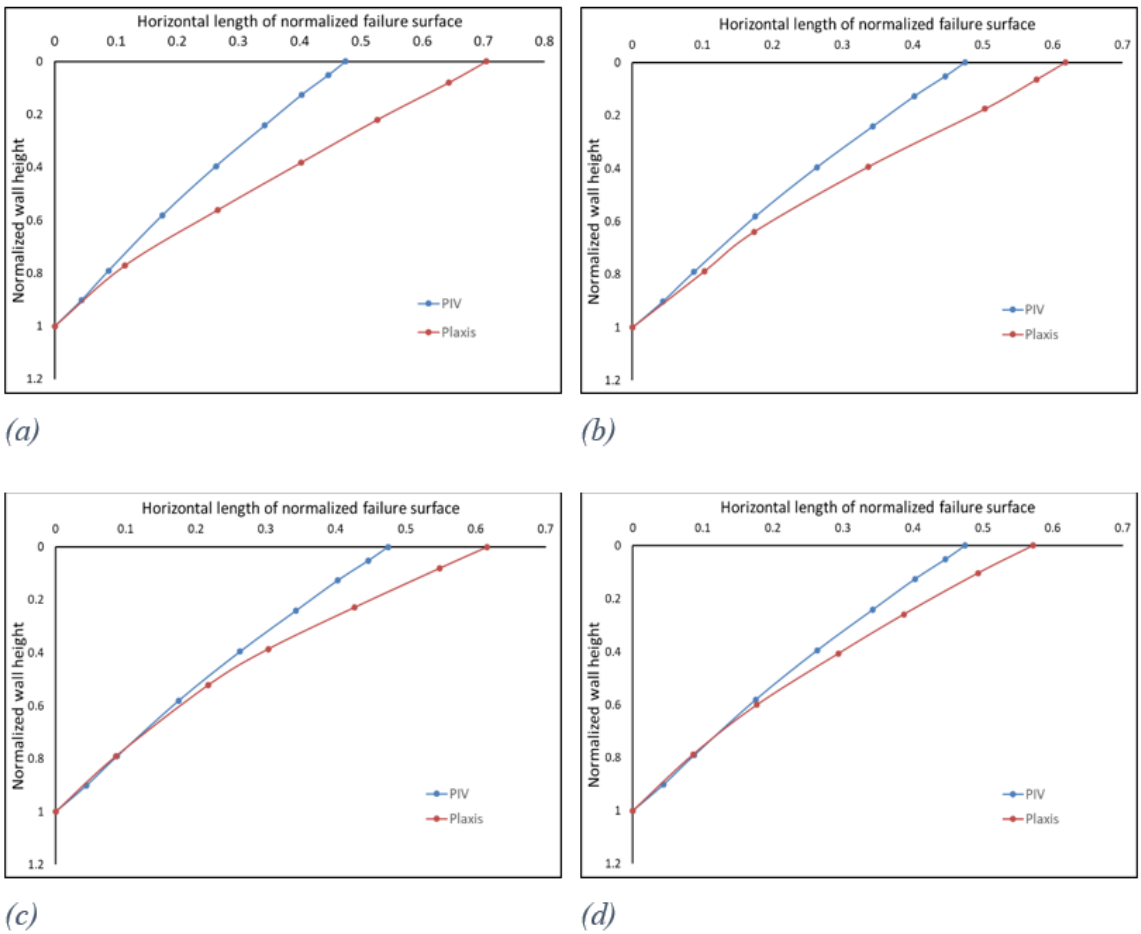

Figure 4.15. Comparison of the Results of Physical models with the Results of the Verification Models for Soil 1. Interface Strength Reduction Factor (R_{inter}); (a) 0.5 (b) 0.6 (c) 0.7 (d) 0.8.

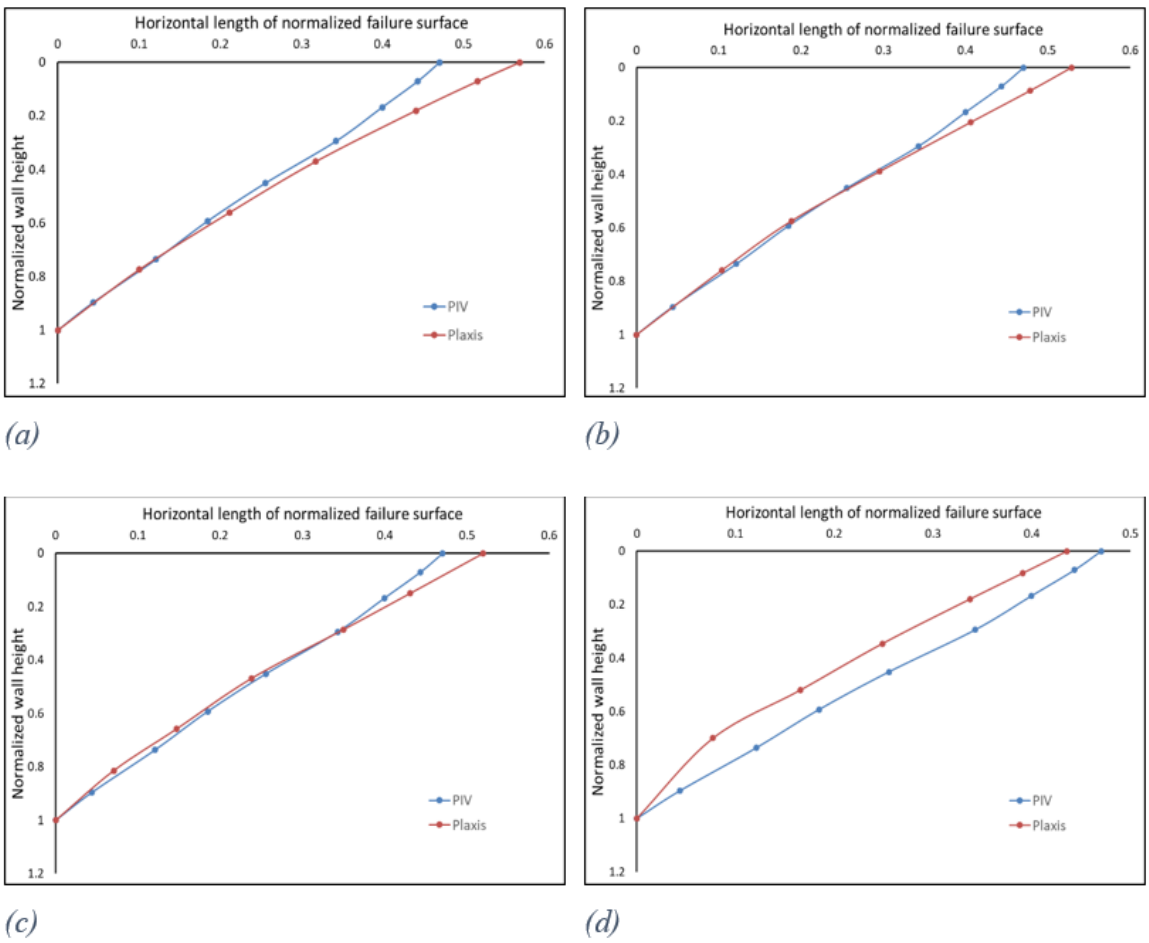

Figure 4.16. Comparison of the Results of Physical models with the Results of the Verification Models for Soil 2. Interface Strength Reduction Factor (R_{inter}); (a) 0.5 (b) 0.6 (c) 0.7 (d) 0.8.

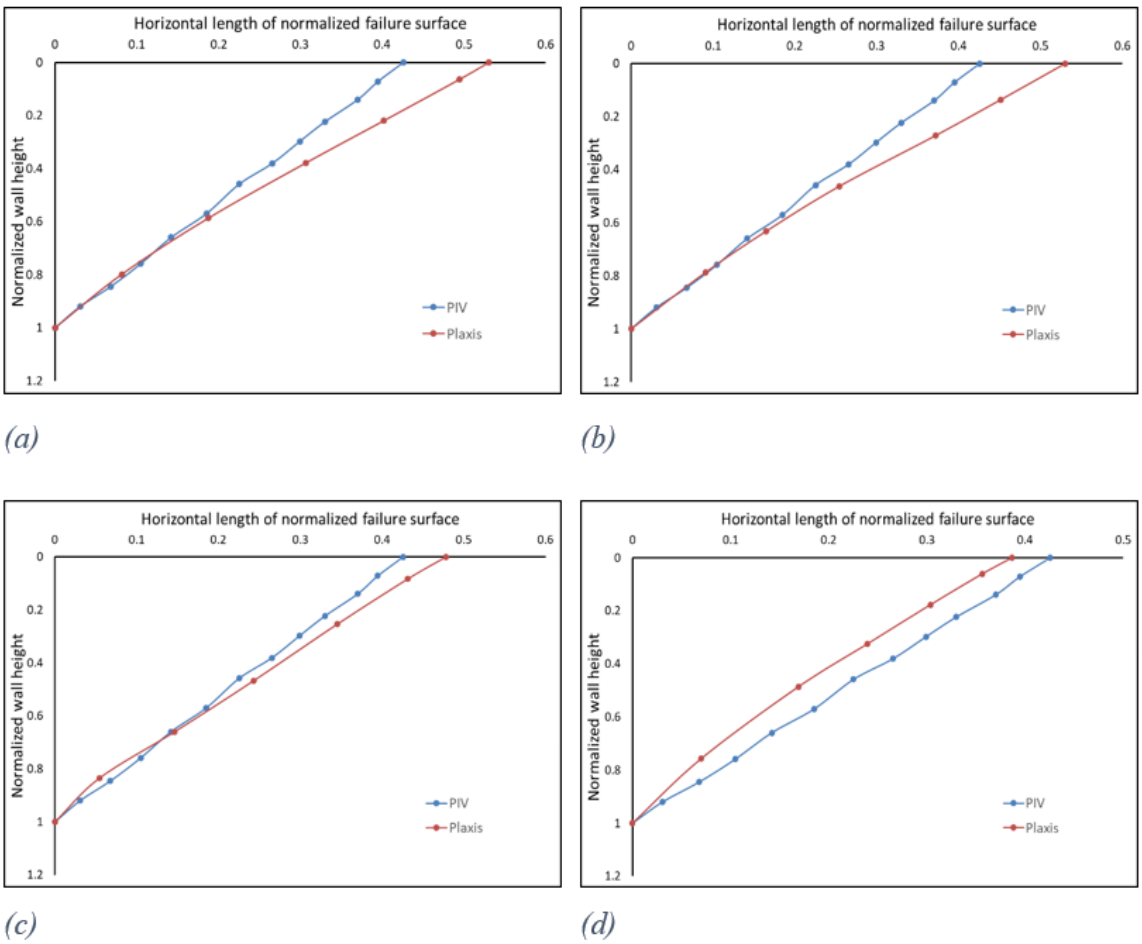

Figure 4.17. Comparison of the Results of Physical models with the Results of the Verification Models for Soil 3. Interface Strength Reduction Factor (R_{inter}); (a) 0.5 (b) 0.6 (c) 0.7 (d) 0.8.

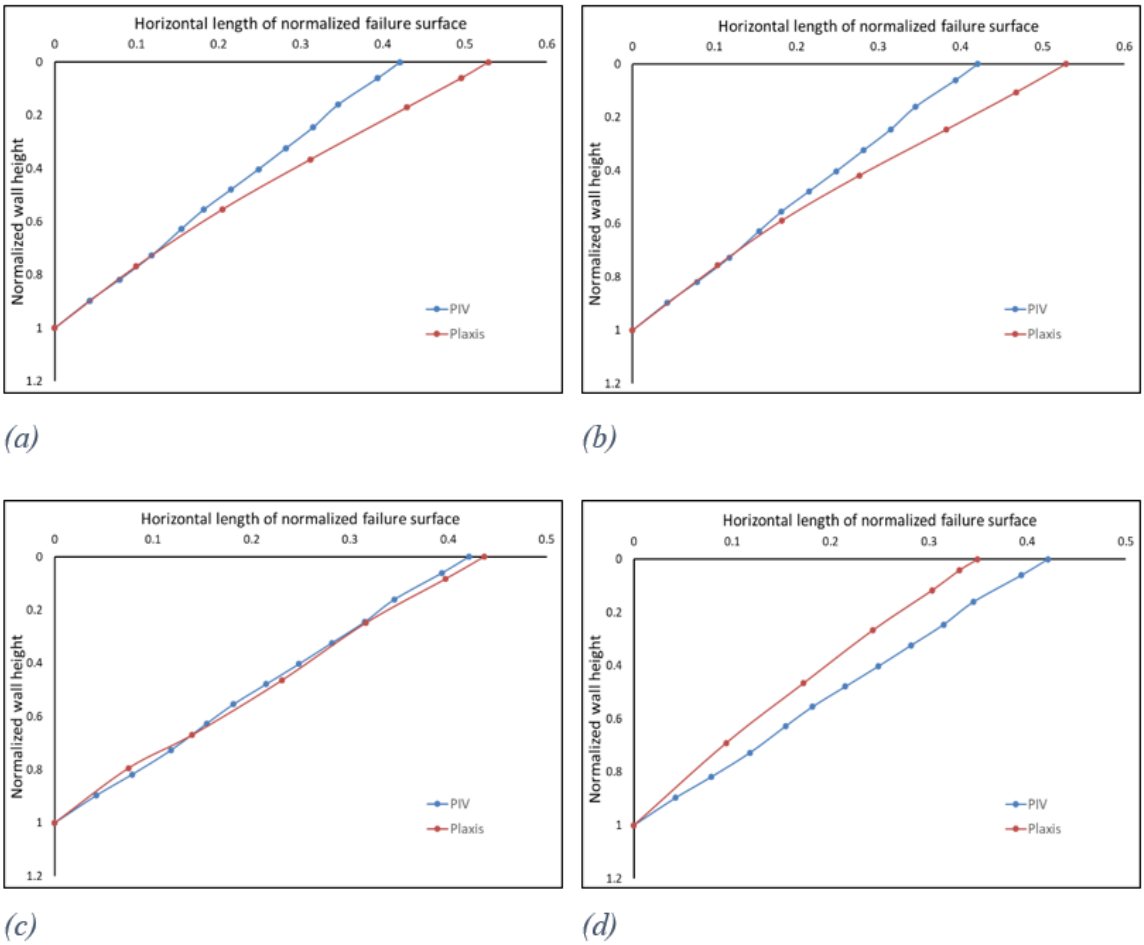

Figure 4.18. Comparison of the Results of Physical models with the Results of the Verification Models for Soil 4. Interface Strength Reduction Factor (R_{inter}); (a) 0.5 (b) 0.6 (c) 0.7 (d) 0.8.

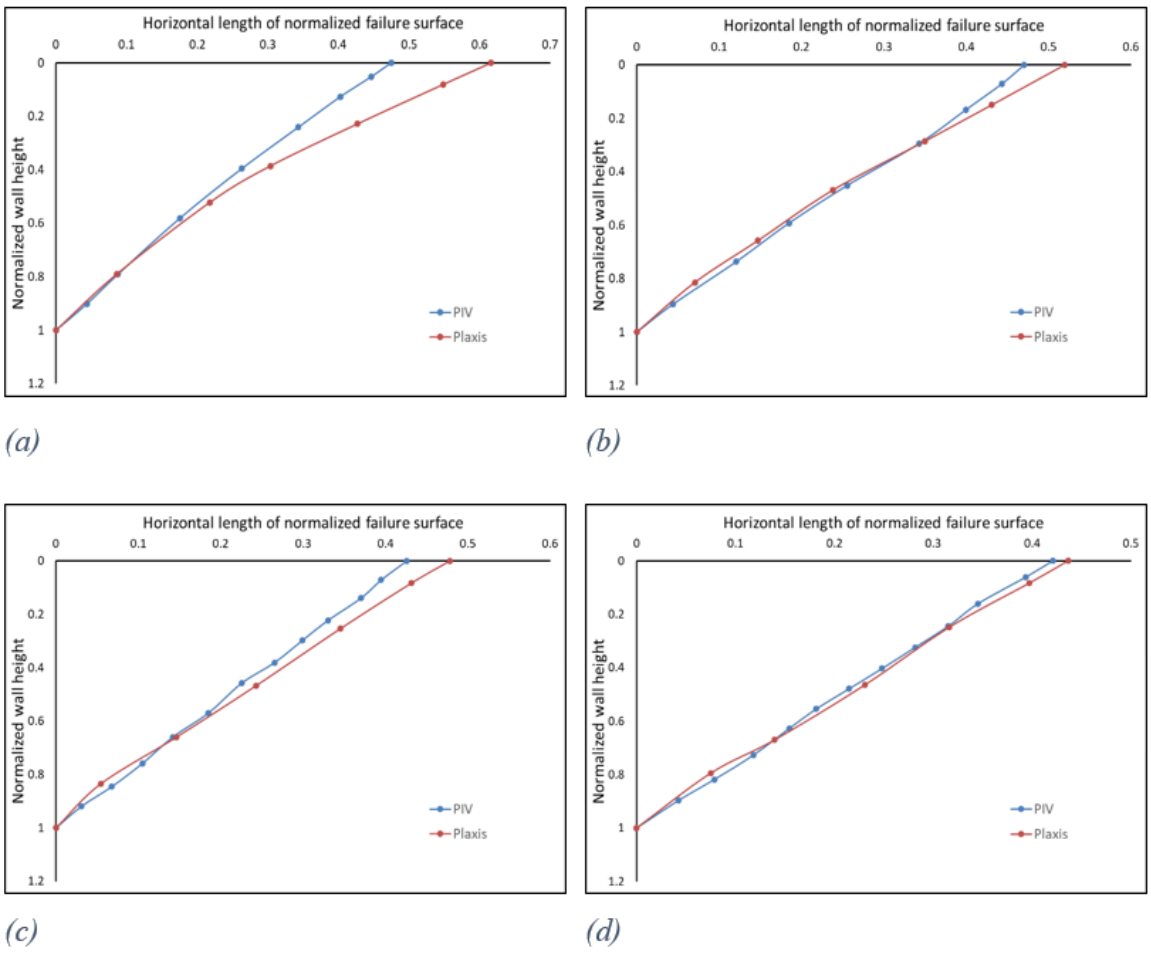

Figure 4.19. Comparison of the Results of Physical models with the Results of the Verification Models for Four Different Sands with 0.7 Interface Strength Reduction Factor (R_{inter}); (a) 0.5 (b) 0.6 (c) 0.7 (d) 0.8.

5. INVESTIGATION OF BACKFILL FAILURE ZONE BASED ON PROBLEM GEOMETRY WITH NUMERICAL MODEL

5.1. Parametric Study

The main purpose of the study is determining the effects of corner angle, the distance from the corner and soil strength parameters on the outer boundary of failure surface at deep excavations. Therefore, these three factors are defined as three different variable groups in the study.

First group is associated with the corner angle between two moving wall at numerical model. Nine different corner angle is selected for the parametric study. Accordingly, these corner angles are chosen as 30, 60, 90, 120, 150, 180, 210, 240 and 270 degrees.

Second group is associated with the distance from the corner. Twelve different distances from the corner are selected for the parametric study. These distances are chosen as 0 m, 0.1 m, 0.3 m, 0.5 m, 0.8 m, 1 m, 3 m, 7 m, 10 m, 15 m, 30 m and 50 m.

Last group is associated with soil strength parameters. In the study, strength parameters of Sile sand are used. Four different relative densities are selected to investigate the effect of relative density on the outer failure surface geometry. These relative densities are chosen as 40%, 51%, 61% and 67%.

5.2. Definition and Assumptions of Numerical Model

Graphical illustration of numerical model is shown in Figure 5.1. The goal of the model is to determine the outer boundary of the slip surface.

Assumptions made for numerical model are summarized below. If required, detailed explanations regarding the assumptions stated below will be given later.

- The height of the walls is 20 m.
- All walls are represented with rigid plate elements. Only two walls can move and their lengths are 100 m for each. Other walls are fixed.
- Hardening Soil is used as a constitutive model to provide precise soil behaviour.
- It is assumed that soil strength parameters do not change with depth.
- 10 cm displacement (0.005H) in x coordinate and 10 cm (0.005H) displacement in y coordinate is defined on the moving walls.
- A fixed connection is defined between 2 moving wall to prevent discontinuity. Free connections are defined between the moving walls and other walls.

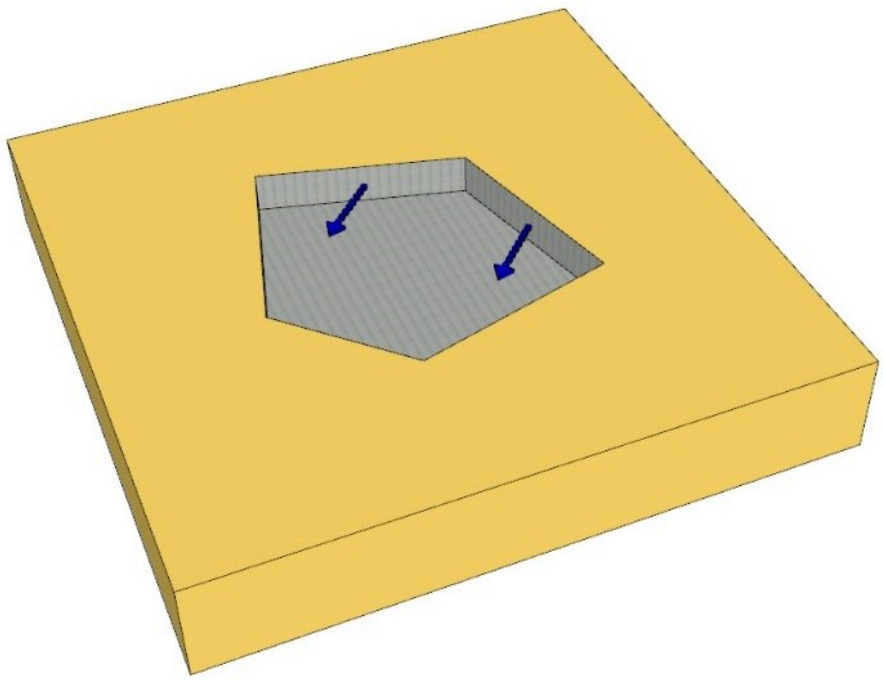

Figure 5.1. Graphical Illustration of Numerical Model.

5.3. Creating Structure of Model

In order to calculate the effect of corner effects on the failure zone geometry, 9 different numerical models are created for 9 different corner angles. As shown in the Figure 5.2, two movable walls of 100 m wide and 20 meters deep are modelled and the effect of the angle between these two moving walls on the failure zone was examined. In all numerical models, stationary walls in contact with moving walls are modelled to be perpendicular to each other. As in the verification model, Plate elements are used to model the base and all the walls of the numerical models. After that, positive and negative interface elements are defined on all plate elements. Then, prescribed displacements are defined for the model base, moving and stationary walls. The model base and the stationary walls are fixed in the x, y, and z directions. As shown Figure 5.2, the moving walls are fixed in z direction and are allowed to move 0.10 m out of the box in the x-direction and y-direction.

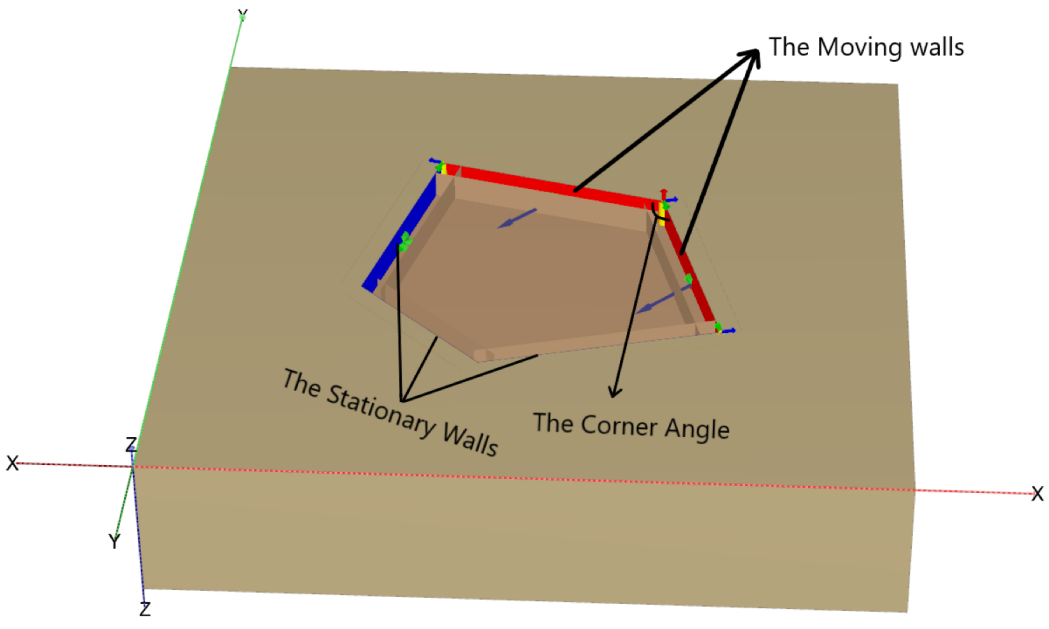

Figure 5.2. Plaxis 3D the Numerical Model Geometry

5.4. Mesh Generation and Connections

After the numerical model is geometrically modelled, it must be divided into finite elements to make the calculations. In this study, element distribution is defined as very fine as same as the verification models.

In order for the movable walls to move smoothly, the connections between the movable wall and the other walls are defined as shown in the Figure 5.3. After that, rotation 1, translation 1, 2 and 3 are defined as free in these connections except for the connection between two moving wall. The connection between walls is defined as fixed because it is not desirable to separate the moving walls when they are moving.

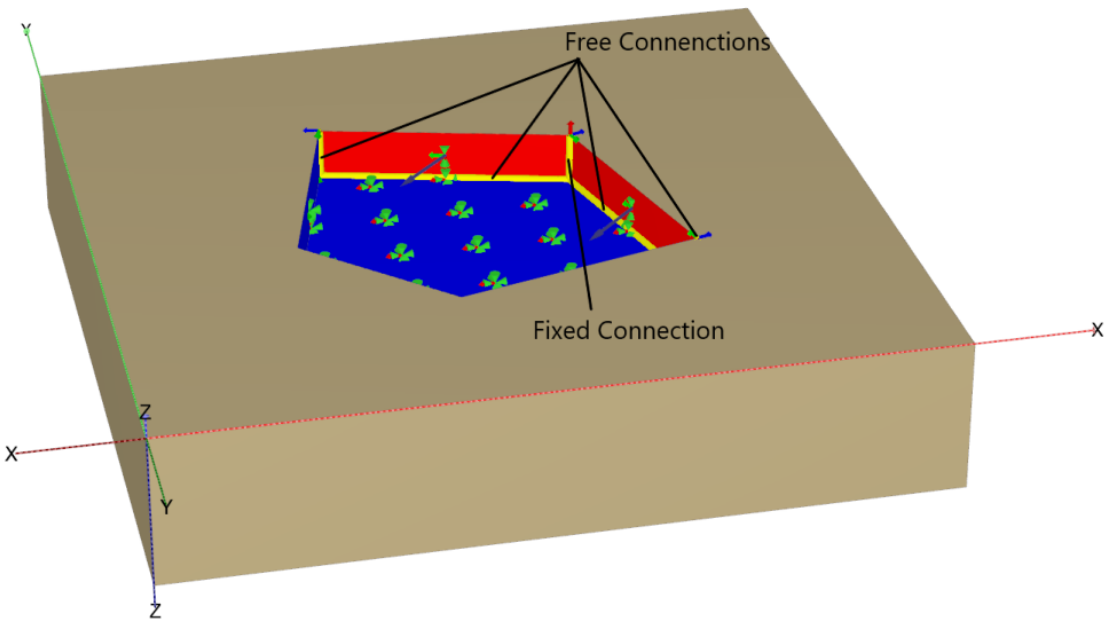

Figure 5.3. The Connections of the Numerical Models

5.5. Construction Stages

Staged construction, which is the last part of the modelling stage of the numerical model, consists of 4 stages and the first of which is the initial phase as the same as verification models. In the next phase, Phase 1, all plates, interfaces, connections and

prescribed displacements are activated, but prescribed displacements were fixed in all directions. In Phase 2, the soil inside the numerical model is deactivated. In the final phase, Phase 3, 0.10 m prescribed displacements are applied to the moving walls in negative x-direction and negative y-direction. After that, all stage construction stages are completed.

6. DISCUSSION OF THE RESULTS

In this part of the study, outer boundaries of the slip surfaces are investigated, according to the results of the numerical model analysis. These results are obtained through the "Output" part of Plaxis 3D program. Same as with the verification models, to determine the slip surfaces and the outer boundary of these slip surfaces, total deviatoric strains, γ_s, of the taken cross-sections are investigated. To determine the outer boundary of the slip surface, the line corresponding to 10^{-3} the total deviatoric strain is considered to be the outer boundary of the slip surface. In this work, only the horizontal distances on the surface of the slip planes are investigated and therefore these distances are assumed as linear lines, according to Rankine (1857). In the cross section shown Figure 6.1, the position of the slip surface (locations of maximum total deviatoric strains) and the outer boundary of the slip surface are highlighted.

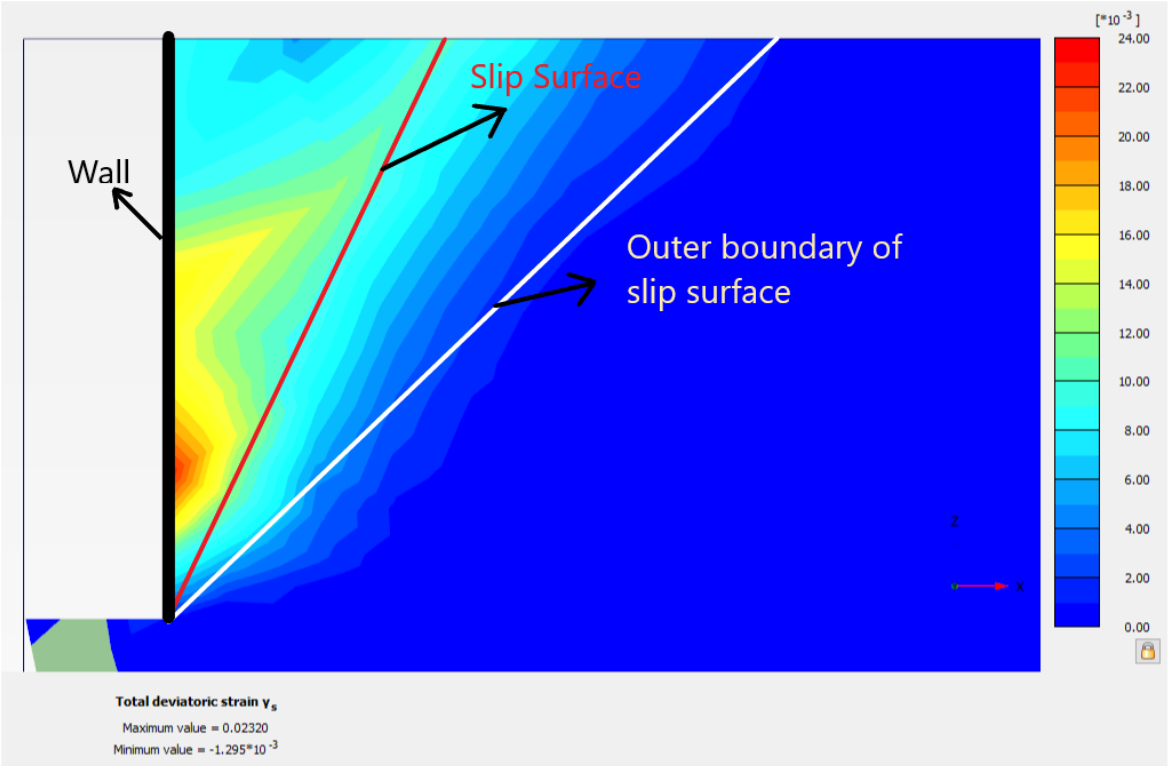

Figure 6.1. Slip Surface and Outer Boundary of Slip Surface for Soil 4, at 90 Degree Angle, with a Distance of 3 Meters from the Wall.

In this research, all lengths are normalized according to the height of the wall. Therefore, the effect of the height of the wall does not influence the nature of the results.

6.1. Distance from the Corner

In this research, the changes in the outer boundary of the slip surfaces are also investigated, in relation with the increasing distance from the corner. 12 cross sections are taken per model, starting from the corner of the model. As in the Figure 6.2 shown below, the corner cross section is located at the intersection of two movable walls and the other 11 cross sections are located at different distances from the corner, all perpendicular to their respective wall. All investigations are made according to this assumption.

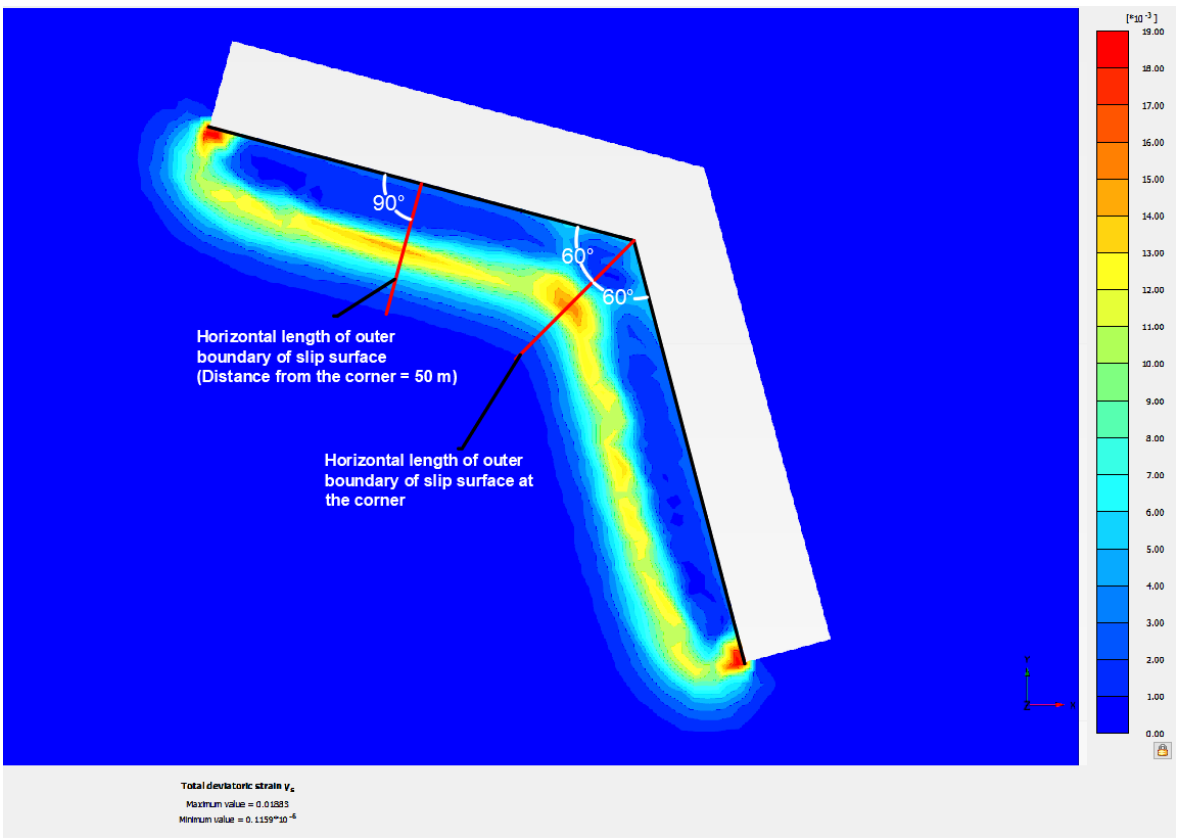

Figure 6.2. The Locations of Two Cross Sections in Soil 1, One at the Corner with 240 Degrees and the Other 50 m Away from the Corner.

These cross sections are taken without a problem at corners with 30°, 60°, 90°, 120°, 150° and 180°. For models with corner angles greater than 180°, like 210°, 240° and 270°, only two cross sections could be taken at the corner and at a distance of 50 m (2.5H) from the corner. The reason for that is shown in Figure 6.3. As the cross sections get closer to the corner, slip surfaces of the adjacent walls tend to mix with each other. In light of this information, in cases where the corner angle is greater than 180°, the locations of the anchorages must be carefully chosen. While installing anchorages, they should be placed at the outer part of the outer boundary of the slip surface of the adjacent wall. One way to counter this problem is to install anchorages longer than normal, if they were being installed perpendicular to the wall. Another way to counter this problem is to install the anchorages at an angle, but this may cause the end of the anchorages to intersect and affect the integrity of the retaining wall seriously. Implementation of this method is usually very difficult, therefore the adjacent walls are bonded to each other to increase stability.

For each cross section, the horizontal distance of the outer boundary of the slip surfaces are plotted for different corner angles in the Figure 6.4 to Figure 6.12. In the case of the corner angle being 180°, the distance of the outer boundary of the slip surface is the same along the entire length of the wall. Apart from that, the distance of the outer boundary of the slip surface at the corner slowly increases, passing the distance of the outer boundary of the slip surface at a distance of 50 m (2.5H) from the corner after 270° corner angle.

In the case where there are enough cross sections, like the models with a corner angle of 30°, 60°, 90°, 120°, the distance of the outer boundary of the slip surface increases as shown in Figure 6.13 to Figure 6.16. It can be seen that increasing slows down and stops after a distance of 0.5-0.6 of the wall height. There are little to no increase in the distance of the outer boundary of the slip surface in the model with a corner angle of 150°. Plane-strain conditions are valid in the case of the model with 180° corner angle, therefore there are no changes in the distance of the outer boundary of the slip surface. A useful way to implement these results in the practice is to shorten the free length of the anchorages 0.5-0.6 wall height away from the corner to decrease

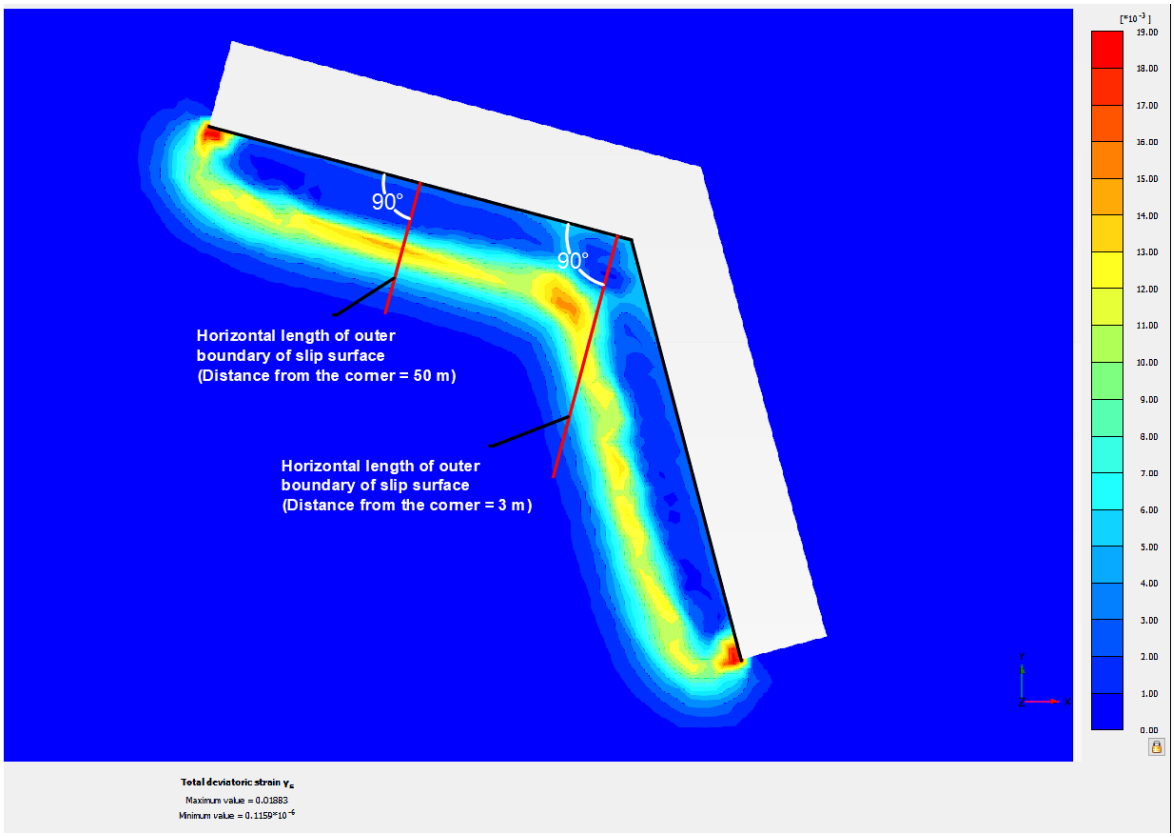

Figure 6.3. The Locations of Two Cross Sections in Soil 1, Taken at Different Distances from the 240 Degree Corner.

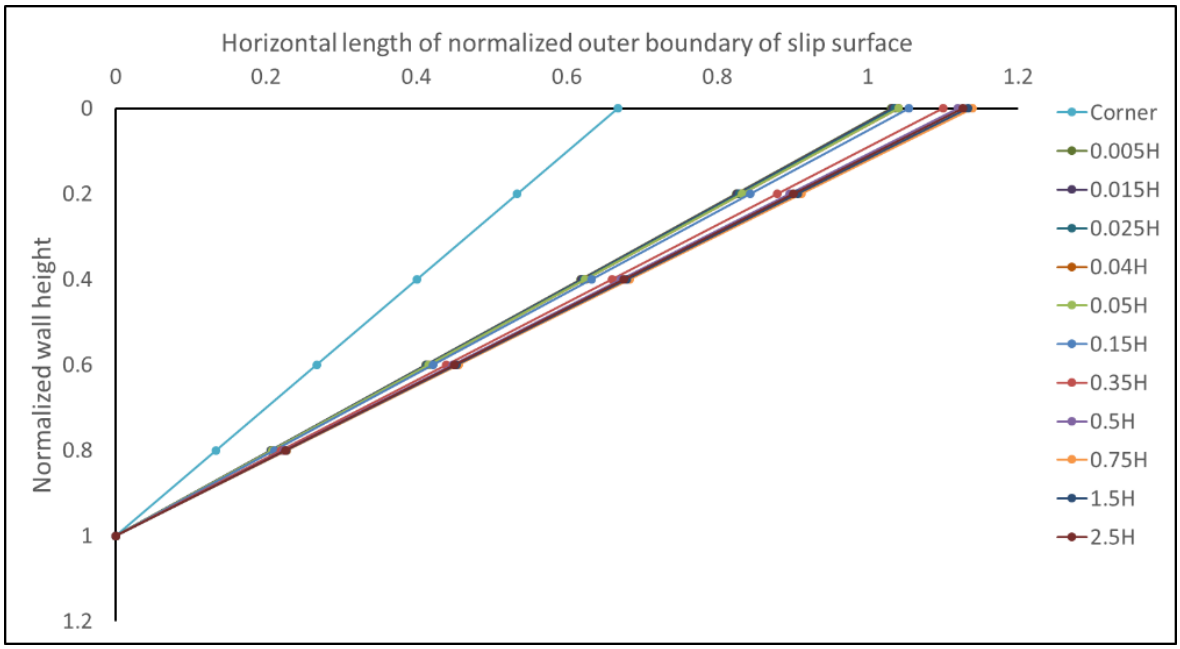

Figure 6.4. Horizontal Length of Normalized Outer Boundary of Slip Surfaces in Soil 1, at Corner with 30 Degree.

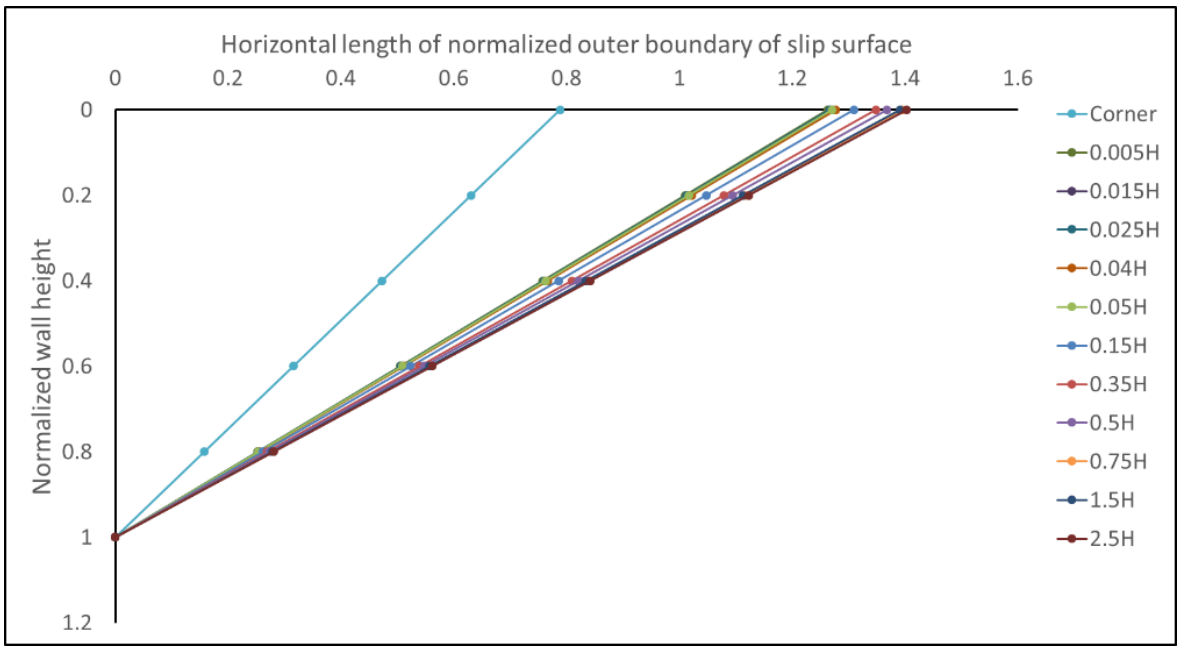

Figure 6.5. Horizontal Length of Normalized Outer Boundary of Slip Surfaces in Soil 1, at Corner with 60 Degree.

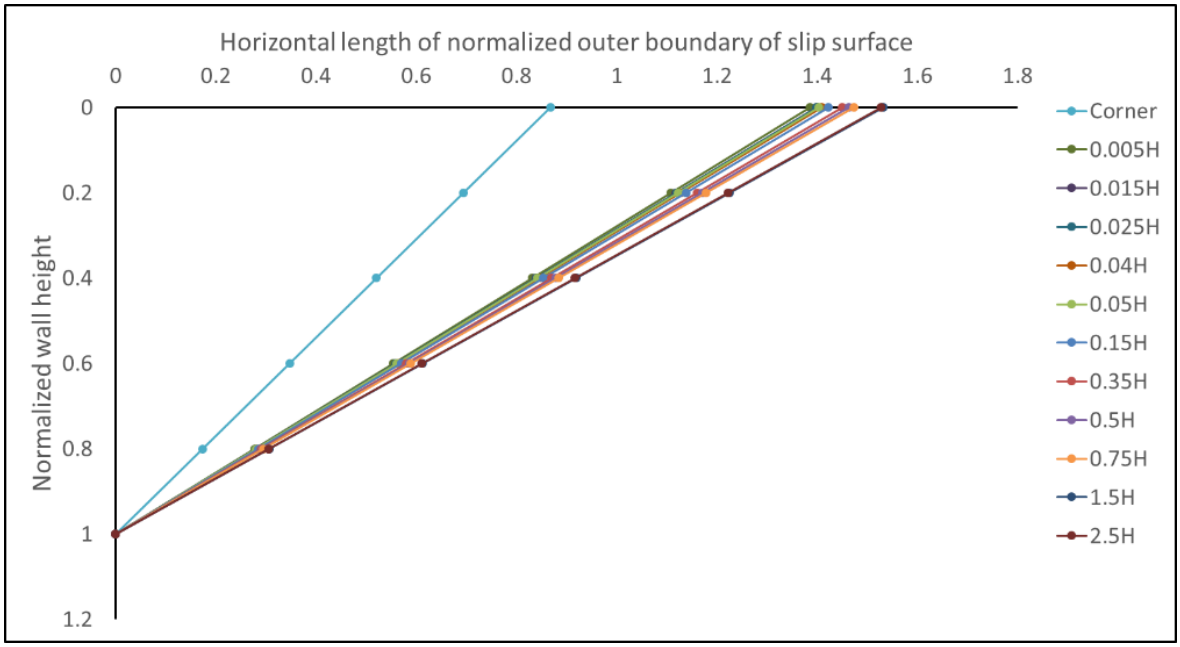

Figure 6.6. Horizontal Length of Normalized Outer Boundary of Slip Surfaces in Soil 1, at Corner with 90 Degree.

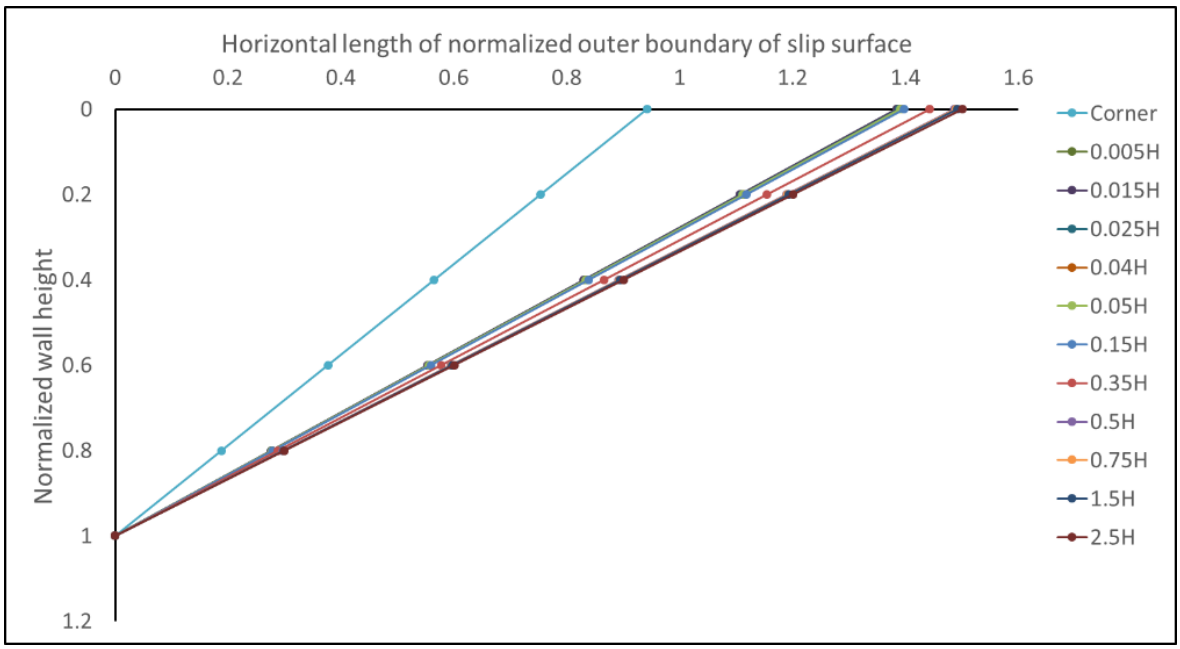

Figure 6.7. Horizontal Length of Normalized Outer Boundary of Slip Surfaces in Soil 1, at Corner with 120 Degree.

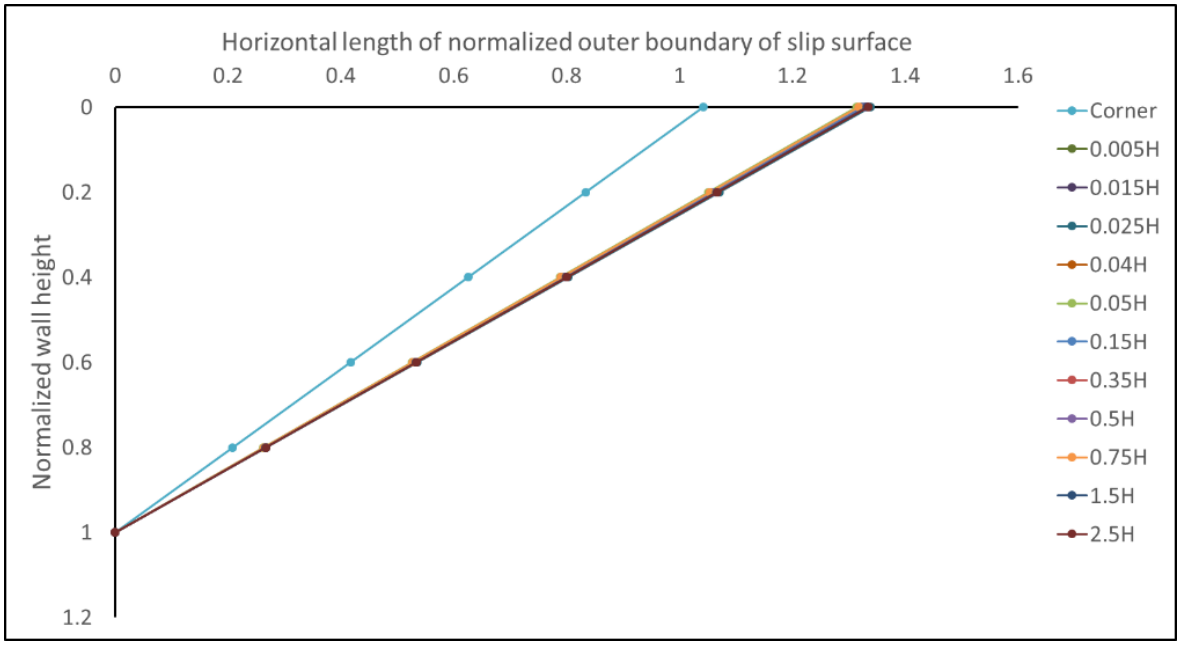

Figure 6.8. Horizontal Length of Normalized Outer Boundary of Slip Surfaces in Soil 1, at Corner with 150 Degree.

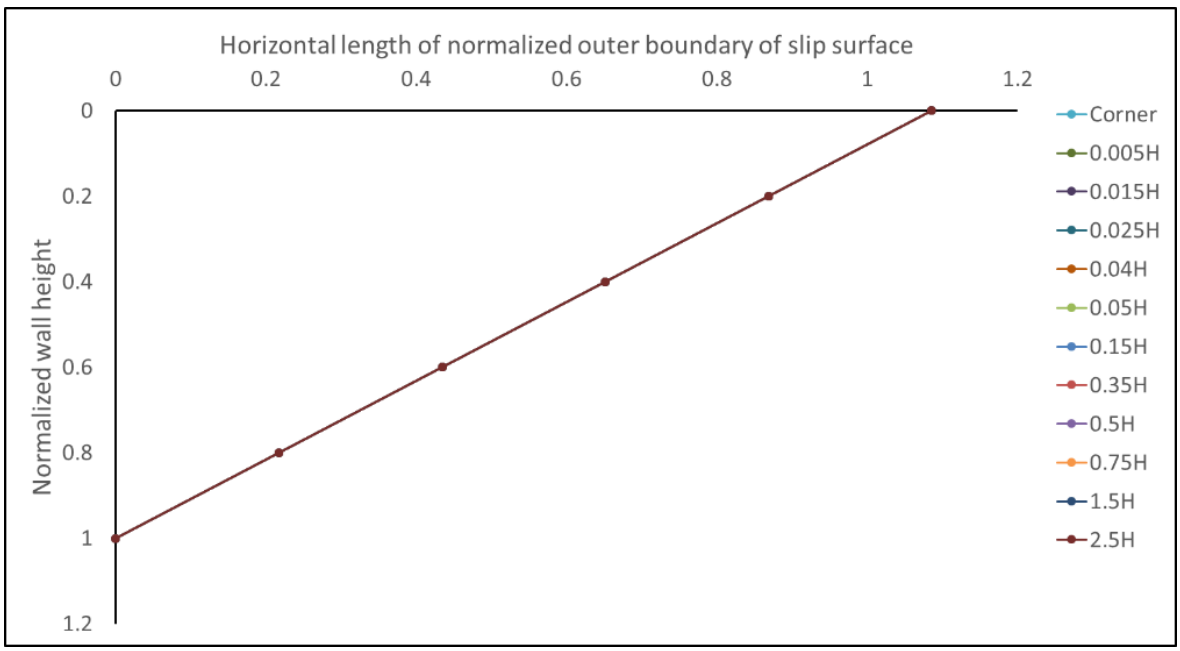

Figure 6.9. Horizontal Length of Normalized Outer Boundary of Slip Surfaces in Soil 1, at Corner with 180 Degree.

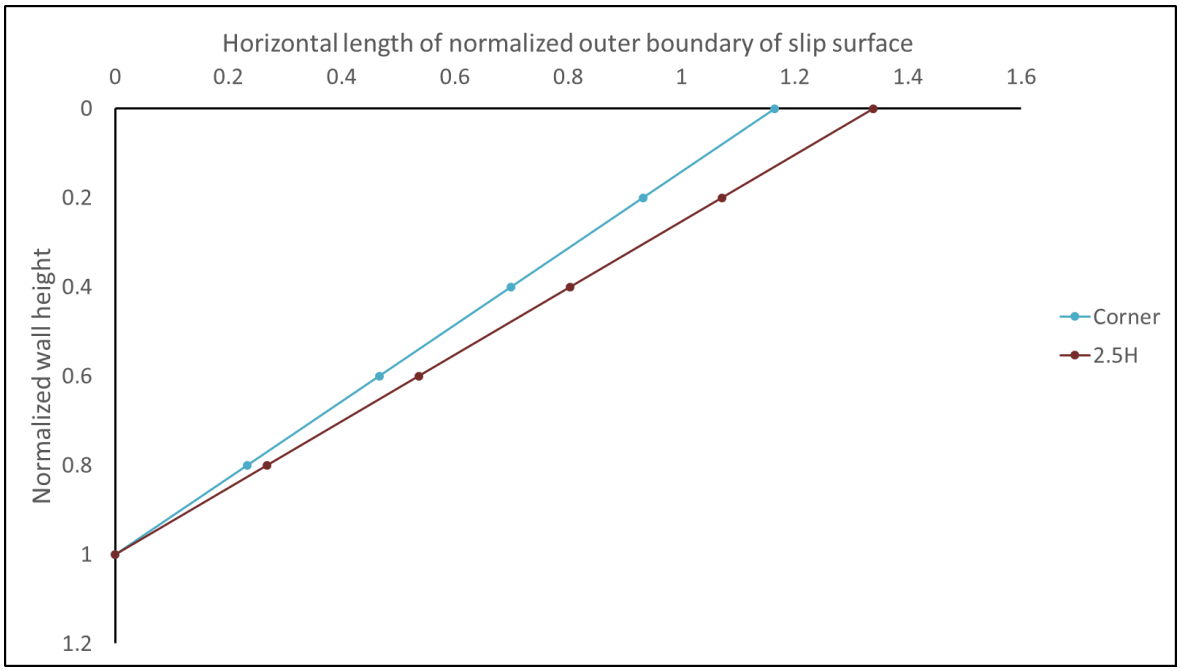

Figure 6.10. Horizontal Length of Normalized Outer Boundary of Slip Surfaces in Soil 1, at Corner with 210 Degree.

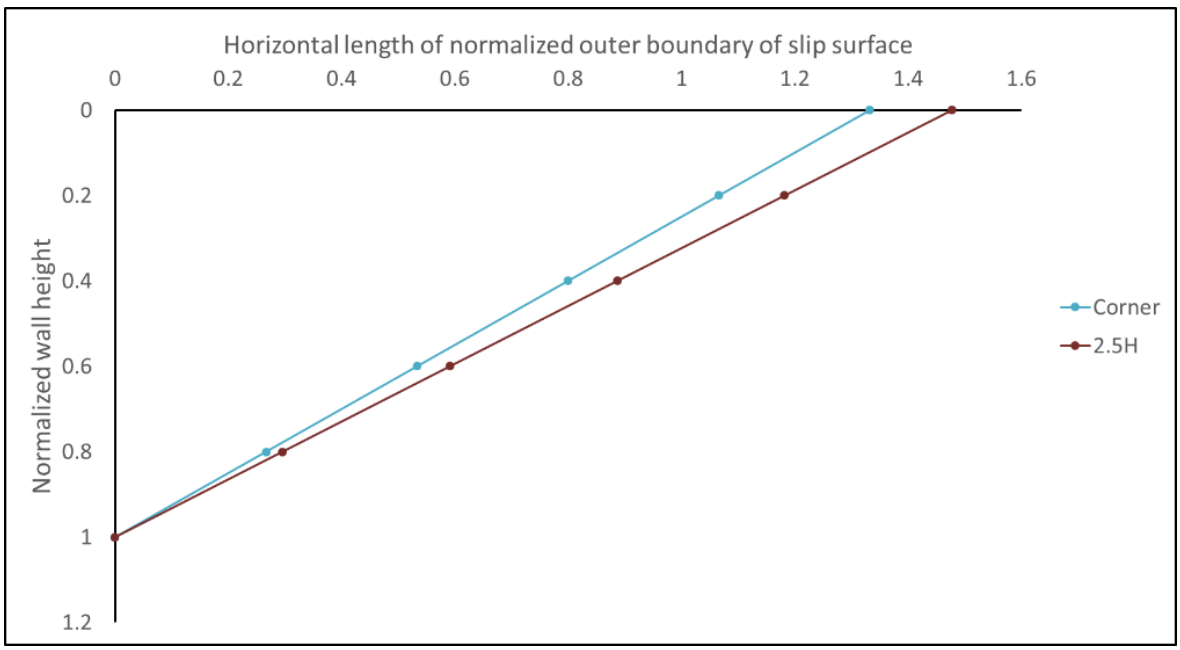

Figure 6.11. Horizontal Length of Normalized Outer Boundary of Slip Surfaces in Soil 1, at Corner with 240 Degree.

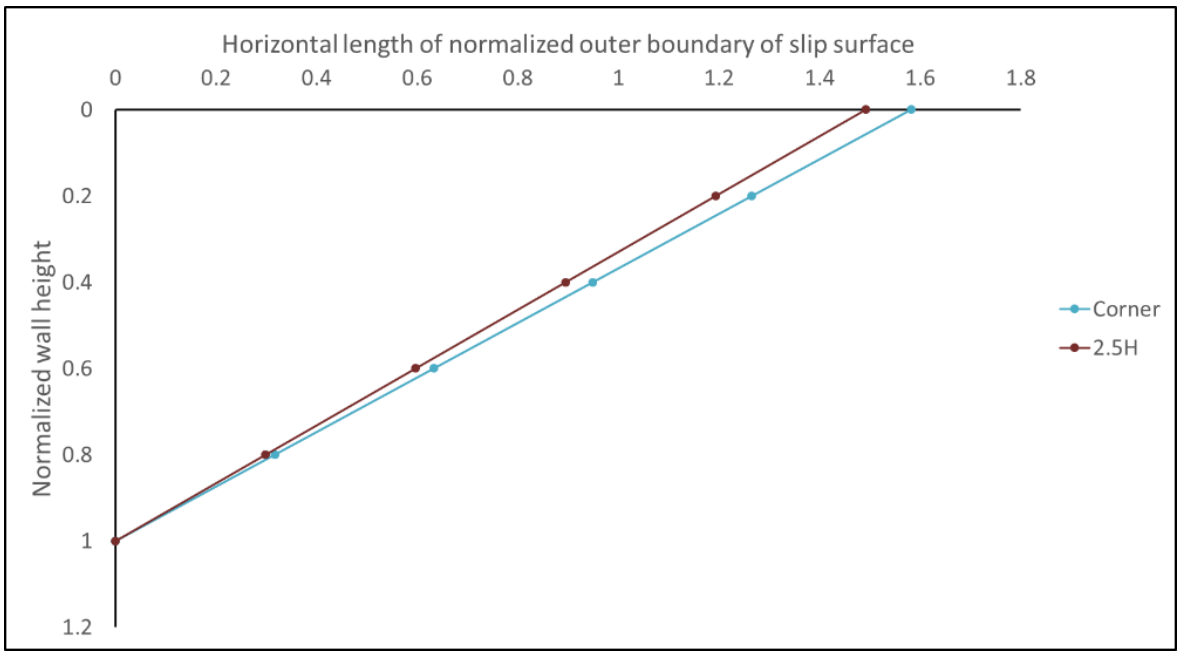

Figure 6.12. Horizontal Length of Normalized Outer Boundary of Slip Surfaces in Soil 1, at Corner with 270 Degree.

the cost of anchorages, in the case the corner angle is either 30°, 60°, 90°, 120°.

6.2. Corner Angle Effect

The models are made for 9 different corner angles, as stated in the researches stated before. These corner angles are 30°, 60°, 90°, 120°, 150°, 180°, 210°, 240° and 270°. Keeping distance from the corner constant for 4 different types of soil, horizontal length of the normalized outer boundary of the slip surfaces created by different corner angles are plotted. The results for Soil 1 are given in Figure 6.17 to Figure 6.28.

As shown in Figure 6.17, it is observed that the outer boundary of the slip surface at the corner cross section gets longer as the corner angle increases. This trend does not occur at other cross sections. The change in length of the distance of the outer boundary of the slip surface for different cross sections according to the corner angle is given in Figure 6.29. To observe this change more accurately, the results of the cross section at 2.5 wall height (2.5H) from the corner and the cross section at the

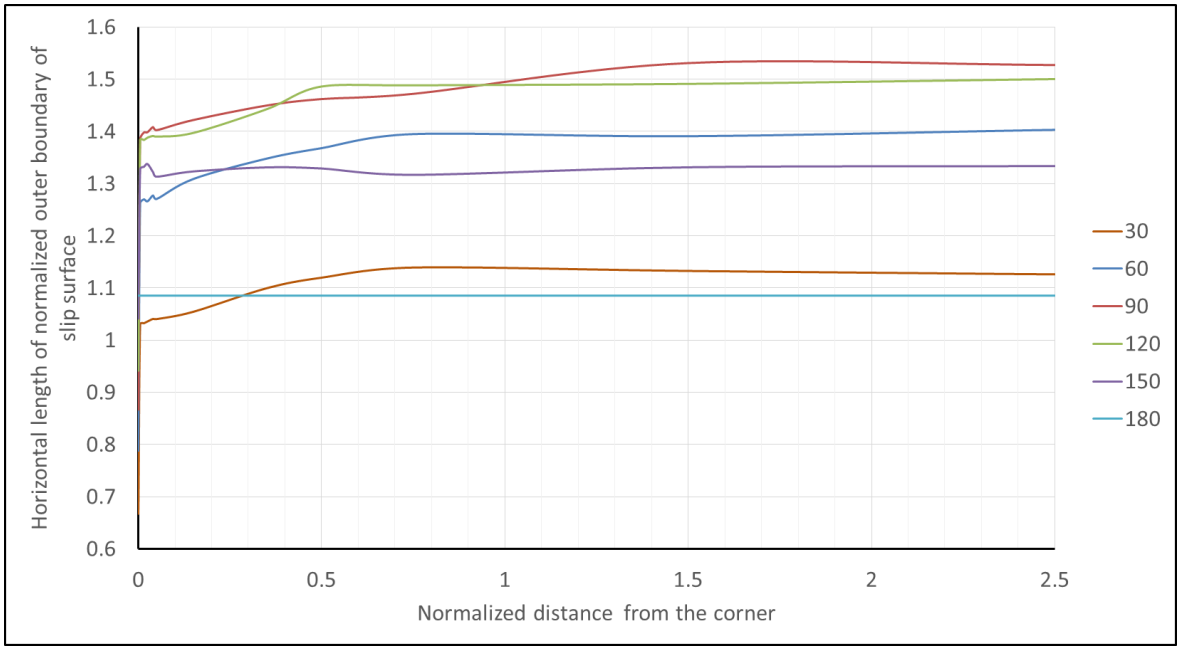

Figure 6.13. The Change of Outer Boundary of Slip Surface with Increasing Distance from the Corner in Soil 1, with Different Corner Angles.

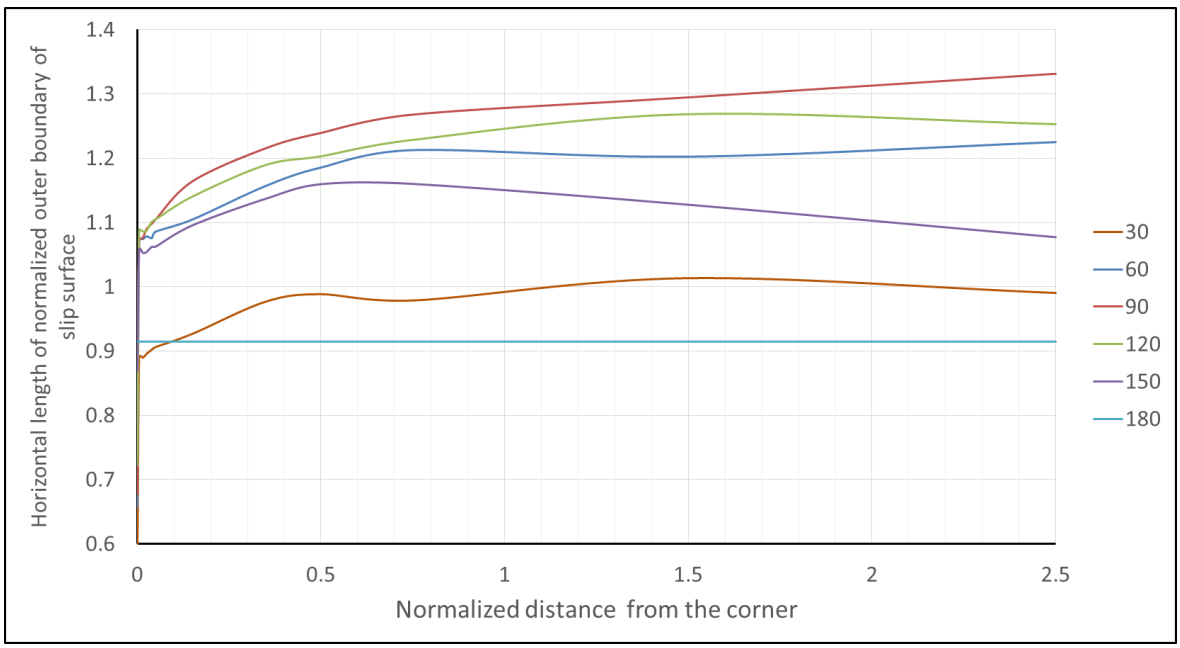

Figure 6.14. The Change of Outer Boundary of Slip Surface with Increasing Distance from the Corner in Soil 2, with Different Corner Angles.

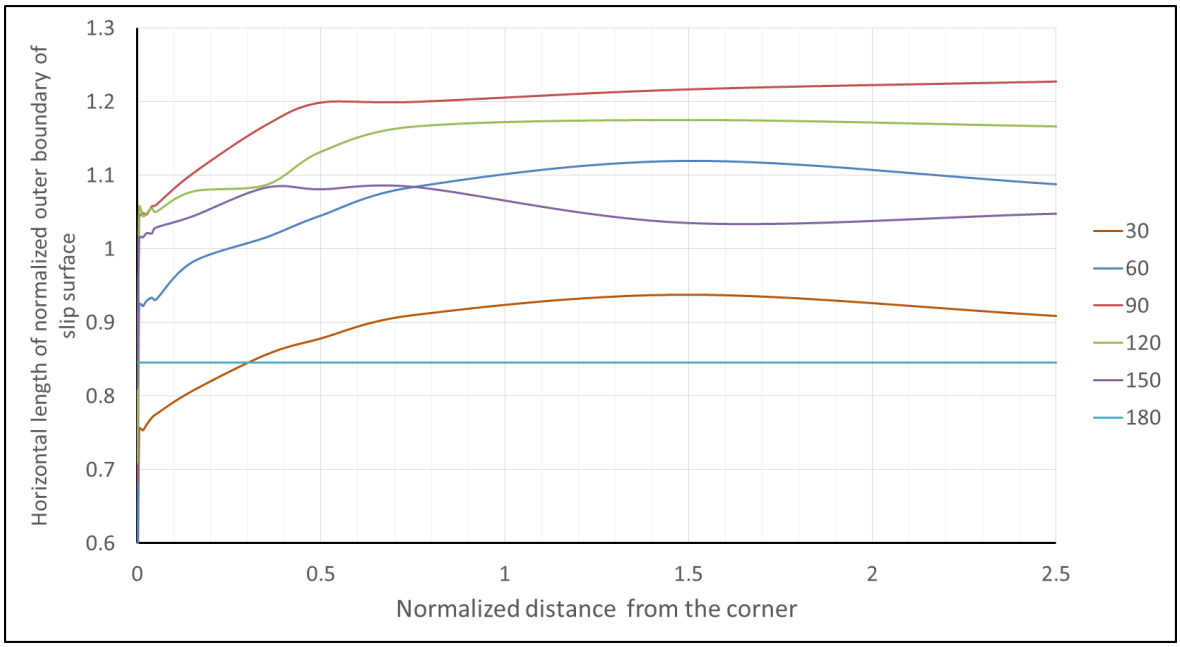

Figure 6.15. The Change of Outer Boundary of Slip Surface with Increasing Distance from the Corner in Soil 3, with Different Corner Angles.

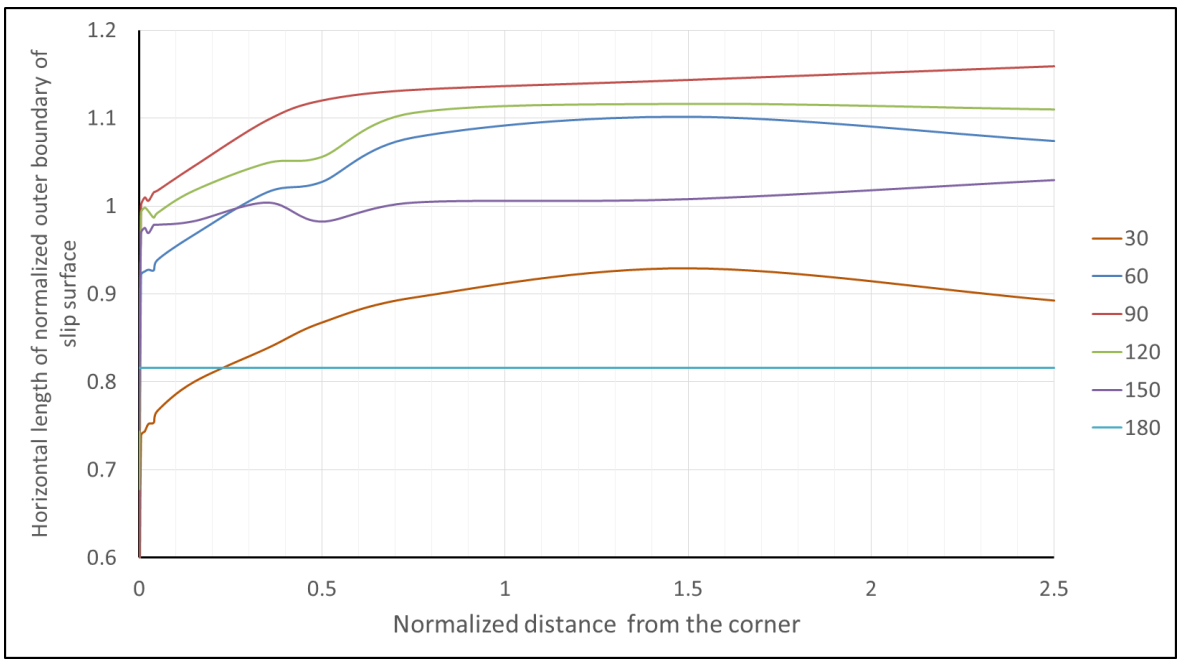

Figure 6.16. The Change of Outer Boundary of Slip Surface with Increasing Distance from the Corner in Soil 4, with Different Corner Angles.

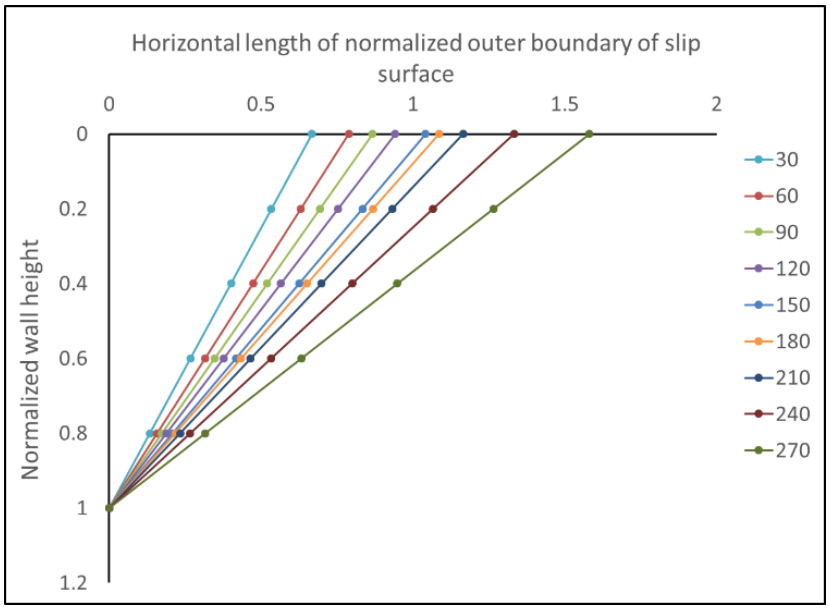

Figure 6.17. Horizontal Length of Normalized Outer Boundary of Slip Surface with Changing Corner Angles at the Corner in Soil 1.

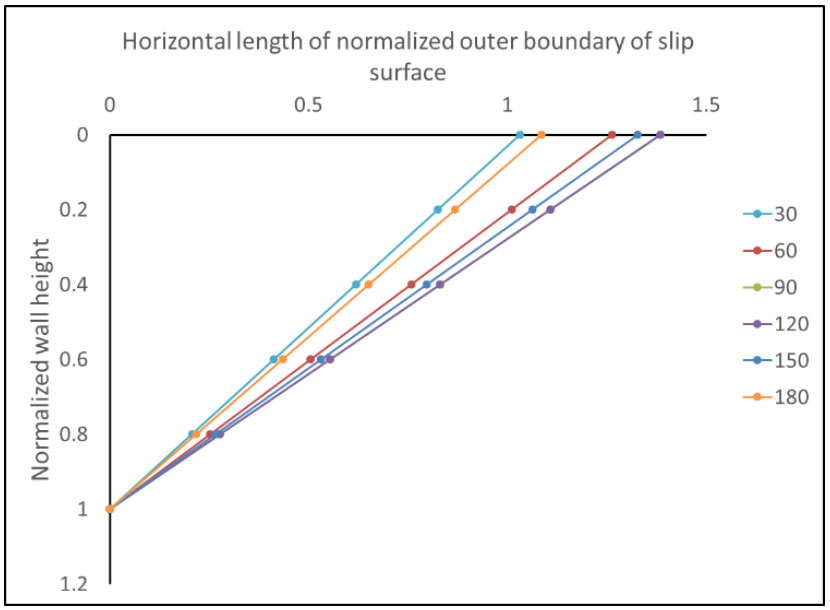

Figure 6.18. Horizontal Length of Normalized Outer Boundary of Slip Surface with Changing Corner Angles at 0.005H in Soil 1.

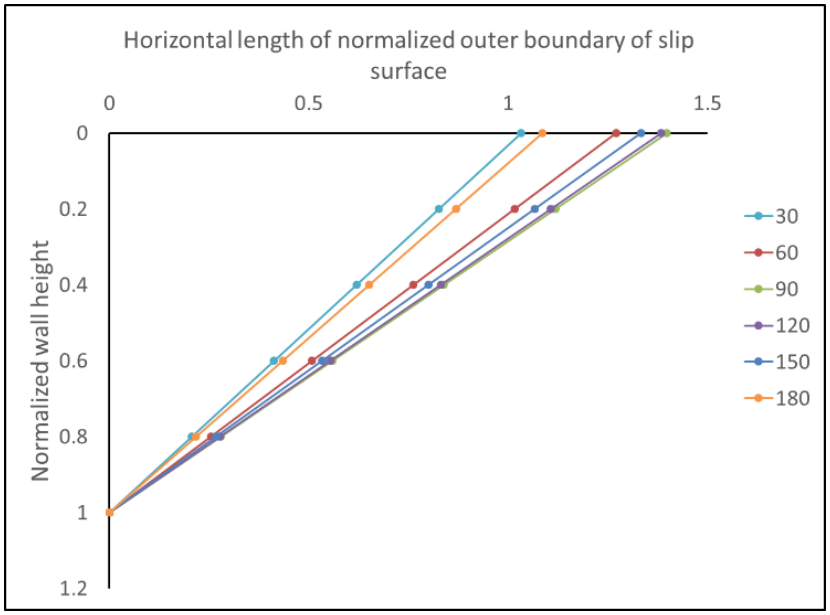

Figure 6.19. Horizontal Length of Normalized Outer Boundary of Slip Surface with Changing Corner Angles at 0.015H in Soil 1.

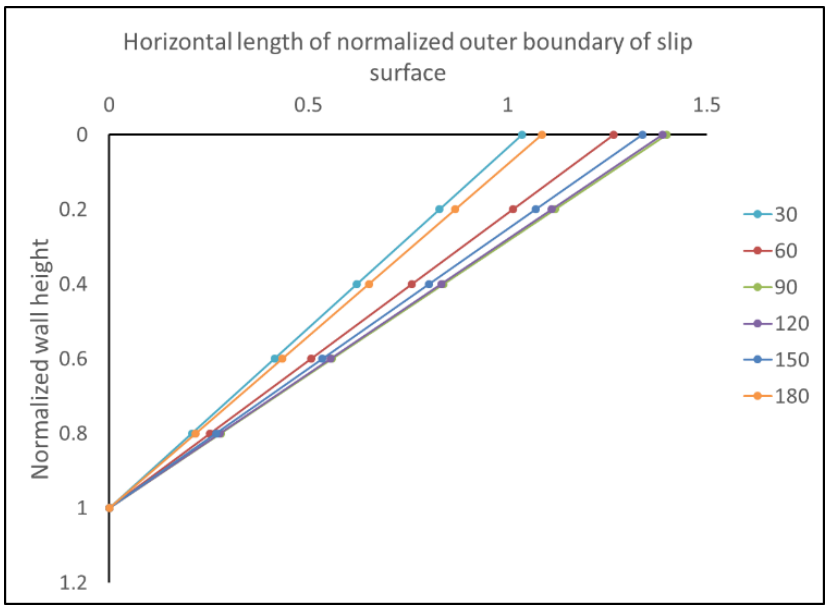

Figure 6.20. Horizontal Length of Normalized Outer Boundary of Slip Surface with Changing Corner Angles at 0.025H in Soil 1.

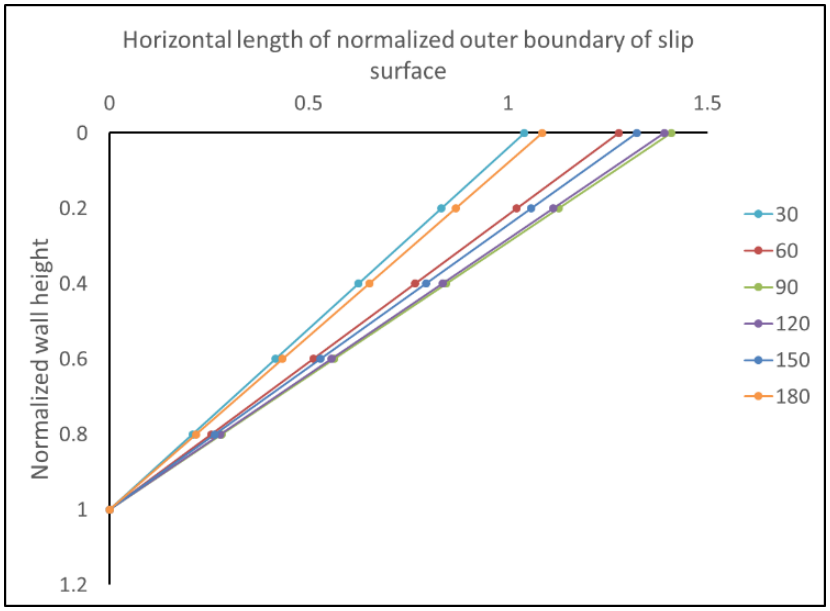

Figure 6.21. Horizontal Length of Normalized Outer Boundary of Slip Surface with Changing Corner Angles at 0.04H in Soil 1.

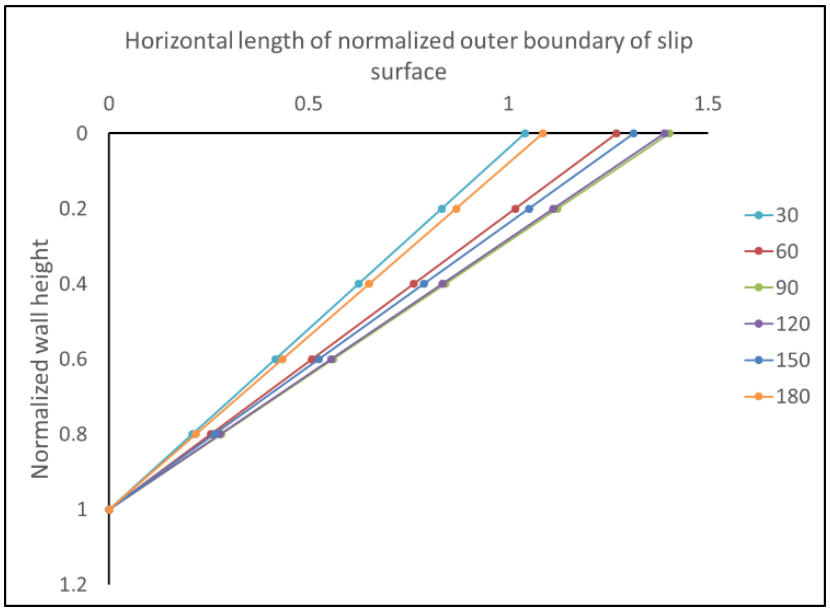

Figure 6.22. Horizontal Length of Normalized Outer Boundary of Slip Surface with Changing Corner Angles at 0.05H in Soil 1.

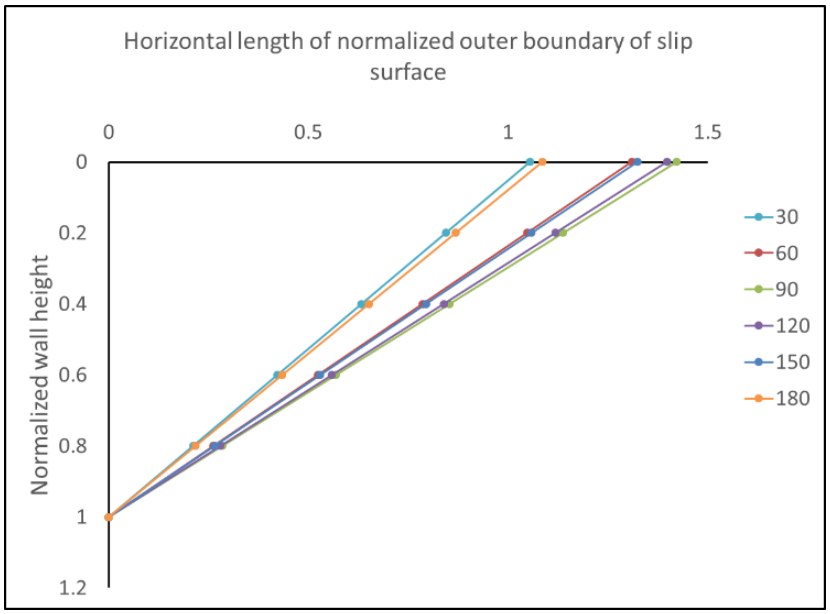

Figure 6.23. Horizontal Length of Normalized Outer Boundary of Slip Surface with Changing Corner Angles at 0.15H in Soil 1.

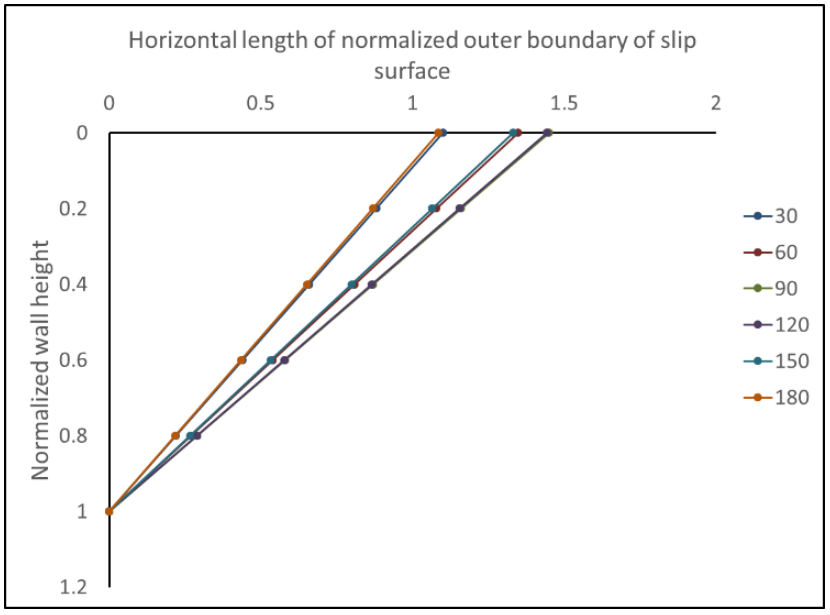

Figure 6.24. Horizontal Length of Normalized Outer Boundary of Slip Surface with Changing Corner Angles at 0.35H in Soil 1.

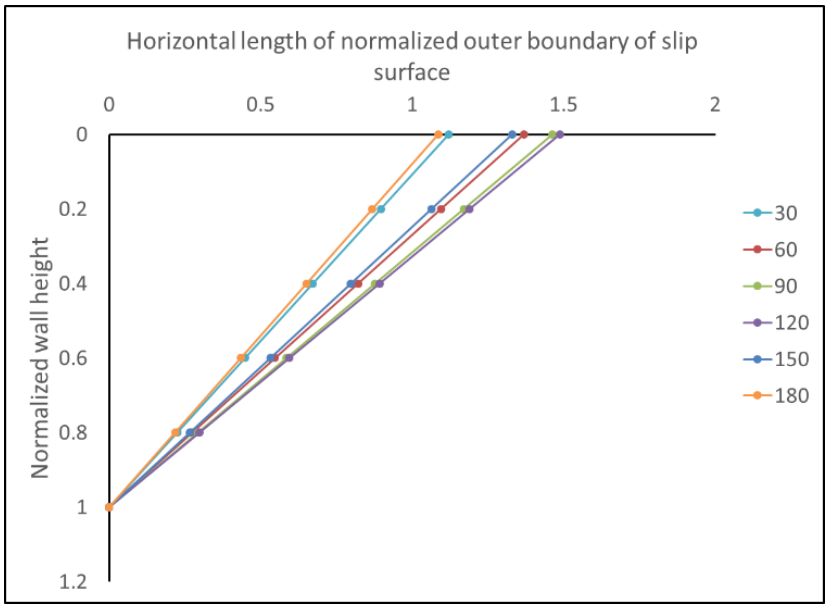

Figure 6.25. Horizontal Length of Normalized Outer Boundary of Slip Surface with Changing Corner Angles at 0.5H in Soil 1.

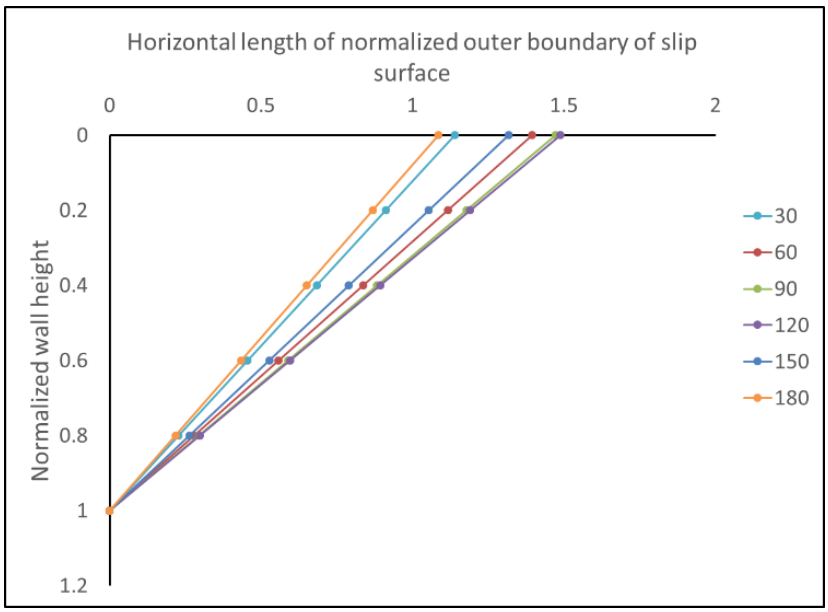

Figure 6.26. Horizontal Length of Normalized Outer Boundary of Slip Surface with Changing Corner Angles at 0.75H in Soil 1.

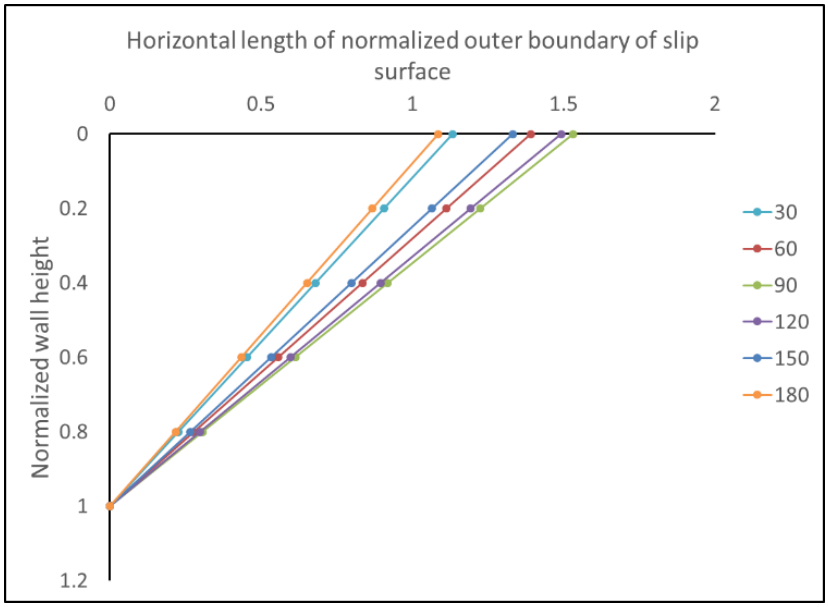

Figure 6.27. Horizontal Length of Normalized Outer Boundary of Slip Surface with Changing Corner Angles at 1.5H in Soil 1.

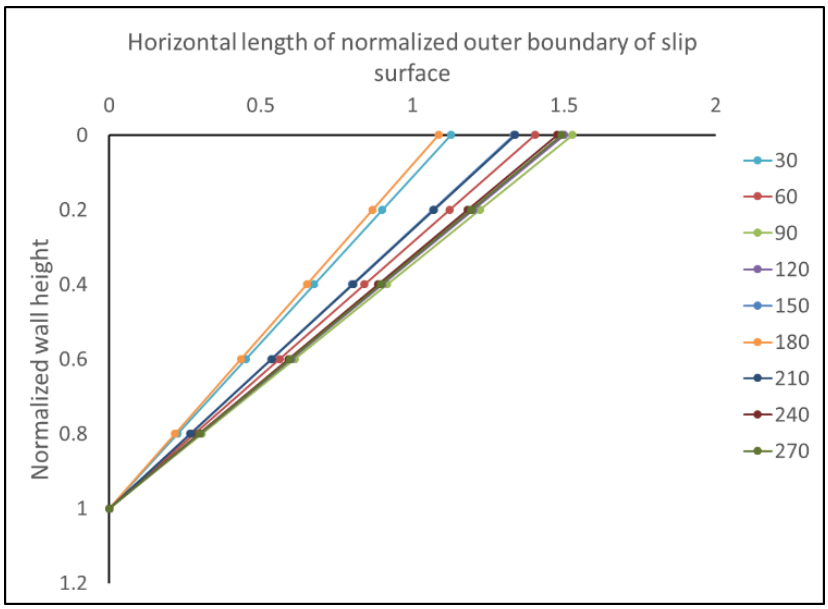

Figure 6.28. Horizontal Length of Normalized Outer Boundary of Slip Surface with Changing Corner Angles at 2.5H in Soil 1.

corner are plotted in Figure 6.30 with this, the results of the angles greater than 180° can also be seen. As shown in the graph, the distance of the outer boundary of the slip surface reaches its maximum at 90° corner angle and reaches its minimum at 180° corner angle. The behaviour in the change of the distance of the outer boundary of the slip surface according to the corner angle can be seen as an absolute sinusoidal curve, with a recurring period of 180°. This means that while making retaining structures, 2D models are not reliable, since they assume the problem to be plain-strain. Corner angles which have similar outer boundary of slip surface are given below in Table 6.1.

Table 6.1. Corner Angle Groups Which Have Similar Outer Boundary of Slip Surface.

Group No:	**Corner Angle (°)**			
1	30	180		
2	60	150	210	
3	90	120	240	270

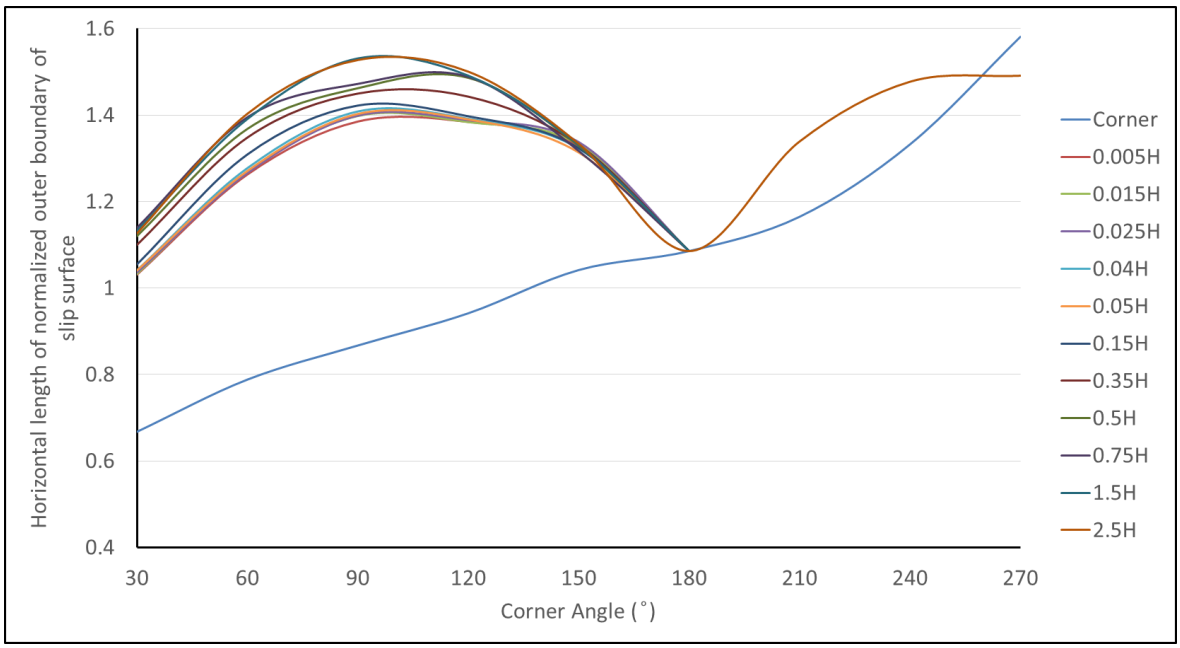

Figure 6.29. The Change in Horizontal Length of the Outer Boundary of the Slip Surface for Different Cross Sections According to the Corner Angle in Soil 1.

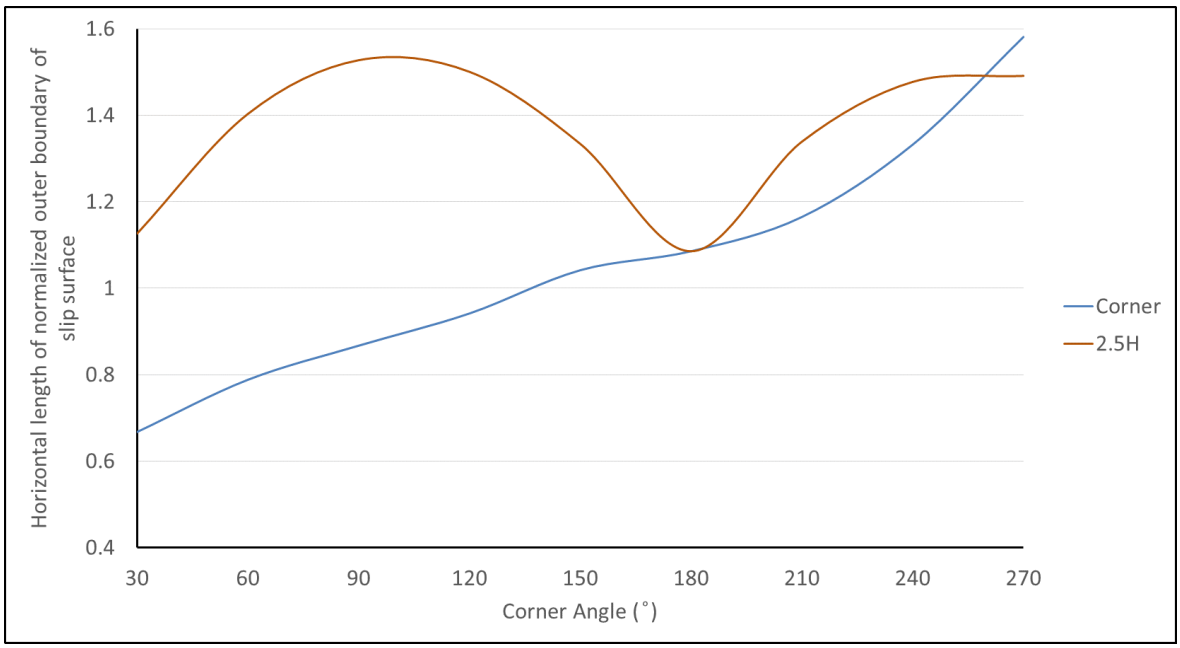

Figure 6.30. The Change in Horizontal Length of the Outer Boundary of the Slip Surface at 2.5H Cross Section According to the Corner Angle in Soil 1.

In the conducted experiments, as seen in Figure 6.13 to Figure 6.16, it is shown that the corners usually increase the distance of the outer surface of the slip surfaces and therefore affect the construction of retaining structures negatively. Also regarding Figure 6.13 to Figure 6.16, there are exceptions to this trend. In the case of the models with a corner angle of 30°, the distance of the outer boundary of the slip surface is shorter than plain-strain case, until a distance of 0.2-0.3 wall height from the corner. This can lower the cost of retaining works in the area.

6.3. Different Soil Types

The researches were conducted on 4 different types of soils with their different relative densities. Keeping the corner angle constant, the change of the distance of the outer boundary of the slip surface can be observed according to the types of the soils. This trend is shown in Figure 6.31 to Figure 6.36 for models with corner angles of 30°, 60°, 90°, 120°, 150° and 180° cross section can be taken at different distances from the corner, therefore the results of all of these cross sections are given. For models with

corner angles of 210°, 240° and 270° the results of the corner cross section and the cross section at a distance of 2.5 wall height are given Figure 6.37 to Figure 6.42.

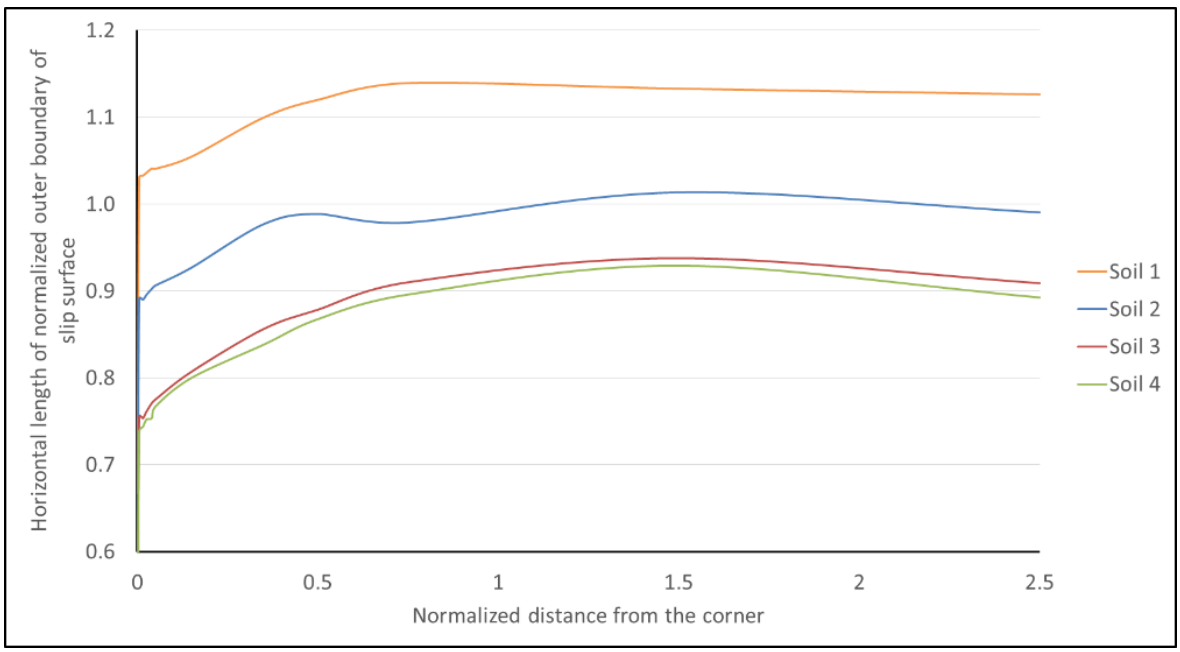

Figure 6.31. The Change of Outer Boundary of Slip Surface with Increasing Distance from the Corner at 30 Degree Corner Angle, with Different Soils

As can be seen from the Figures 6.31 to Figure 6.42, as the friction angle, a strength parameter of the soil, increases, the distance of the outer boundary of the slip surface tend to decrease in all of the models. As the soil strength increases, the cost of retaining structures decrease for all corner angles.

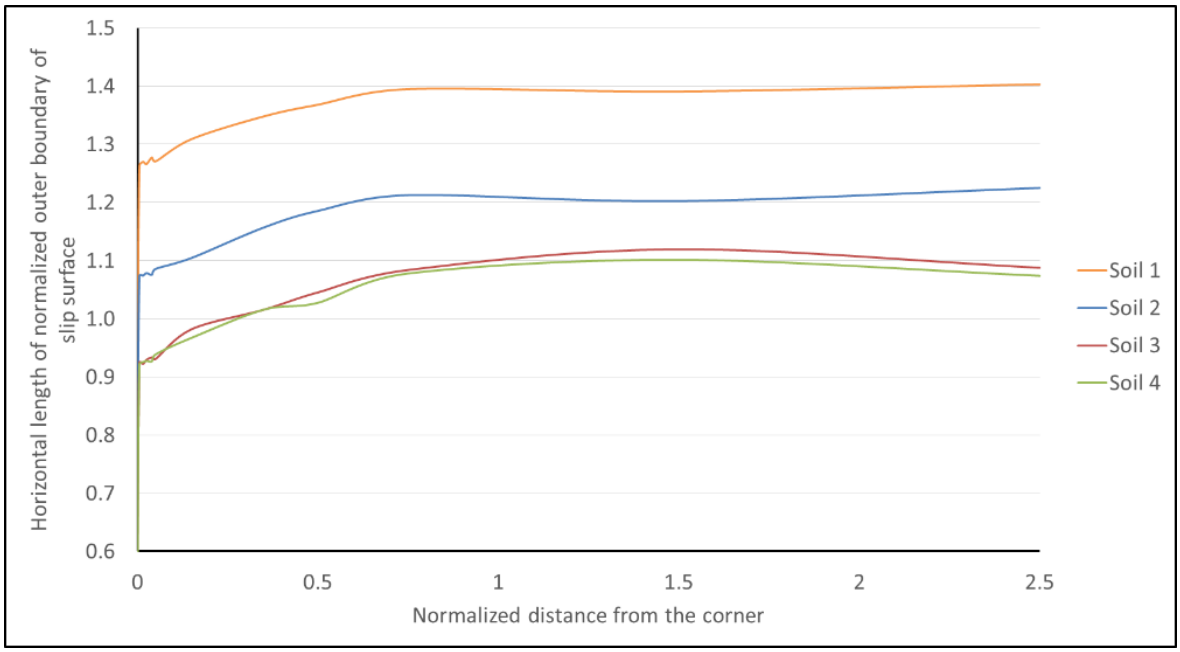

Figure 6.32. The Change of Outer Boundary of Slip Surface with Increasing Distance from the Corner at 60 Degree Corner Angle, with Different Soils

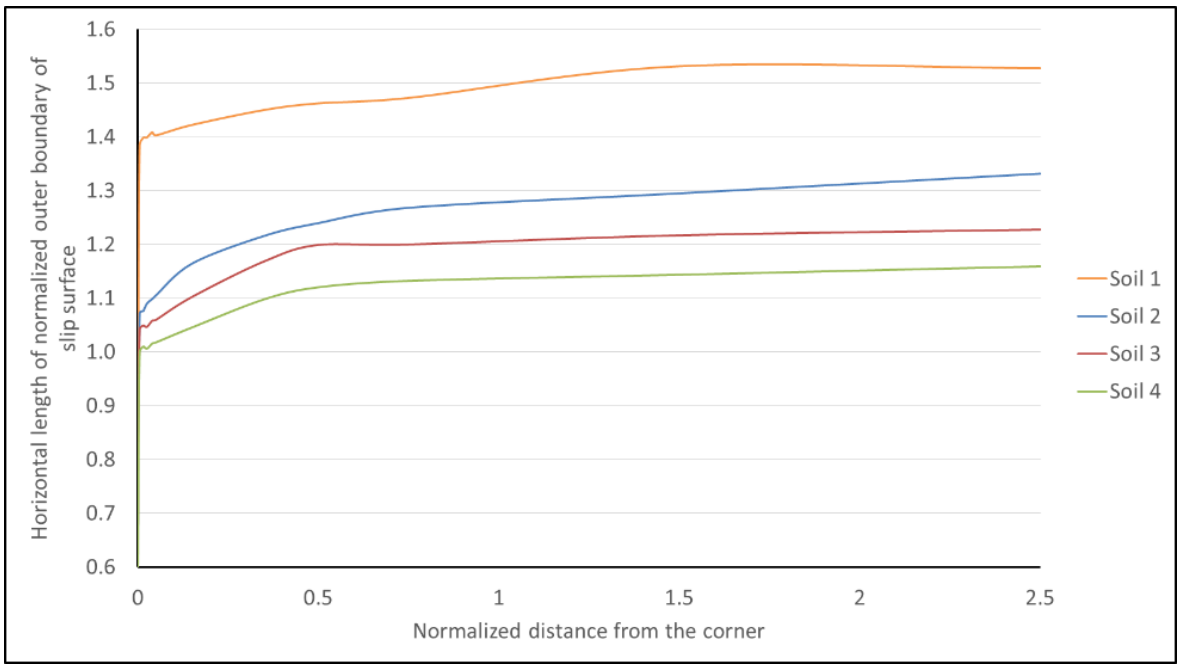

Figure 6.33. The Change of Outer Boundary of Slip Surface with Increasing Distance from the Corner at 90 Degree Corner Angle, with Different Soils

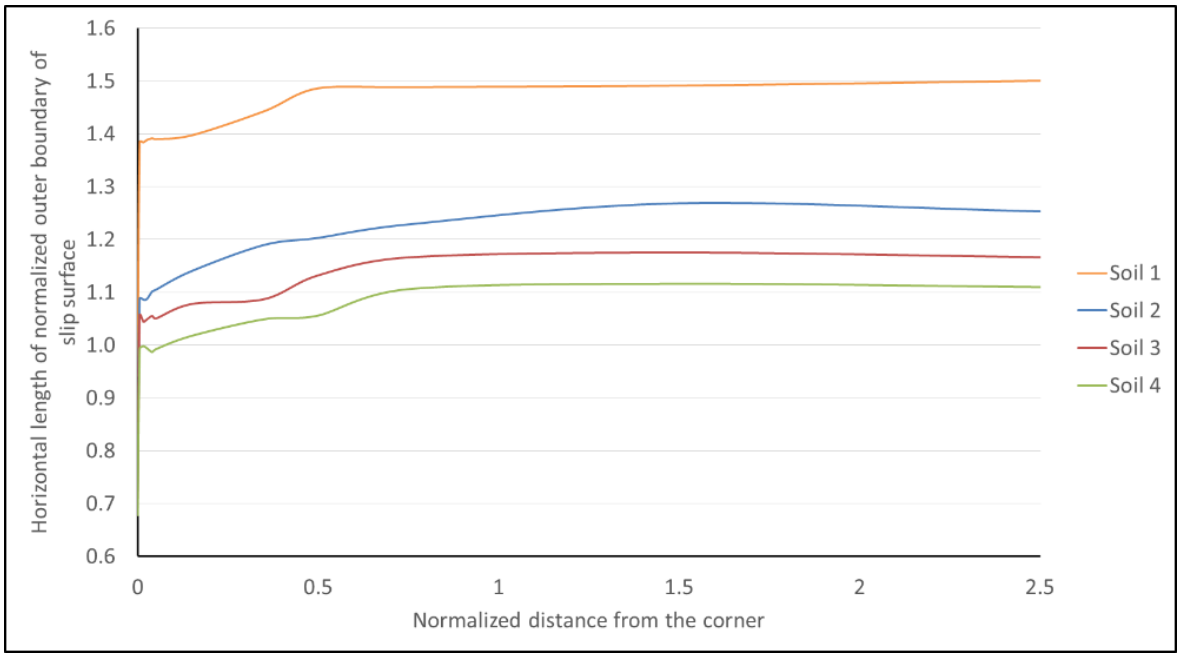

Figure 6.34. The Change of Outer Boundary of Slip Surface with Increasing Distance from the Corner at 120 Degree Corner Angle, with Different Soils

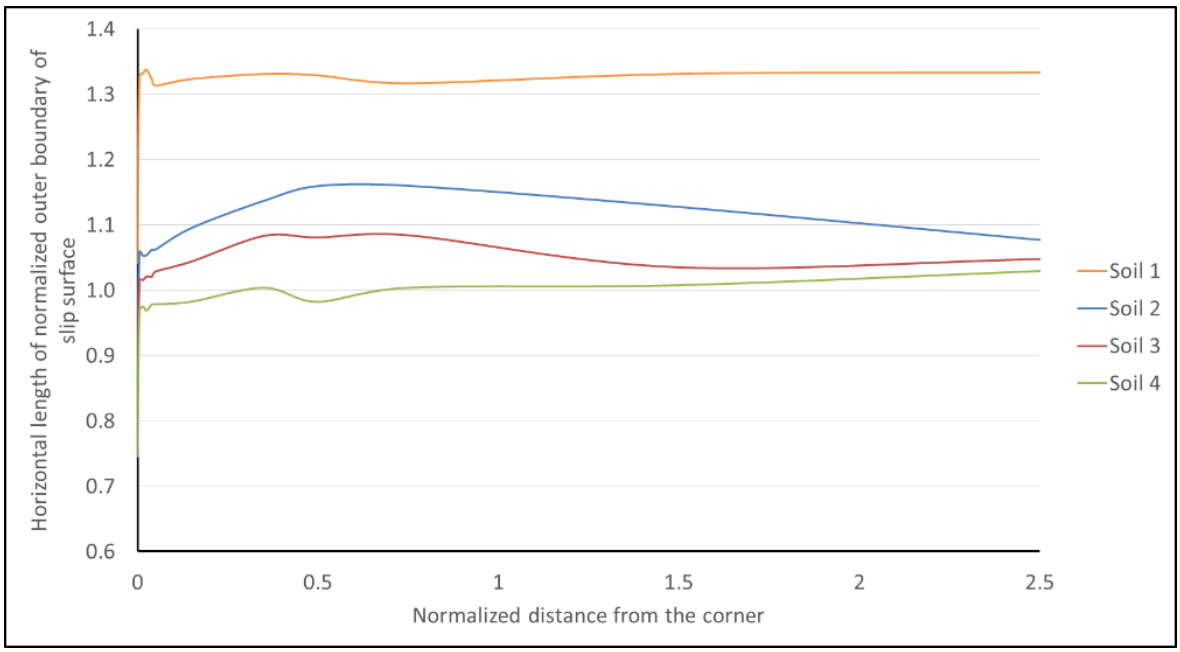

Figure 6.35. The Change of Outer Boundary of Slip Surface with Increasing Distance from the Corner at 150 Degree Corner Angle, with Different Soils

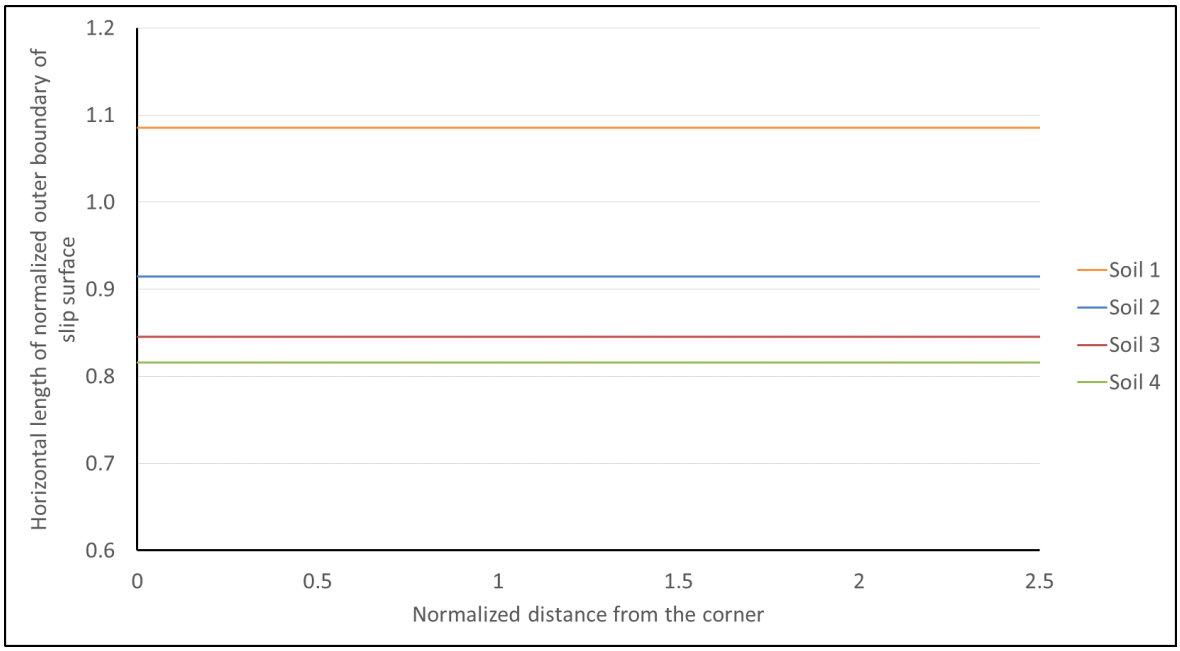

Figure 6.36. The Change of Outer Boundary of Slip Surface with Increasing Distance from the Corner at 180 Degree Corner Angle, with Different Soils

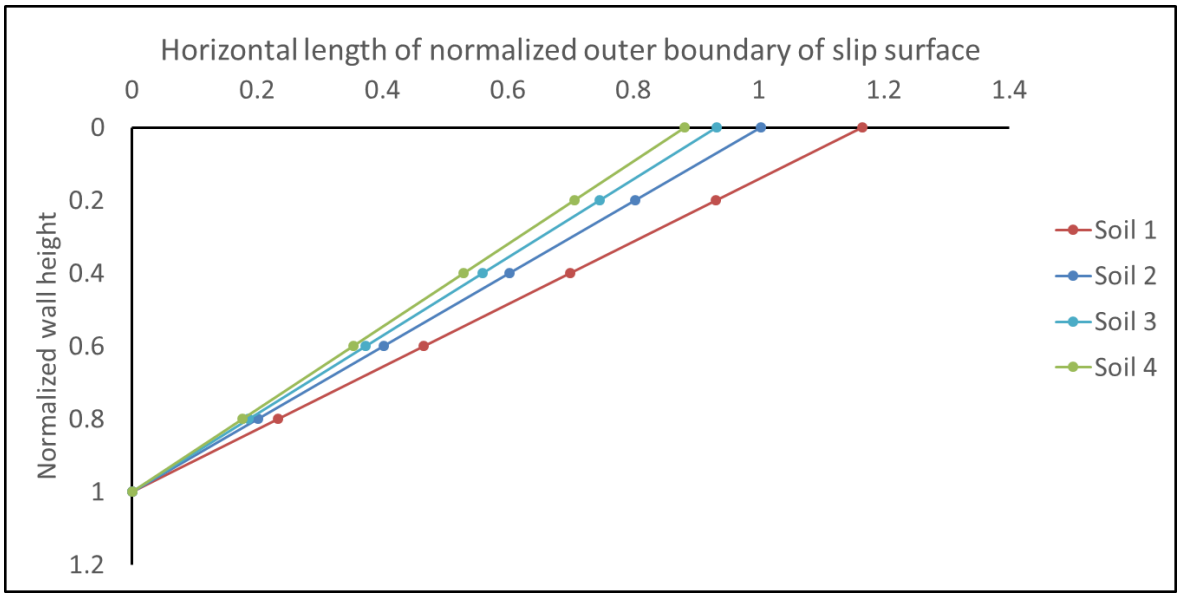

Figure 6.37. Horizontal Length of Normalized Outer Boundary of Slip Surface with Different Soils at the Corner with 210 Degree Corner Angle.

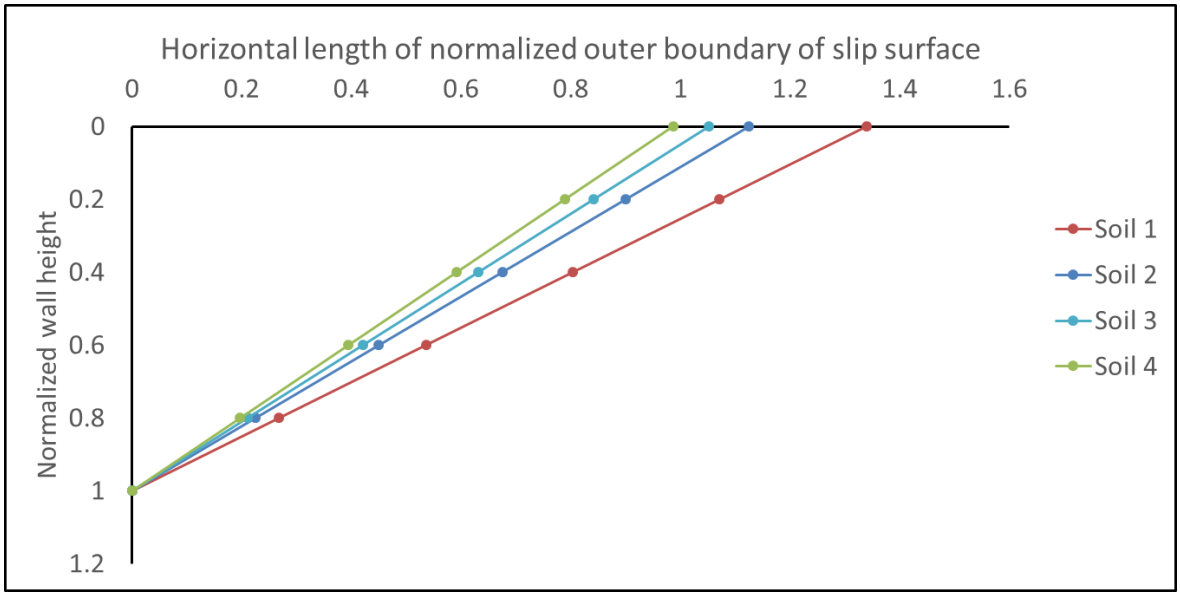

Figure 6.38. Horizontal Length of Normalized Outer Boundary of Slip Surface with Different Soils at 2.5H with 210 Degree Corner Angle.

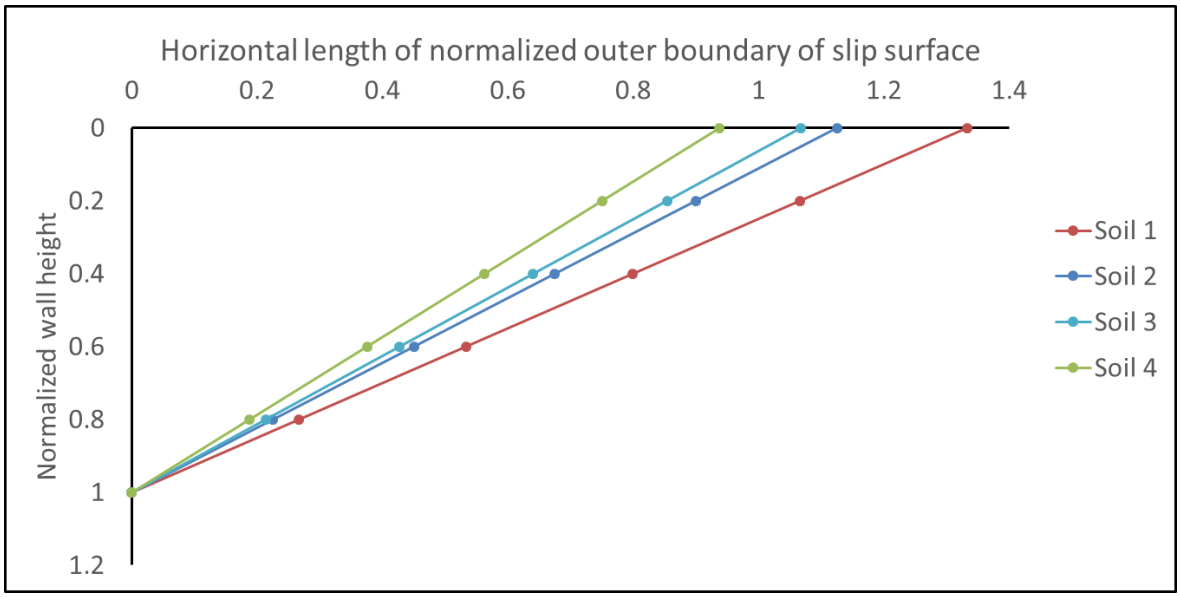

Figure 6.39. Horizontal Length of Normalized Outer Boundary of Slip Surface with Different Soils at the Corner with 240 Degree Corner Angle.

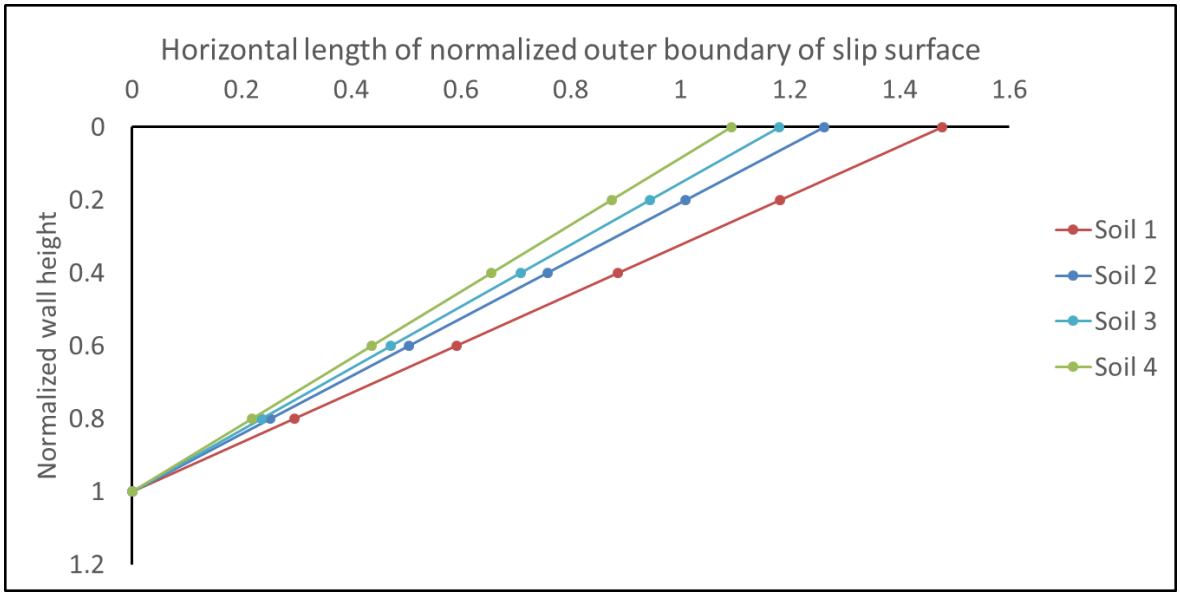

Figure 6.40. Horizontal Length of Normalized Outer Boundary of Slip Surface with Different Soils at 2.5H with 240 Degree Corner Angle.

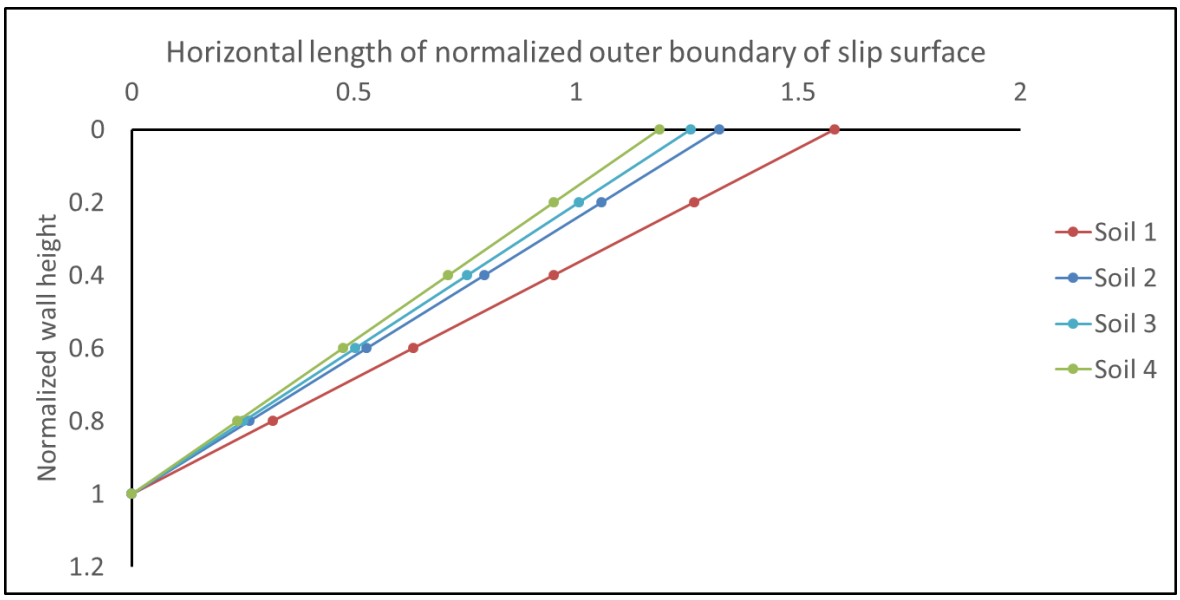

Figure 6.41. Horizontal Length of Normalized Outer Boundary of Slip Surface with Different Soils at the Corner with 270 Degree Corner Angle.

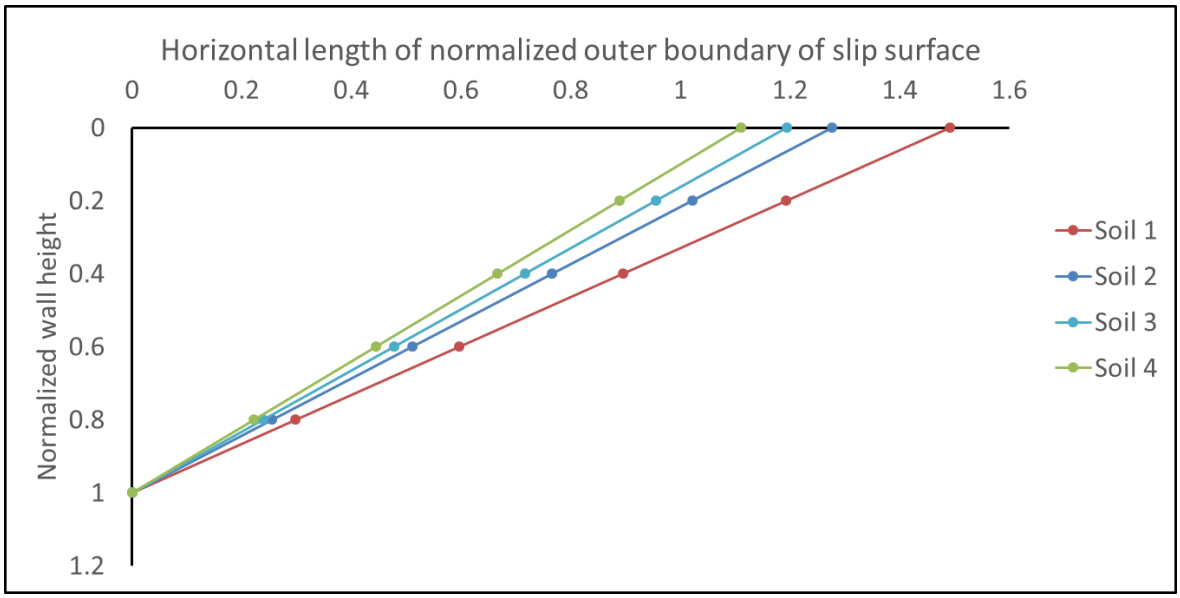

Figure 6.42. Horizontal Length of Normalized Outer Boundary of Slip Surface with Different Soils at 2.5H with 270 Degree Corner Angle.

7. CONCLUSION

In this work, the outer boundaries of the slip surfaces needed for the design of the retaining structures were investigated. In this context, numerical modellings were conducted in Plaxis 3D and the obtained results were investigated. To determine important soil parameters and to ensure the numerical models to work properly, Plaxis models were compared with small-scale retaining wall models carried out within the scope of TUBITAK Project No. 114M329 for verification. Like with the physical models, numerical models were created by using cohesionless soils and assuming the retaining structure to deform only under translation. The effects of 3 different variables on the outer boundary of the slip surface were tried to be determined in this research. These variables are the corner angle in retaining structures, the distance from the corner and peak friction angle and dilatation angle influenced by the relative density of the soil.

Considering the distance from the corner, for corners with smaller angles then 180°, with increasing distance from the corner, it was observed that the distance between the retaining structure and the outer boundary of the slip surface tends to increases with a diminishing rate and the stays constant after reaching a certain distance from the corner. It was observed that the increase of the relative density in the cohesionless soils decreases the distance between the wall and the outer boundary of the slip surface. Regarding the conducted analyses, corners increase the distance of the outer boundary of the slip surface in general. This means that two dimensional analyses, which do not take the corner effect into consideration, are not safe for the design of retaining structures.

REFERENCES

Bolton, M. D., 1986,“ The Strength and Dilatancy of Sands.”, *Geotechnique.*

Chakraborty, T, and R Salgado, 2010, “Dilatancy and Shear Strength of Sand at Low Confining Pressures.”, *Jasce Ournal of Geotechnical and Geoenvironmental Engineering.*

Coduto, D.P. , 2001, “Foundation Design Principles and Practices”, *Prentice-Hall. Inc.*, New Jersey.

Coulomb, C.A., 1776, “Essai sur une application des regles de maximis et minimis quelques problemes de statique, relatits a l’architecture.” *Memoires de Mathematique de l’Academie Royale de Science 7*, Paris.

Craig, R.F., 2004, “Soil Mechanics”, *Chapman and Hall.*

Çinicioğlu, O., A., Abadkon, A., Altunbas, and M., Abzal, 2013, “Variation of Friction Angle and Dilatancy for Anisotropic Coheisonless Soils”, *Proceedings, 18th International Conference on Soil Mechanics and Geotechnical Engineering*; pp. 2-6.

Fang, Yung Show, and Isao Ishibashi, 1986, “Static Earth Pressures with Various Wall Movements.”, *Journal of Geotechnical Engineering.* Huebner, Dewhirst, Smith, Byrom, 2001, “The Finite Element Method for Engineers”, *Wiley-Interscience*, 4th Edition.

Jamilowsky, M., Ghionna V. N., Lancelotto R., ve Pasqualini E., 1988, “New Correlations of Penetrating Testing” Penetration Testing ISOPT-1, AA Balkema, 1: 263 - 296.

Kulhawy, F. H. ve Mayne, P. W., 1990, "Manual on Estimating Soil Properties for Foundation Design", *EL-6800 Project 1493-6 Final Report, Electric Power Research Institute (EPRI)*, New York.

Lesniewska, Danuta, and David Muir Wood, 2009, "Observations of Stresses and Strains in a Granular Material.", *Journal of Engineering Mechanics.*

Lesniewska, D., M. Niedostatkiewicz, and J. Tejchman, 2012, "Experimental Study on Shear Localization in Granular Materials within Combined Strain and Stress Field.", *Strain.*

Niedostatkiewicz, M., D. Lesniewska, and J. Tejchman, 2011, "Experimental Analysis of Shear Zone Patterns in Cohesionless for Earth Pressure Problems Using Particle Image Velocimetry.", *Strain.*

Plaxis 3D Manual, Plaxis Company, 2018

Rankine, W. J. M., 1857, "On the Stability of Loose Earth.", *Philosophical Transactions of the Royal Society of London.*

Reynolds, Osborne, 1885, "LVII. On the Dilatancy of Media Composed of Rigid Particles in Contact. With Experimental Illustrations.", *Philosophical Magazine*, Series 5.

Rowe, P. W., 1962, "The Stress-Dilatancy Relation for Static Equilibrium of an Assembly of Particles in Contact.", *Proceedings of the Royal Society A: Mathematical, Physical and Engineering Sciences.*

Schanz, T., and P. A. Vermeer, 1996, "Angles of Friction and Dilatancy of Sand.", *Geotechnique.*

Soltanbeigi, B., Altunbas, A. And Cinicioglu O., 2015,"Visualization of Shear bands in cohesionless soils, Proc. Symp. Deformation Characteristics of Geomaterials", *Buenos Aires*, Argentina.

Taylor, D.W. , 1948, "Fundamentals of Soil Mechanics", *John Wiley and Sons Inc.*, New York.

Terzaghi, K., 1943, "Theoretical Soil Mechanics", *Wiley*, New York.

Toyosawa, Y Itoh, S B Tamrakar, and N Suemasa, 2006, "Redistribution of Active Earth Pressures Using Movable Earth Support Apparatus in Centrifuge.", *Phys. Model. Geotech.–6th ICPMG.*

Tsagareli, Z. V., 1967, "Experimental Investigation of the Pressure of a Loose Medium on Retaining Walls with a Vertical Back Face and Horizontal Backfill Surface.", *Soil Mechanics and Foundation Engineering.*

Vaid, Y.P., and S. Sasitharan, 1993, "The Strength and Dilatancy of Sand: Reply.", *Canadian Geotechnical Journal.*

White, DJ, Andy Take, and M.D. Bolton, 2001, "Measuring Soil Deformation in Geotechnical Models Using Digital Images and PIV Analysis.", *10th International Conference on Computer Methods and Advances in Geomechanics.*

White, D. J., W. A. Take, and M. D. Bolton, 2003, "Soil Deformation Measurement Using Particle Image Velocimetry (PIV) and Photogrammetry.", *Geotechnique.*

APPENDIX A: FOR EACH CROSS SECTION, THE HORIZONTAL DISTANCE OF THE OUTER BOUNDARY OF THE SLIP SURFACES FOR DIFFERENT CORNER ANGLES

For each cross section, the horizontal distance of the outer boundary of the slip surfaces for different corner angles in soil 2, 3 and 4.

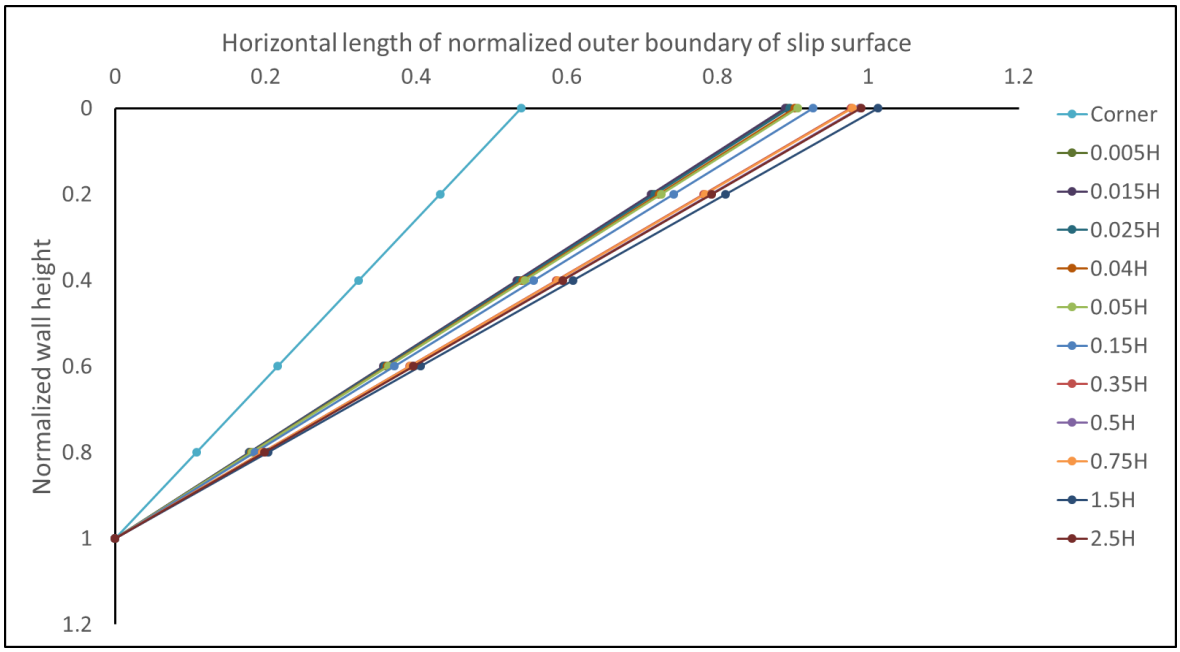

Figure A.1. Horizontal Length of Normalized Outer Boundary of Slip Surfaces in Soil 2, at Corner with 30 Degree.

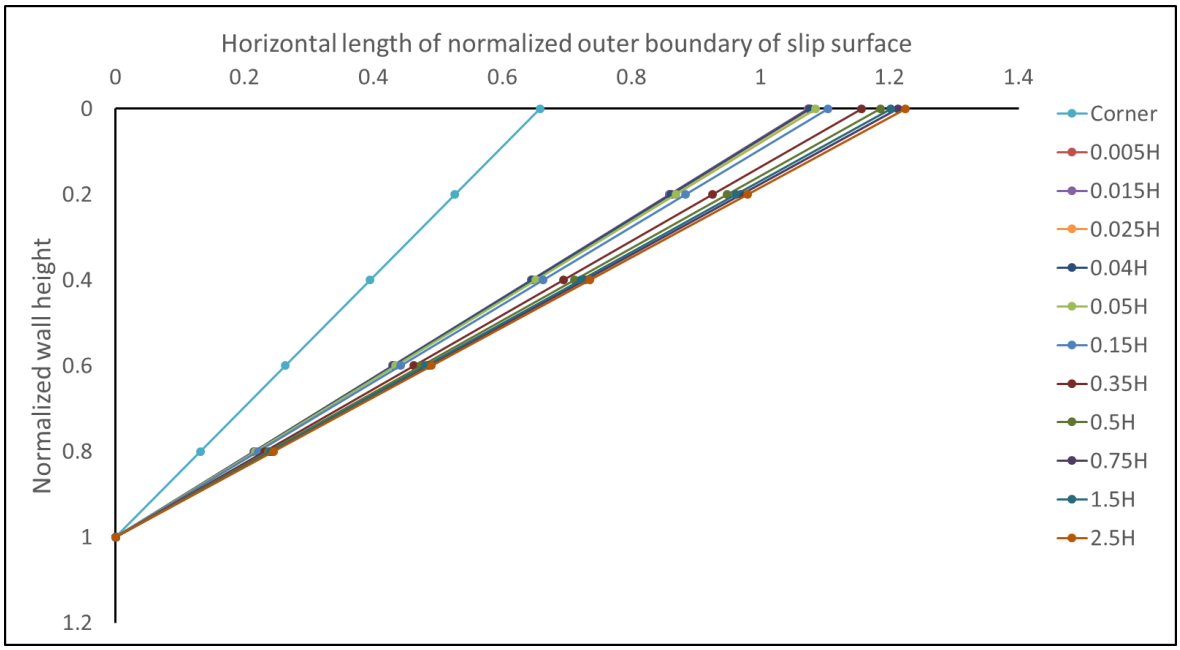

Figure A.2. Horizontal Length of Normalized Outer Boundary of Slip Surfaces in Soil 2, at Corner with 60 Degree.

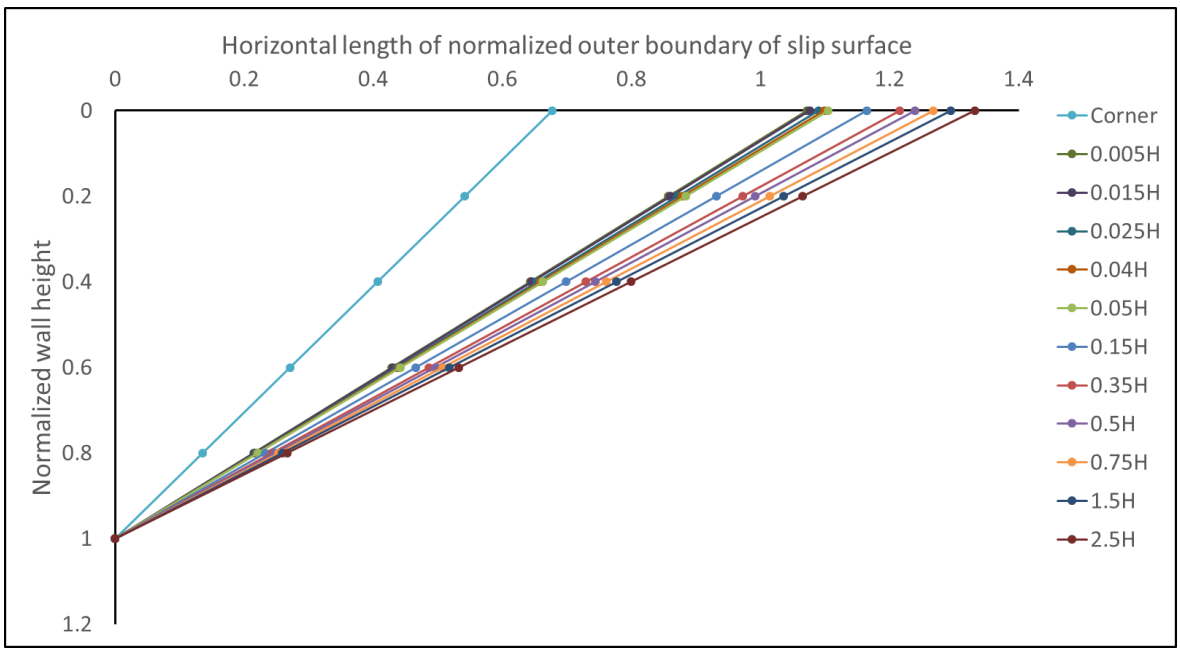

Figure A.3. Horizontal Length of Normalized Outer Boundary of Slip Surfaces in Soil 2, at Corner with 90 Degree.

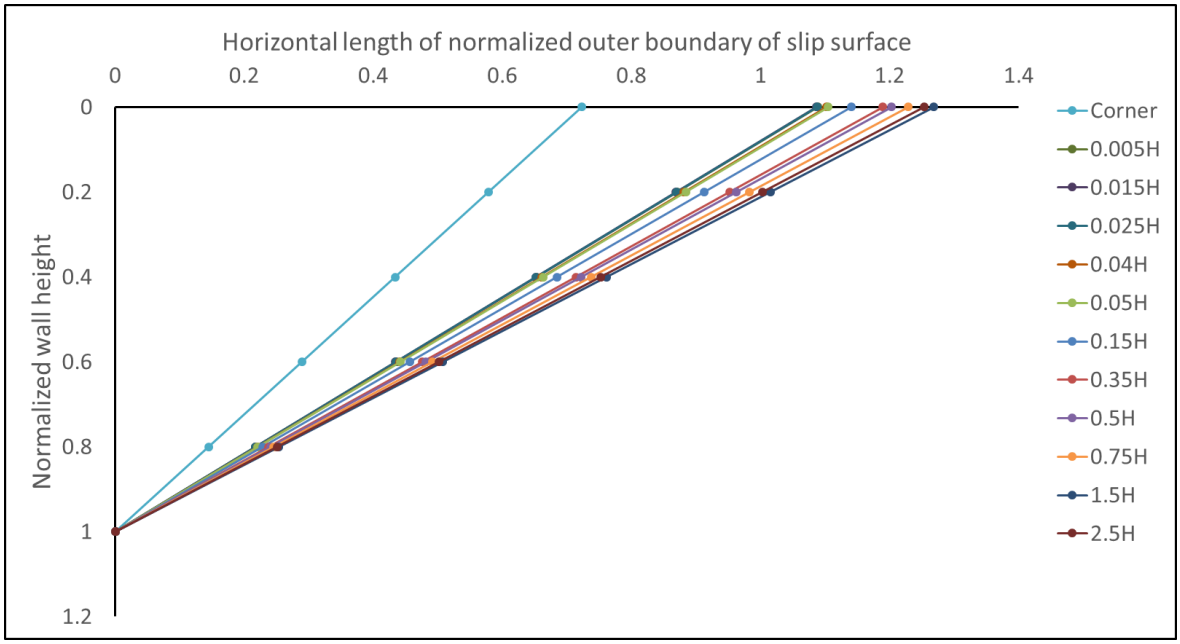

Figure A.4. Horizontal Length of Normalized Outer Boundary of Slip Surfaces in Soil 2, at Corner with 120 Degree.

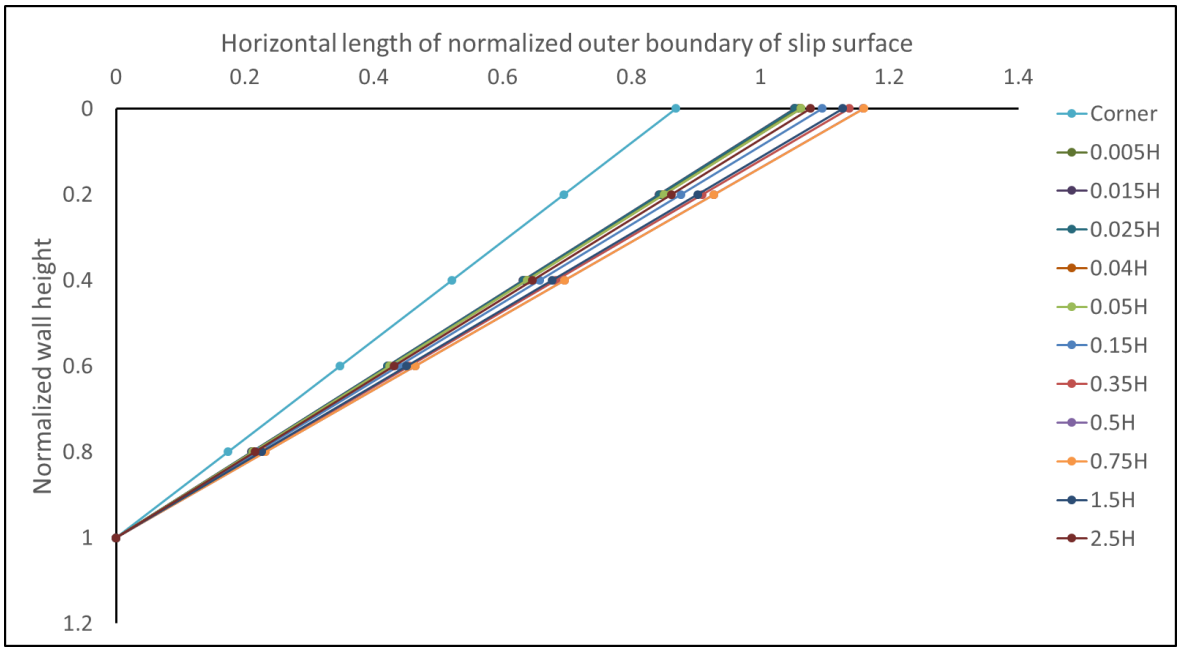

Figure A.5. Horizontal Length of Normalized Outer Boundary of Slip Surfaces in Soil 2, at Corner with 150 Degree.

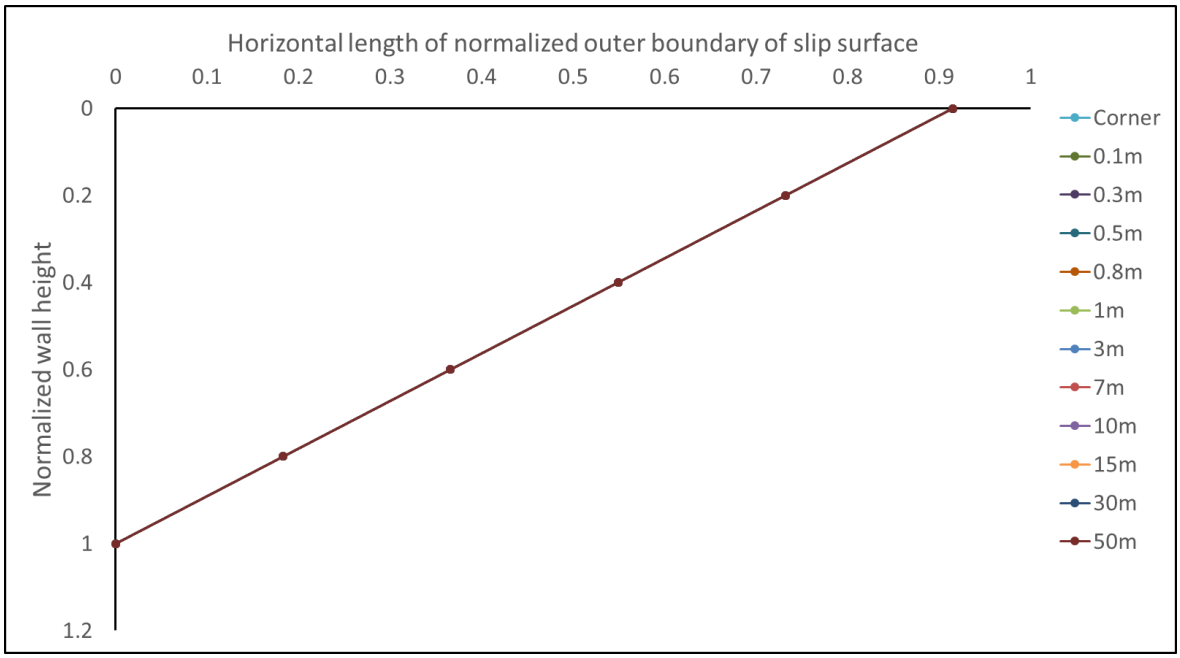

Figure A.6. Horizontal Length of Normalized Outer Boundary of Slip Surfaces in Soil 2, at Corner with 180 Degree.

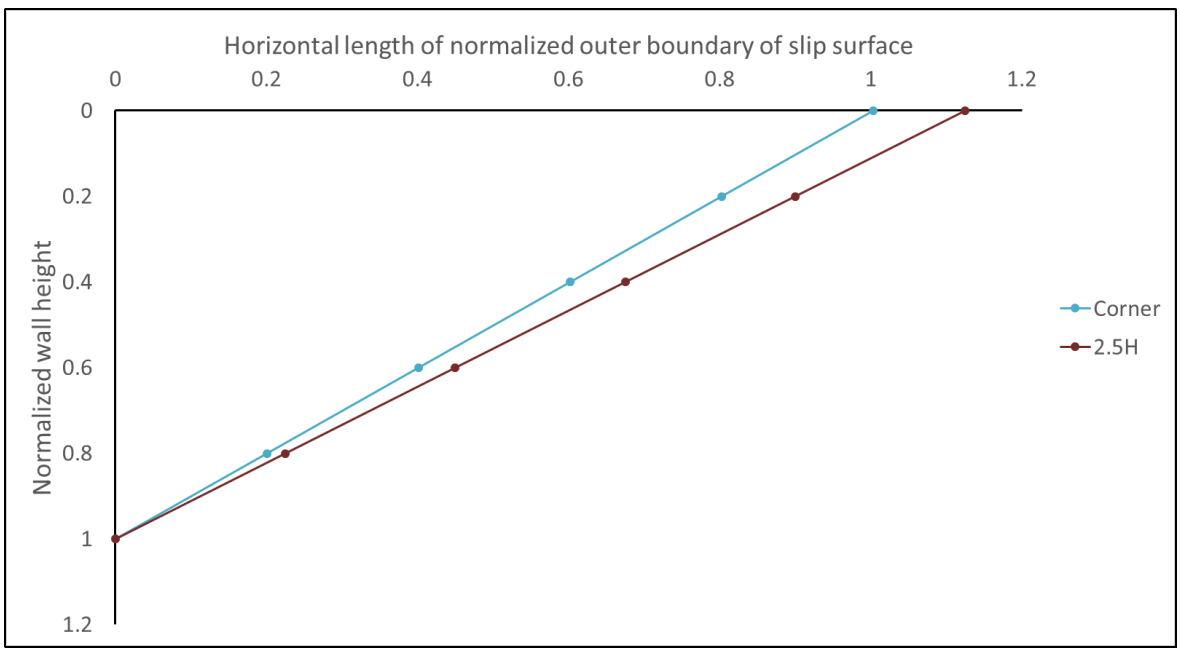

Figure A.7. Horizontal Length of Normalized Outer Boundary of Slip Surfaces in Soil 2, at Corner with 210 Degree.

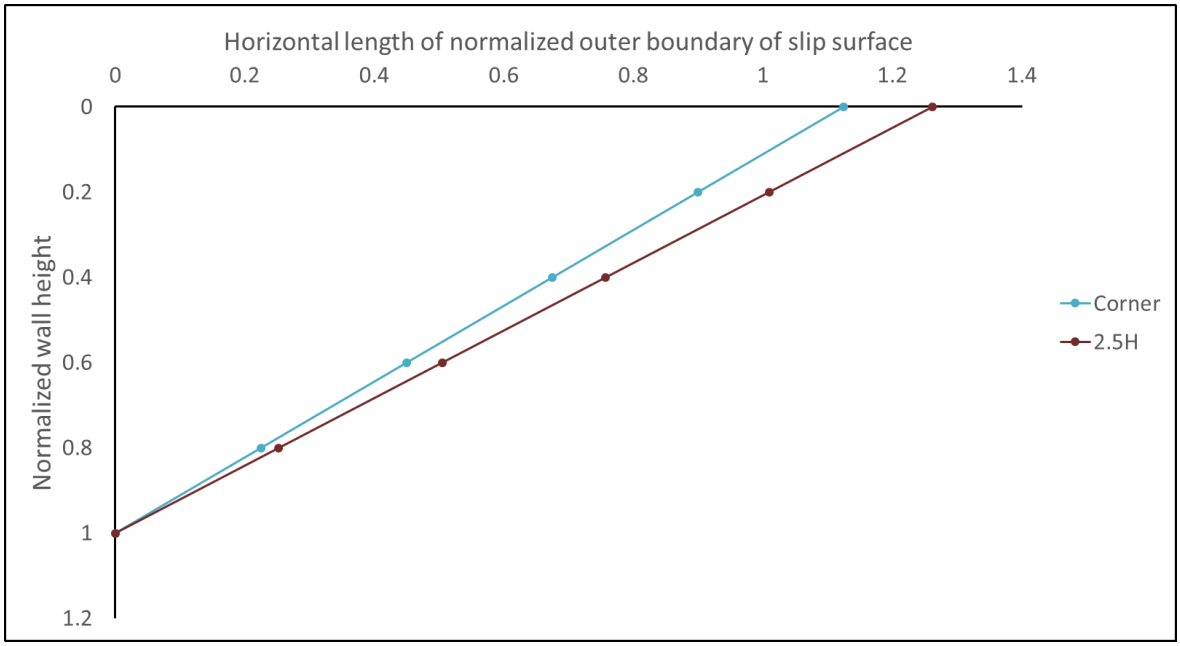

Figure A.8. Horizontal Length of Normalized Outer Boundary of Slip Surfaces in Soil 2, at Corner with 240 Degree.

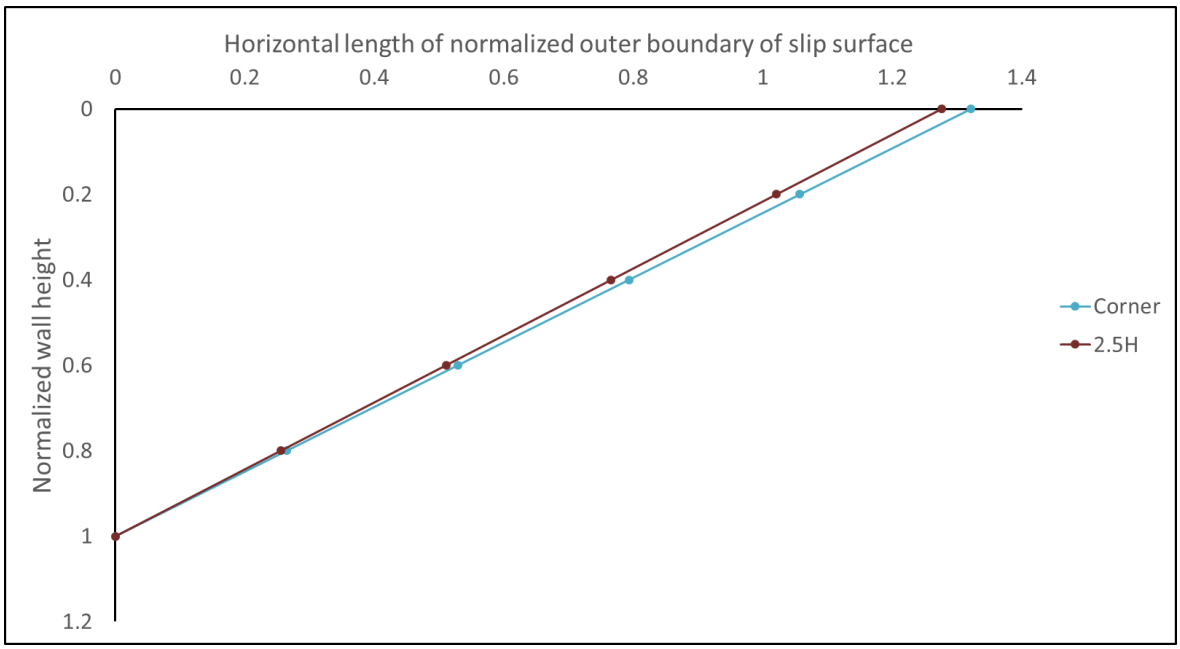

Figure A.9. Horizontal Length of Normalized Outer Boundary of Slip Surfaces in Soil 2, at Corner with 270 Degree.

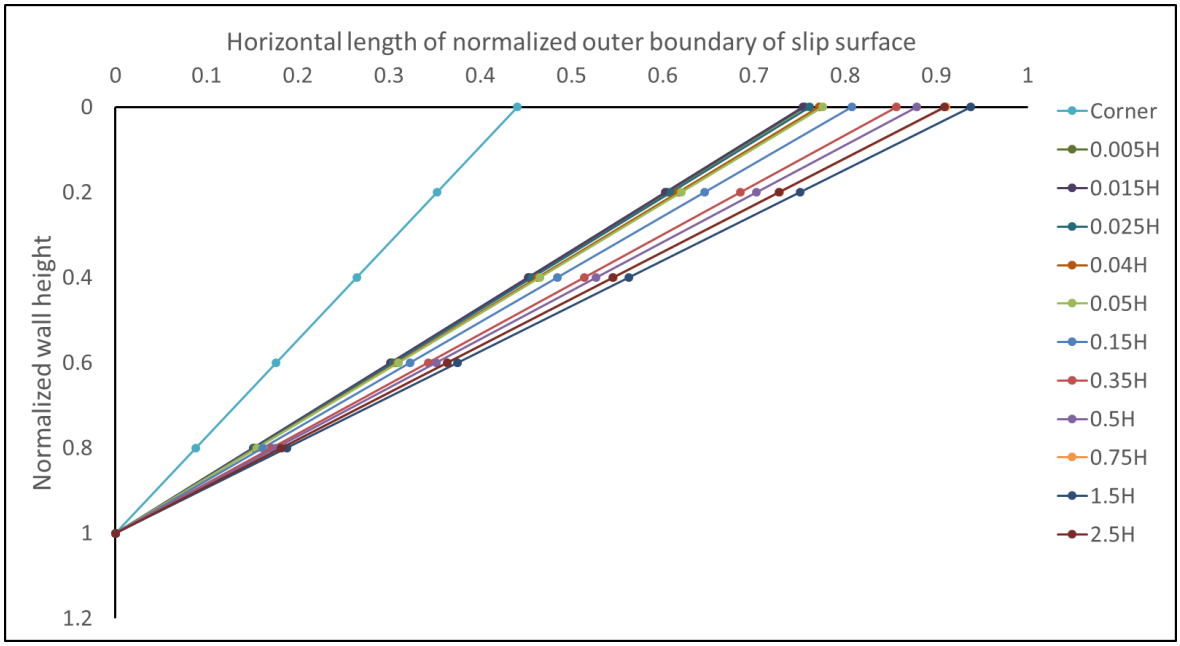

Figure A.10. Horizontal Length of Normalized Outer Boundary of Slip Surfaces in Soil 3, at Corner with 30 Degree.

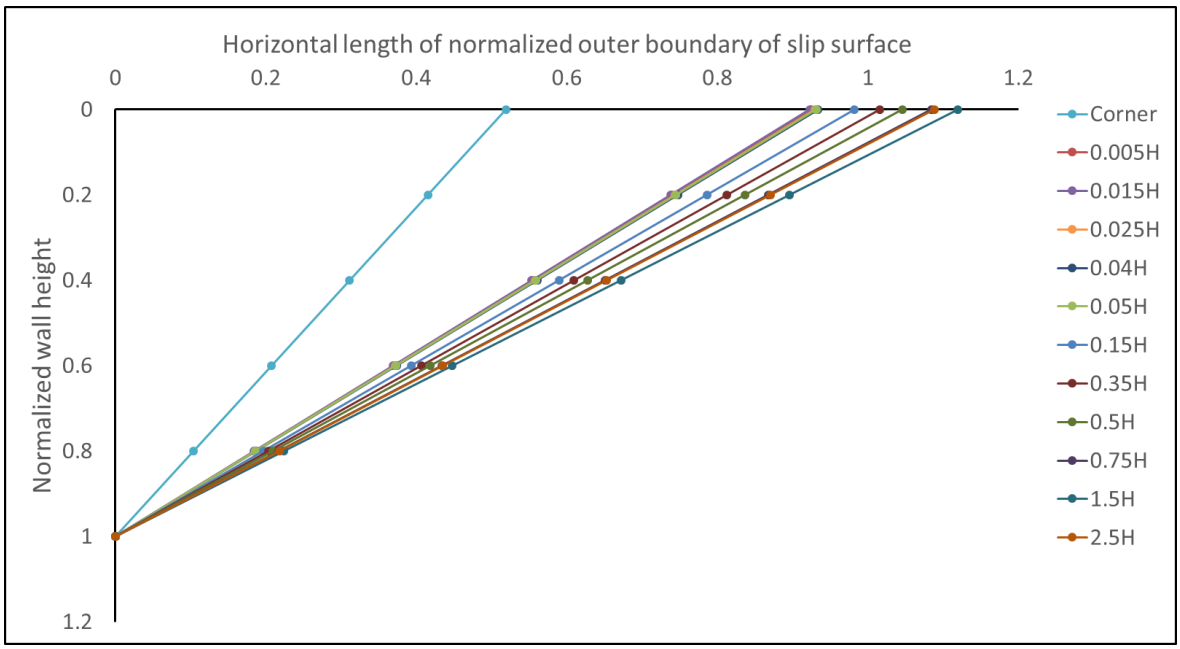

Figure A.11. Horizontal Length of Normalized Outer Boundary of Slip Surfaces in Soil 3, at Corner with 60 Degree.

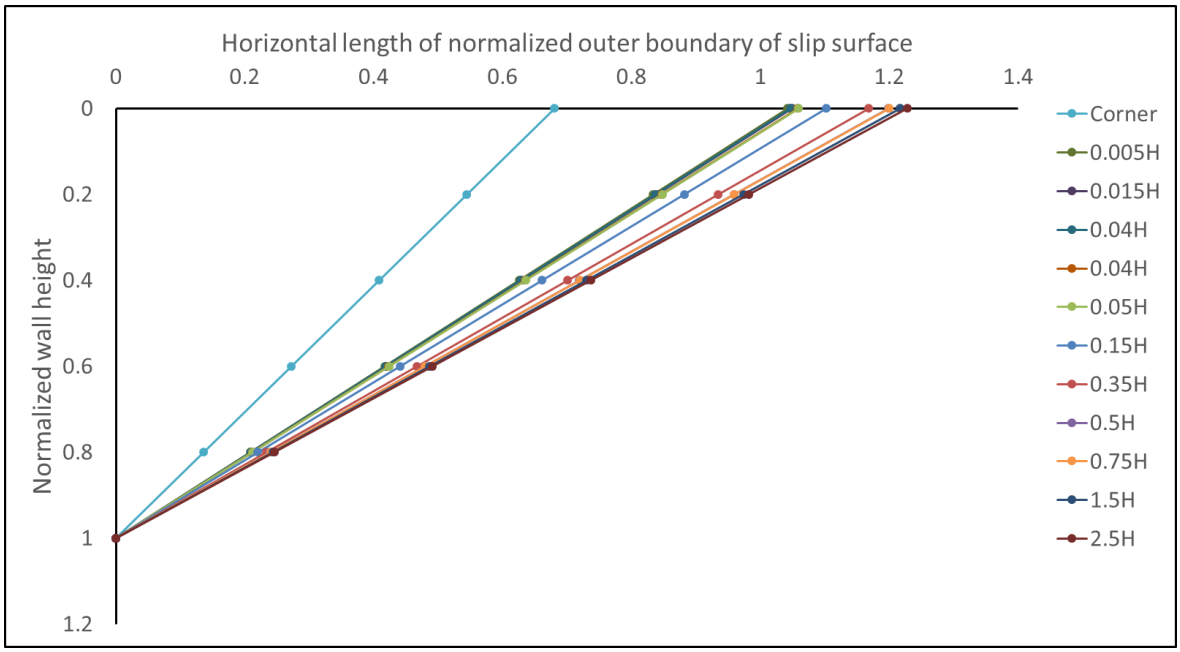

Figure A.12. Horizontal Length of Normalized Outer Boundary of Slip Surfaces in Soil 3, at Corner with 90 Degree.

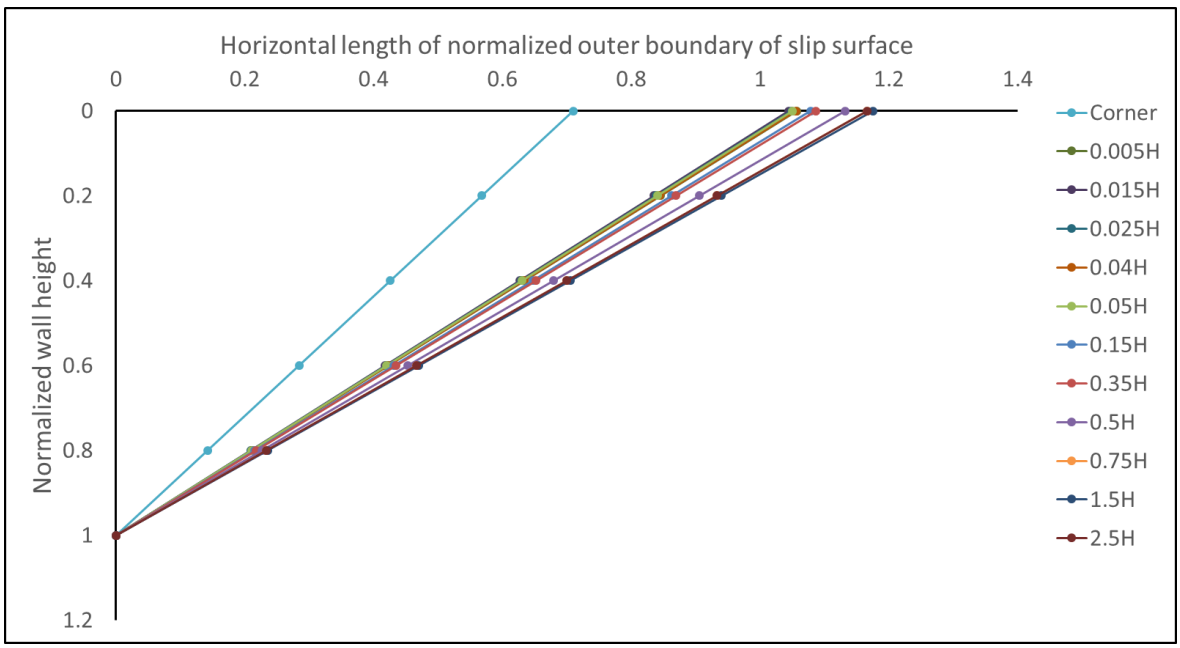

Figure A.13. Horizontal Length of Normalized Outer Boundary of Slip Surfaces in Soil 3, at Corner with 120 Degree.

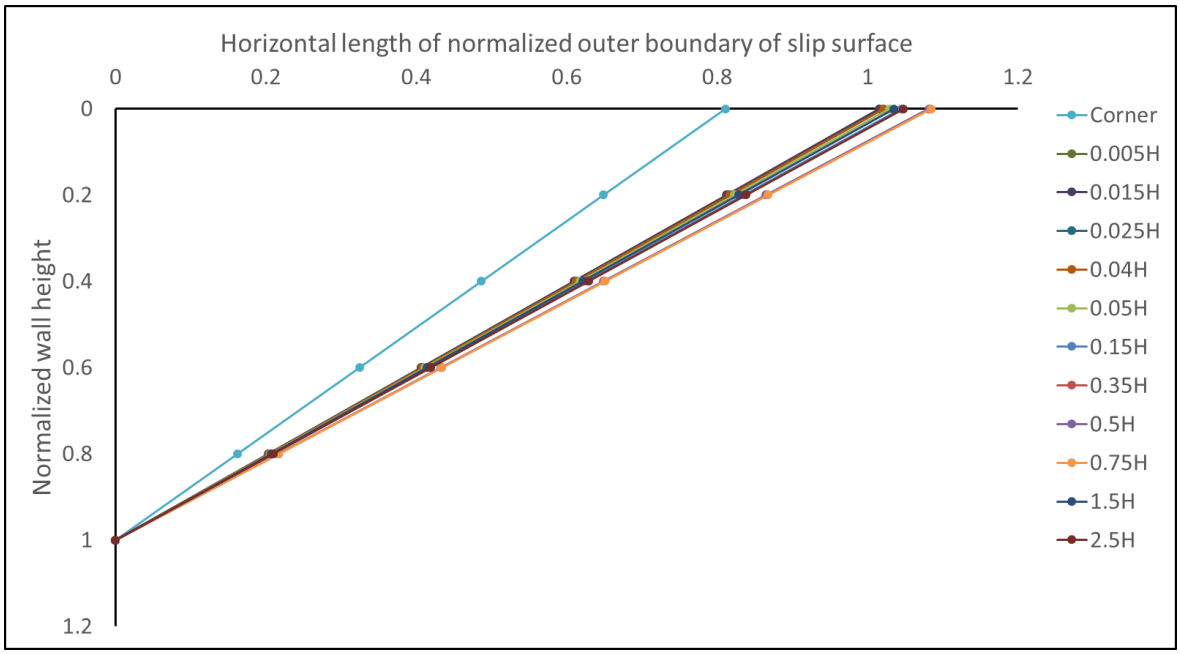

Figure A.14. Horizontal Length of Normalized Outer Boundary of Slip Surfaces in Soil 3, at Corner with 150 Degree.

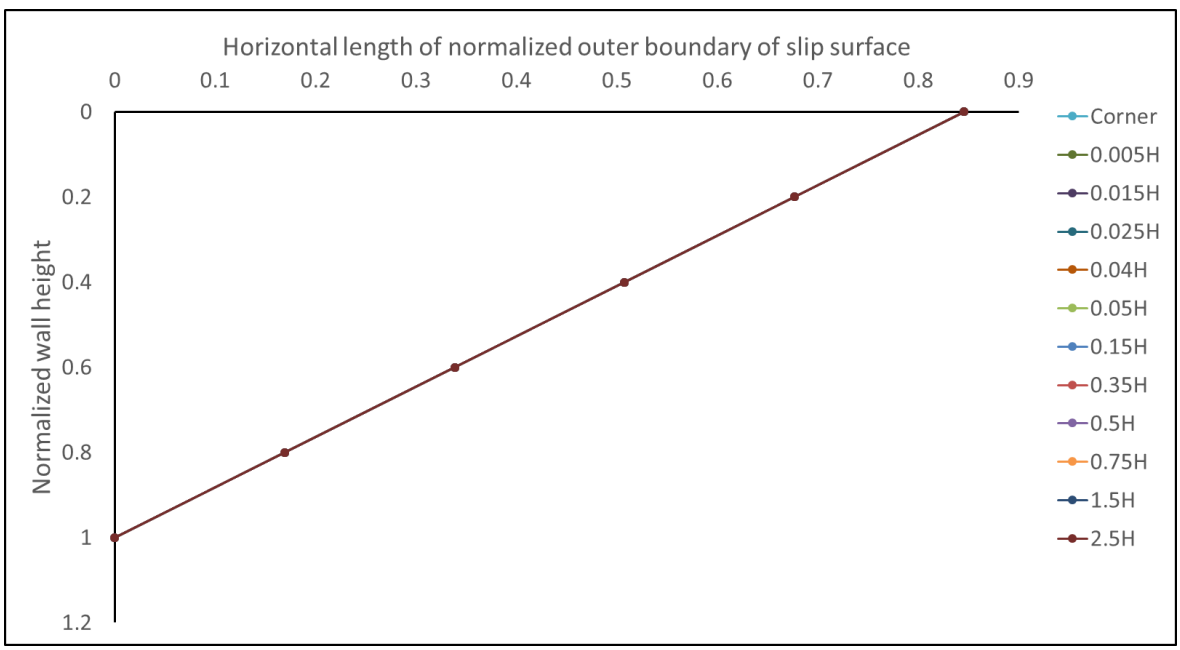

Figure A.15. Horizontal Length of Normalized Outer Boundary of Slip Surfaces in Soil 3, at Corner with 180 Degree.

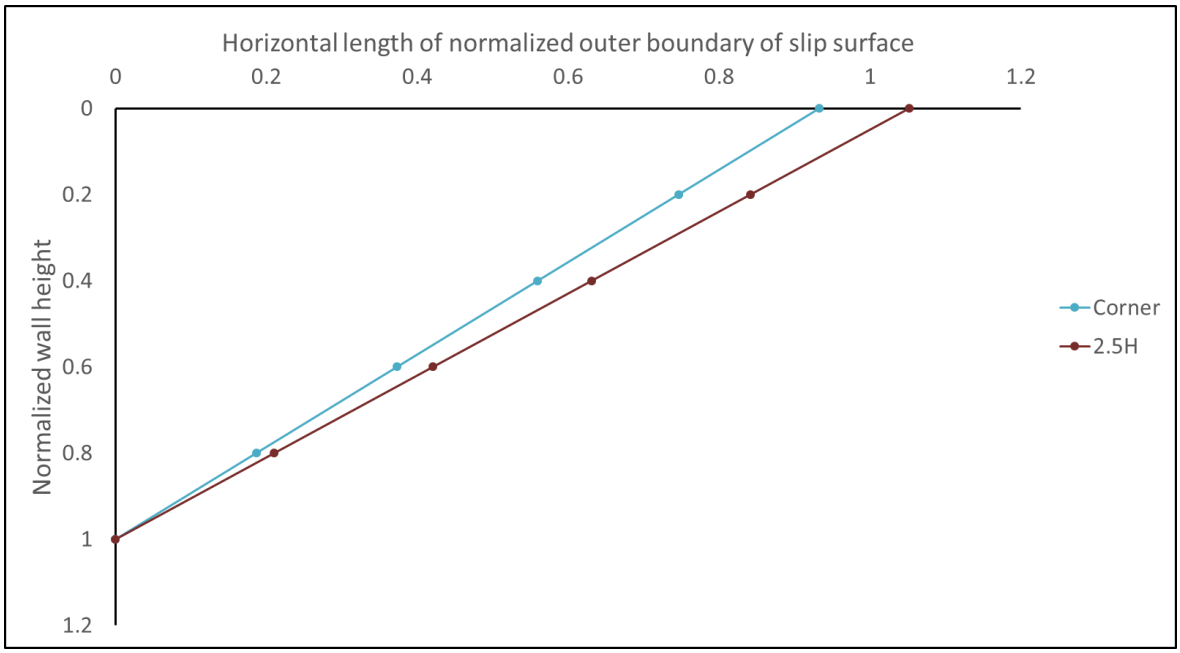

Figure A.16. Horizontal Length of Normalized Outer Boundary of Slip Surfaces in Soil 3, at Corner with 210 Degree.

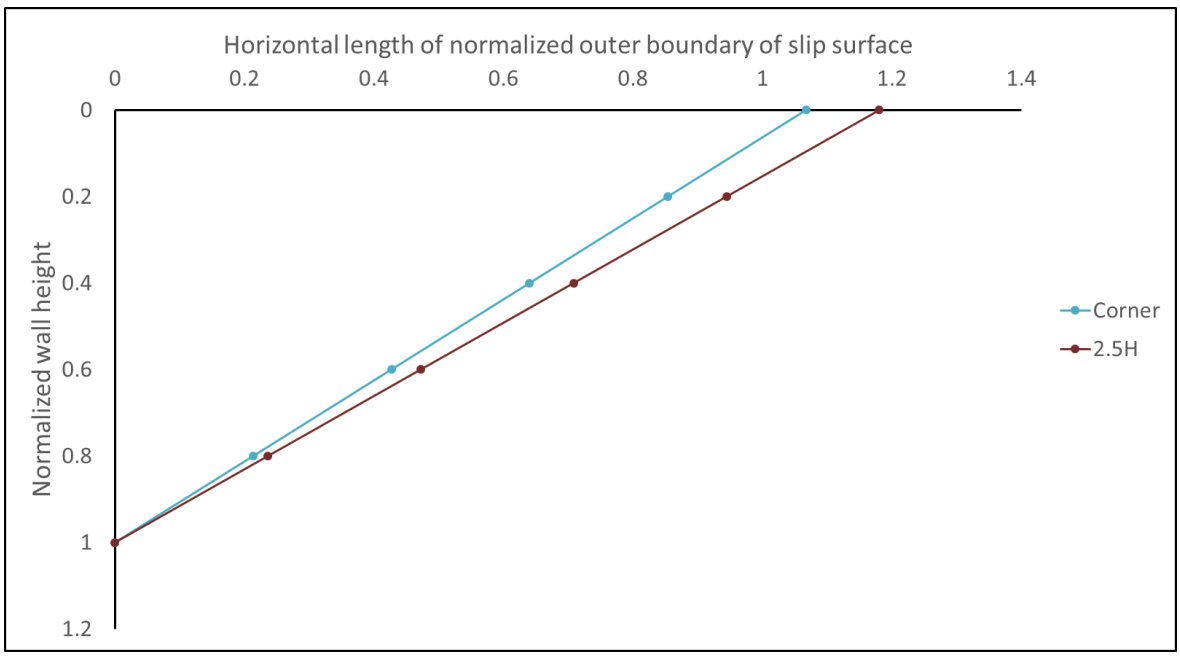

Figure A.17. Horizontal Length of Normalized Outer Boundary of Slip Surfaces in Soil 3, at Corner with 240 Degree.

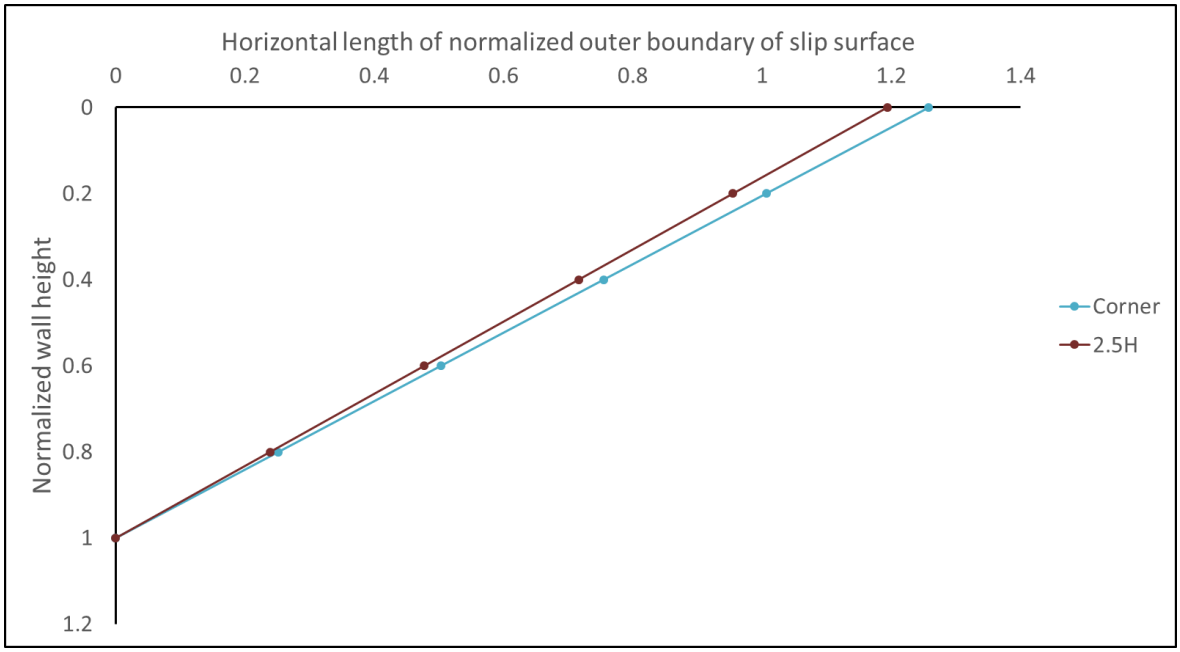

Figure A.18. Horizontal Length of Normalized Outer Boundary of Slip Surfaces in Soil 3, at Corner with 270 Degree.

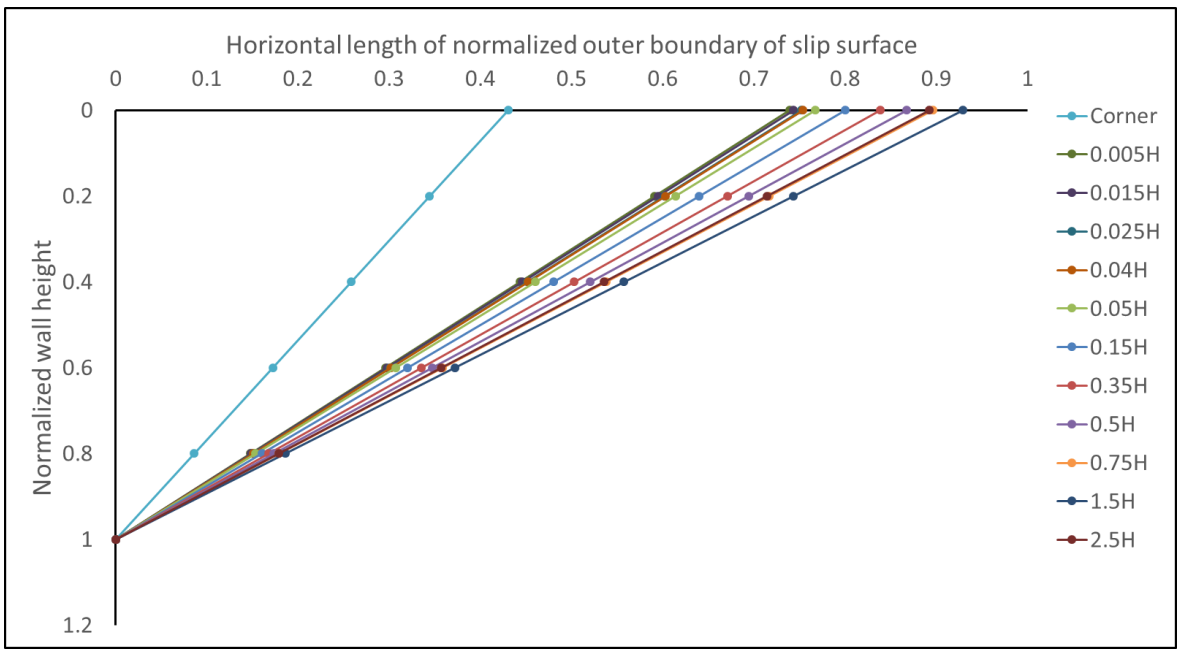

Figure A.19. Horizontal Length of Normalized Outer Boundary of Slip Surfaces in Soil 4, at Corner with 30 Degree.

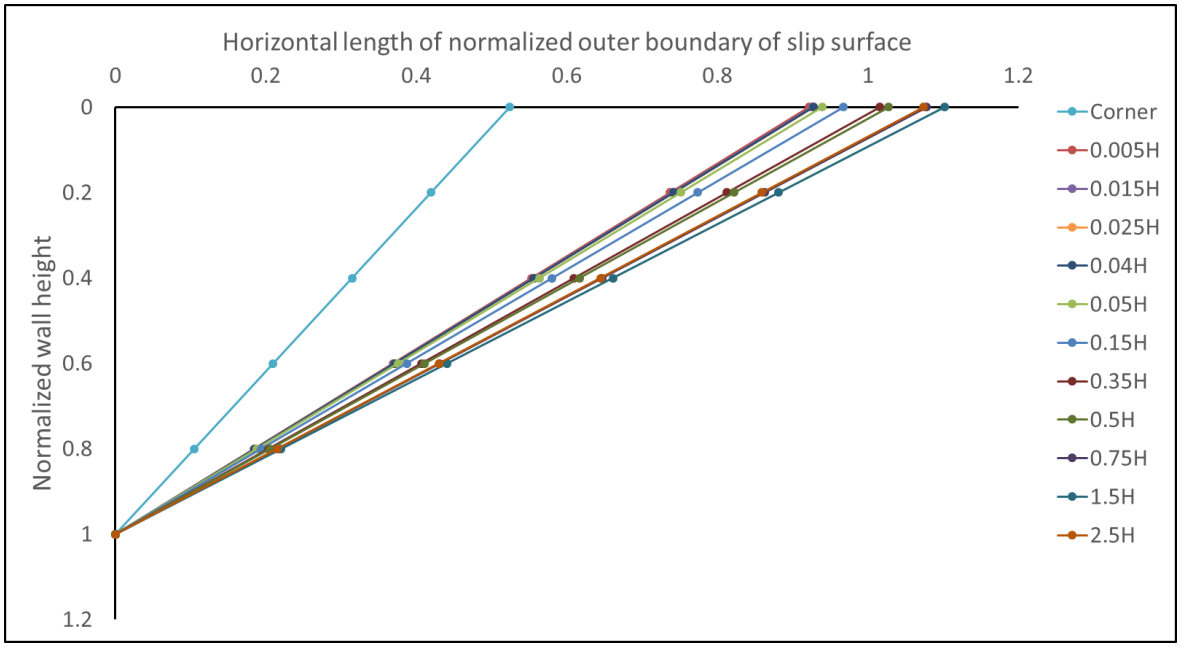

Figure A.20. Horizontal Length of Normalized Outer Boundary of Slip Surfaces in Soil 4, at Corner with 60 Degree.

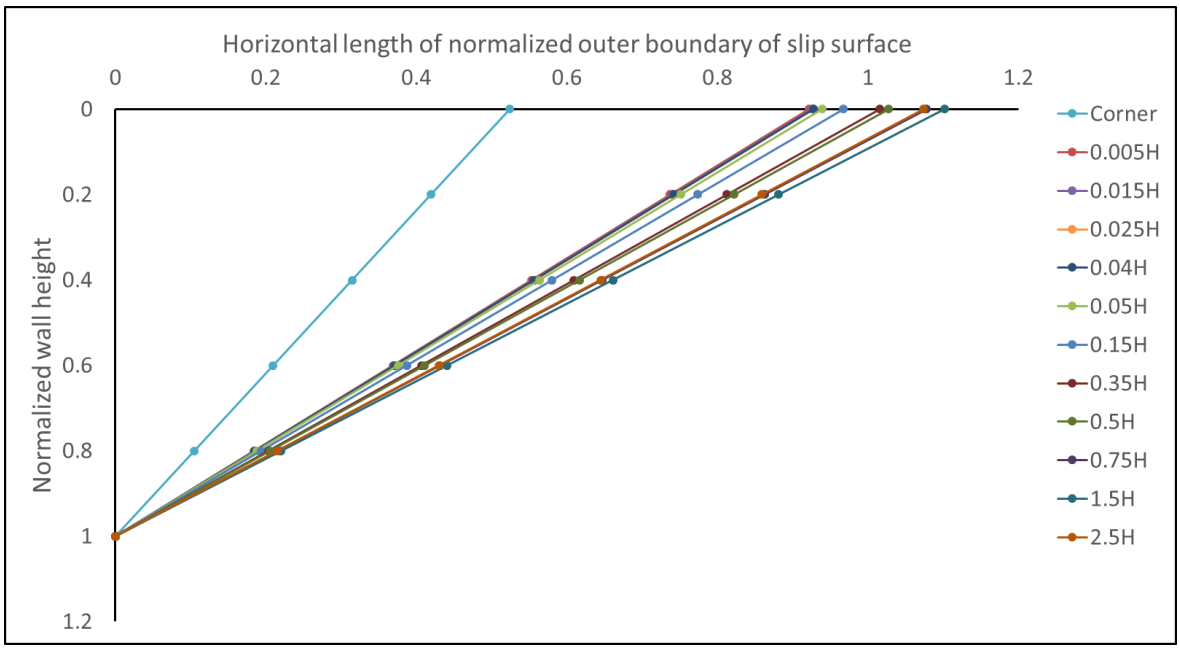

Figure A.21. Horizontal Length of Normalized Outer Boundary of Slip Surfaces in Soil 4, at Corner with 90 Degree.

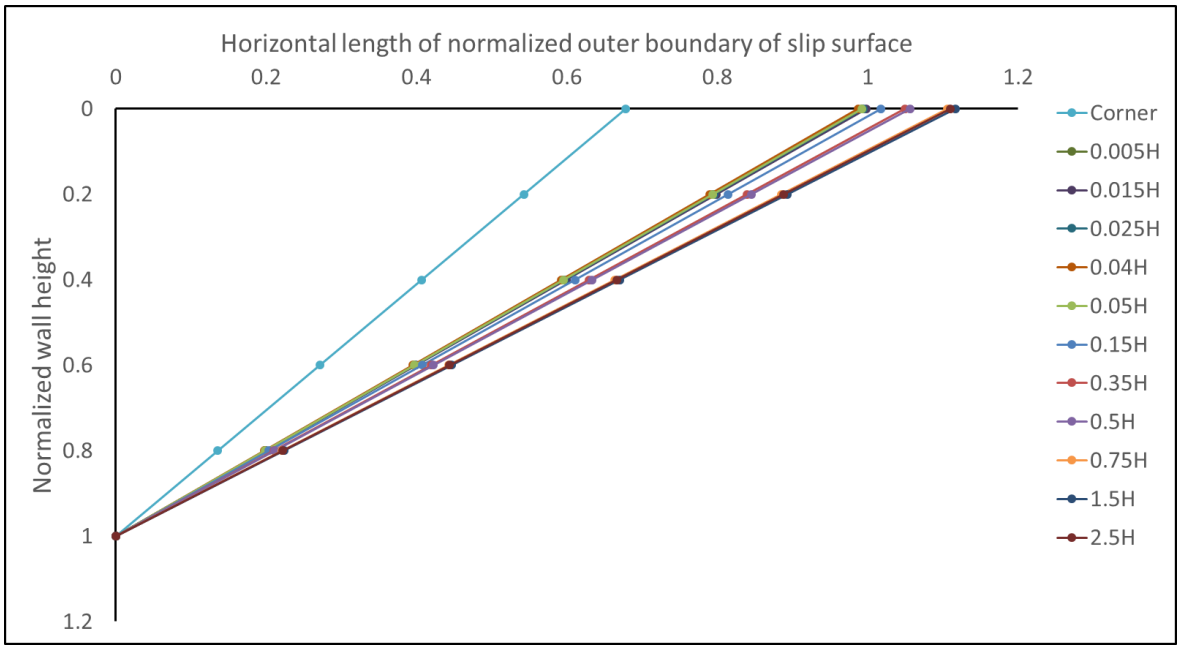

Figure A.22. Horizontal Length of Normalized Outer Boundary of Slip Surfaces in Soil 4, at Corner with 120 Degree.

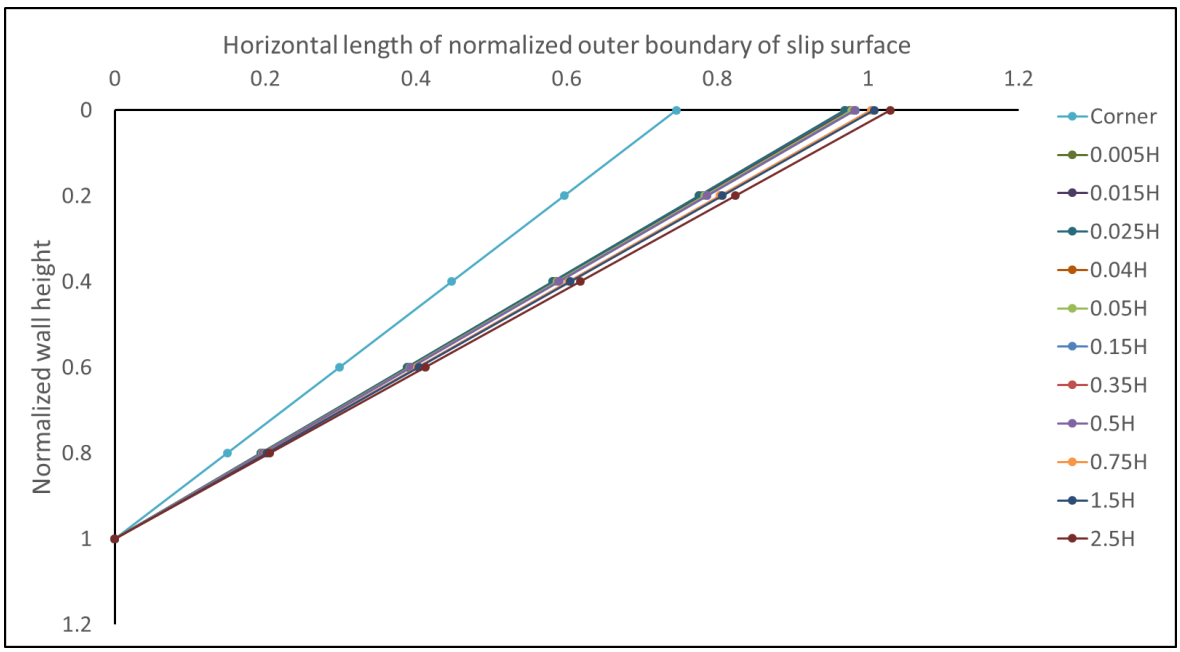

Figure A.23. Horizontal Length of Normalized Outer Boundary of Slip Surfaces in Soil 4, at Corner with 150 Degree.

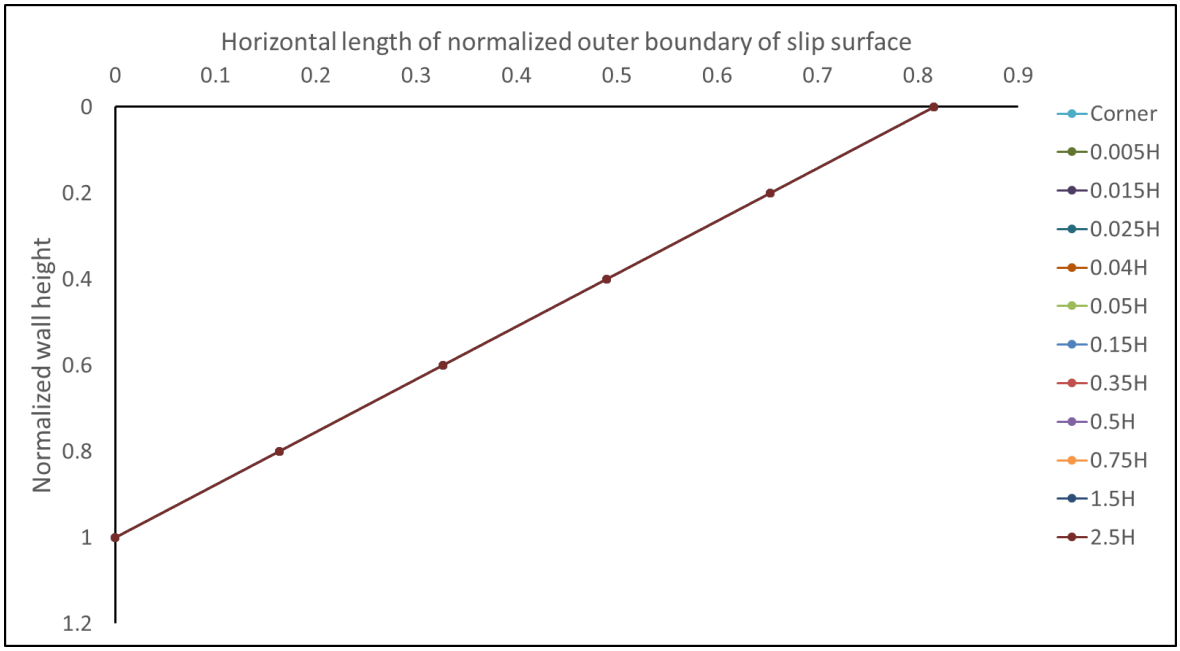

Figure A.24. Horizontal Length of Normalized Outer Boundary of Slip Surfaces in Soil 4, at Corner with 180 Degree.

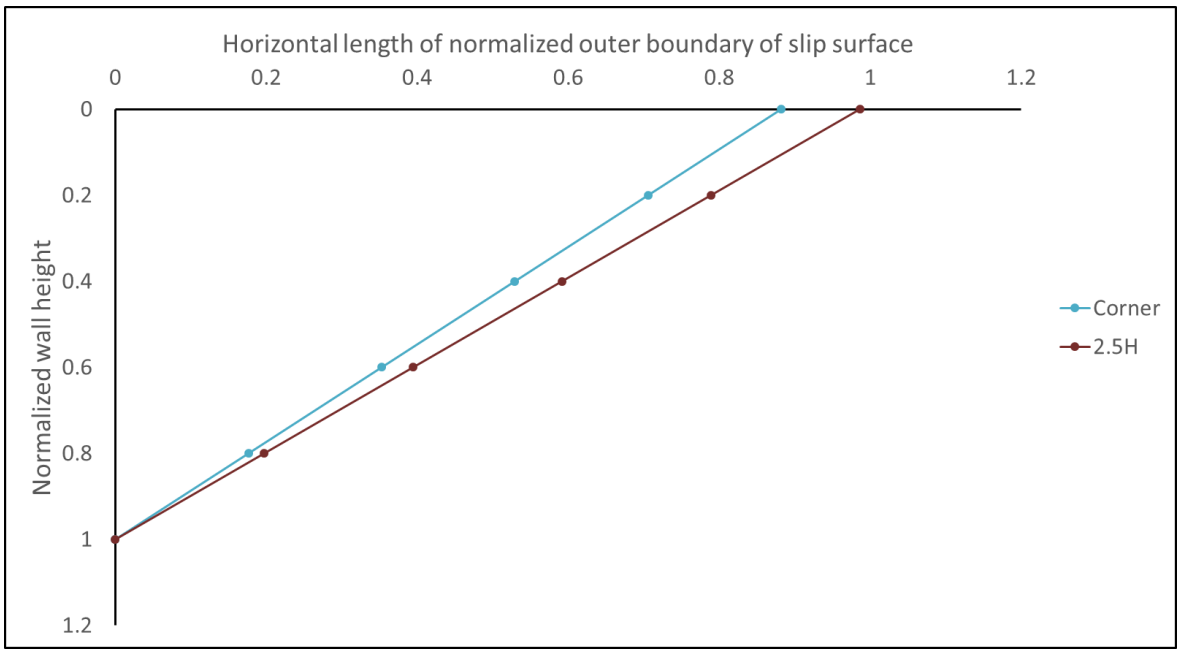

Figure A.25. Horizontal Length of Normalized Outer Boundary of Slip Surfaces in Soil 4, at Corner with 210 Degree.

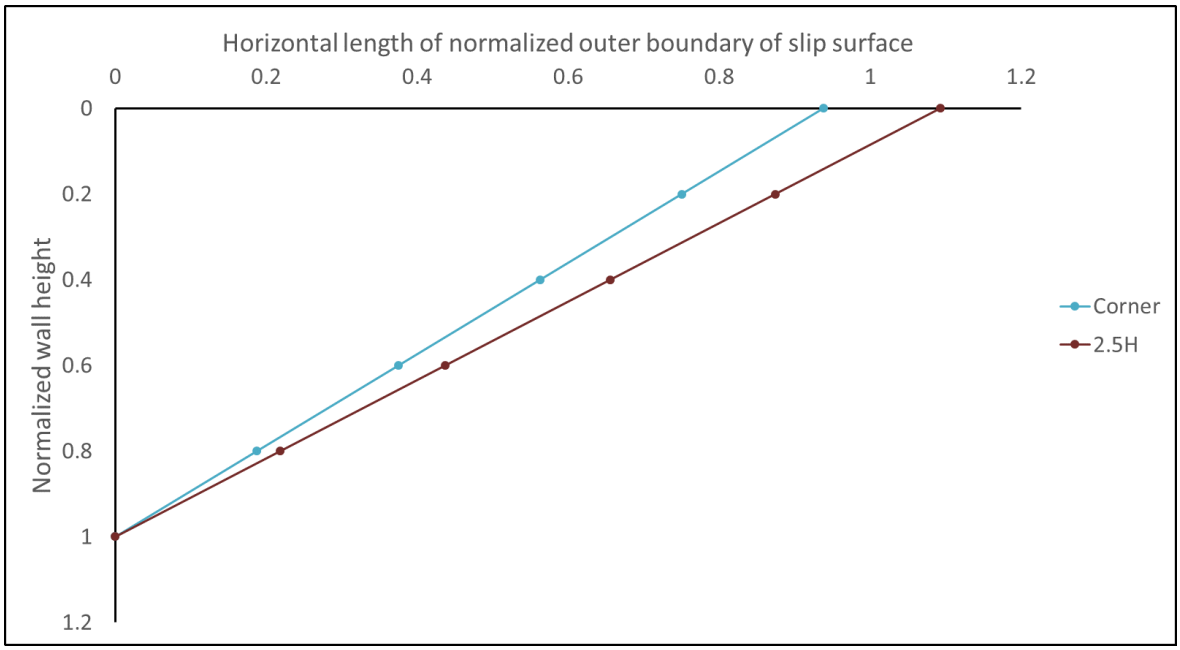

Figure A.26. Horizontal Length of Normalized Outer Boundary of Slip Surfaces in Soil 4, at Corner with 240 Degree.

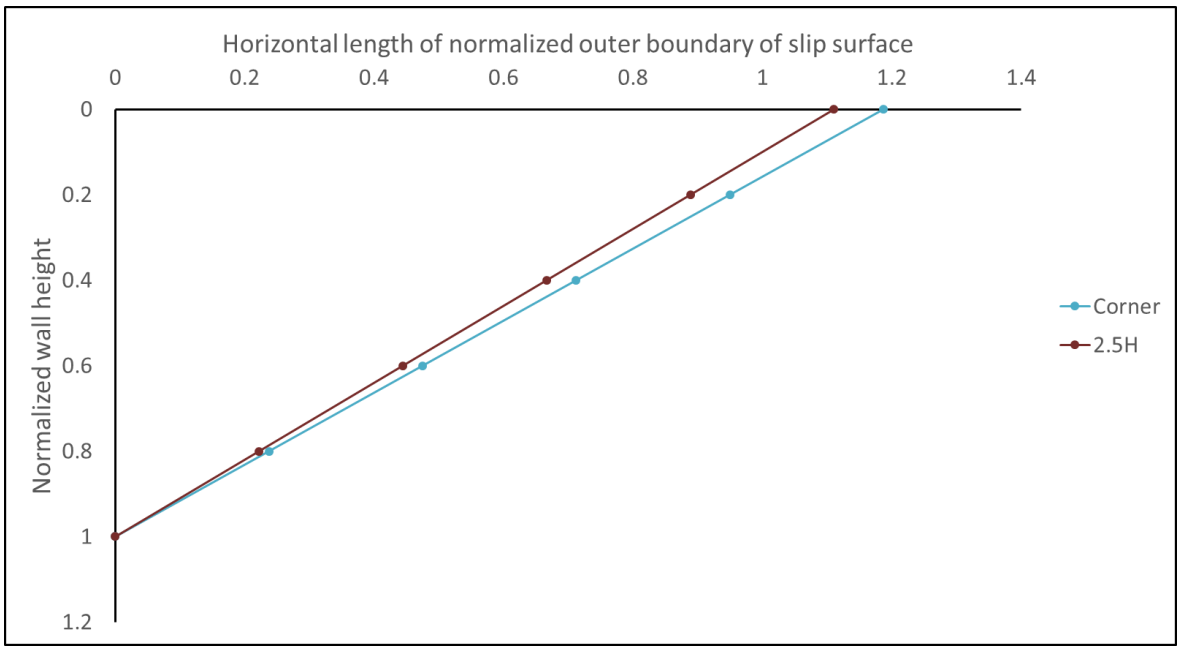

Figure A.27. Horizontal Length of Normalized Outer Boundary of Slip Surfaces in Soil 4, at Corner with 270 Degree.

APPENDIX B: HORIZONTAL LENGTH OF THE NORMALIZED OUTER BOUNDARY OF THE SLIP SURFACES CREATED BY DIFFERENT CORNERS

Keeping distance from the corner constant for soil 2, 3 and 4, horizontal length of the normalized outer boundary of the slip surfaces created by different corner angles are plotted. The results are given as follow.

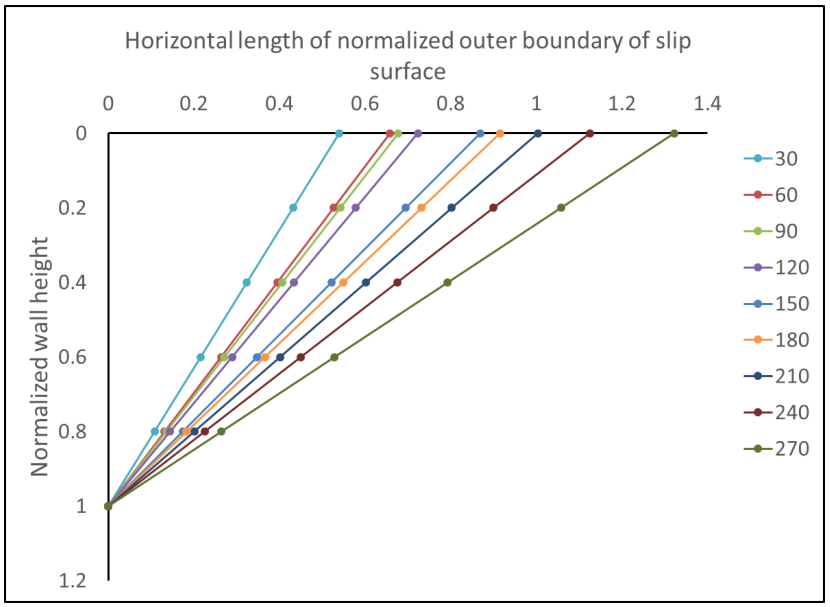

Figure B.1. Horizontal Length of Normalized Outer Boundary of Slip Surface with Changing Corner Angles at the Corner in Soil 2.

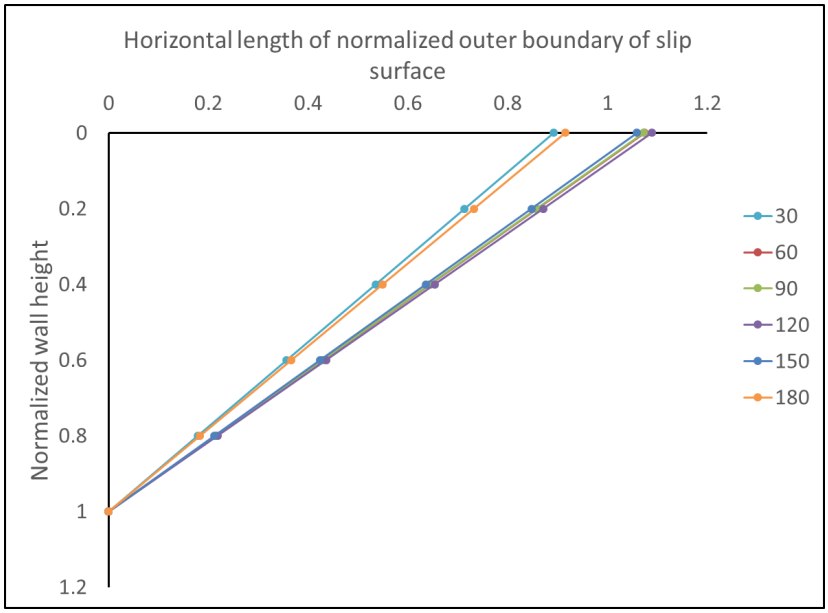

Figure B.2. Horizontal Length of Normalized Outer Boundary of Slip Surface with Changing Corner Angles at 0.005H in Soil 2.

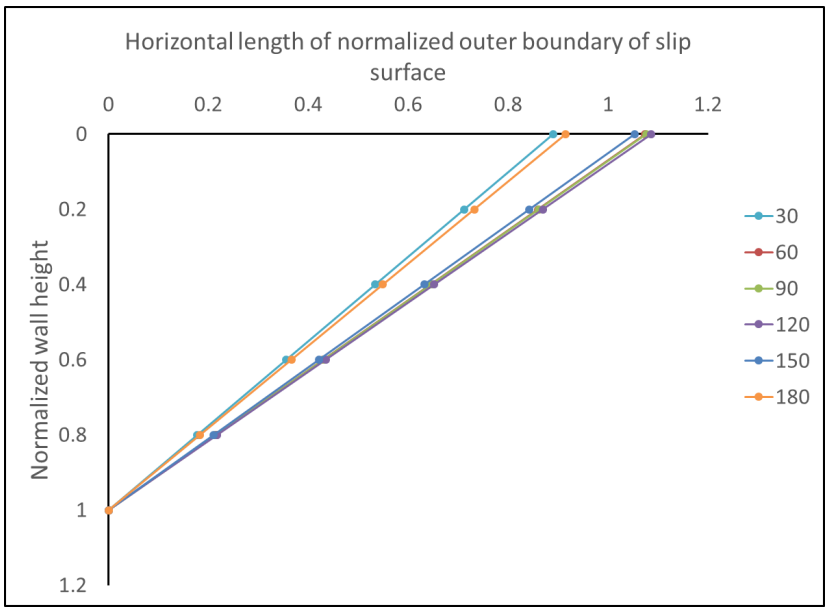

Figure B.3. Horizontal Length of Normalized Outer Boundary of Slip Surface with Changing Corner Angles at 0.015H in Soil 2.

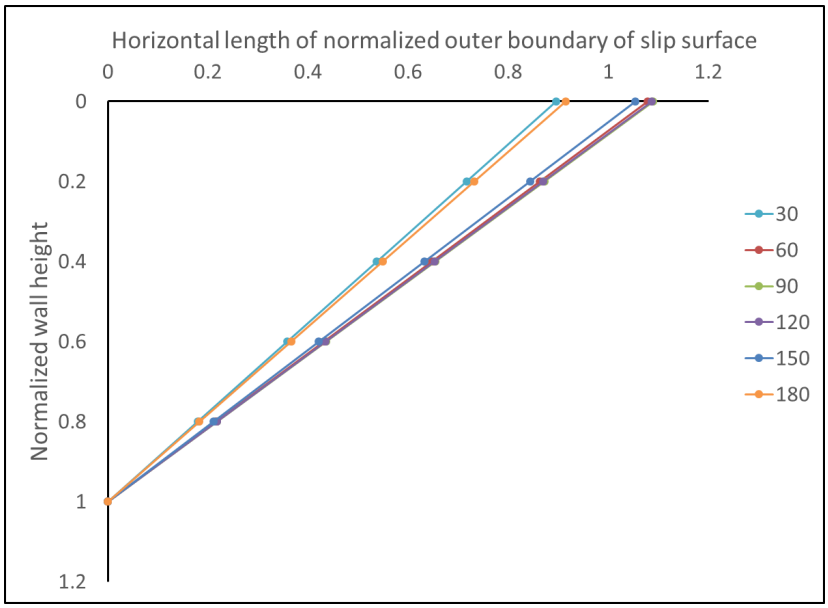

Figure B.4. Horizontal Length of Normalized Outer Boundary of Slip Surface with Changing Corner Angles at 0.025H in Soil 2.

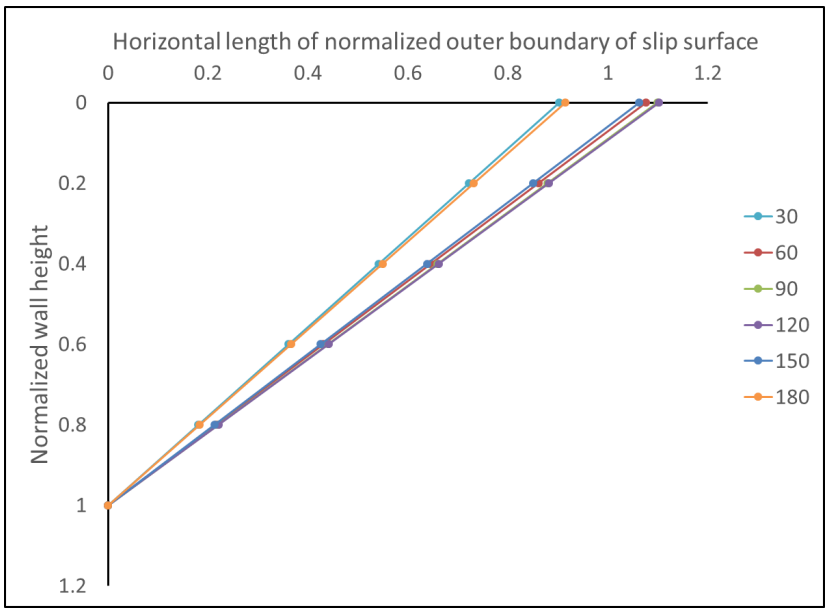

Figure B.5. Horizontal Length of Normalized Outer Boundary of Slip Surface with Changing Corner Angles at 0.04H in Soil 2.

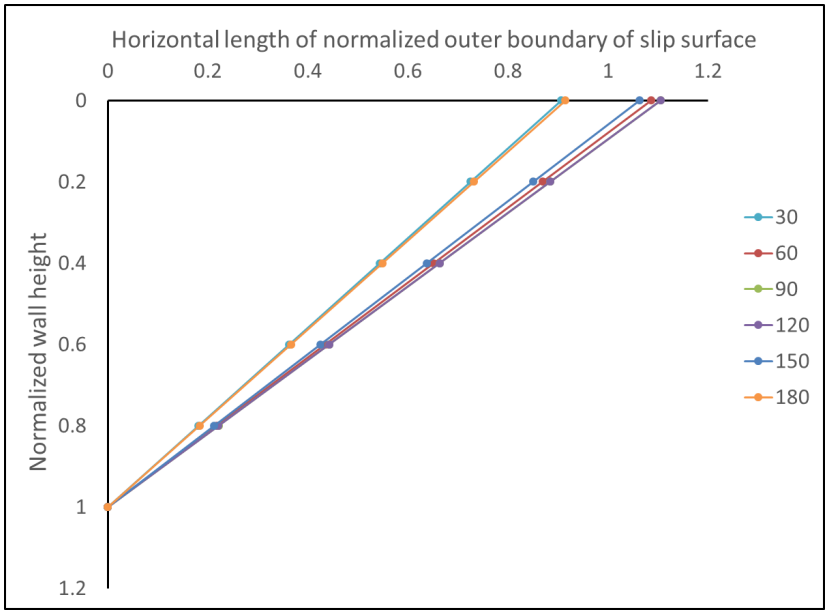

Figure B.6. Horizontal Length of Normalized Outer Boundary of Slip Surface with Changing Corner Angles at 0.05H in Soil 2.

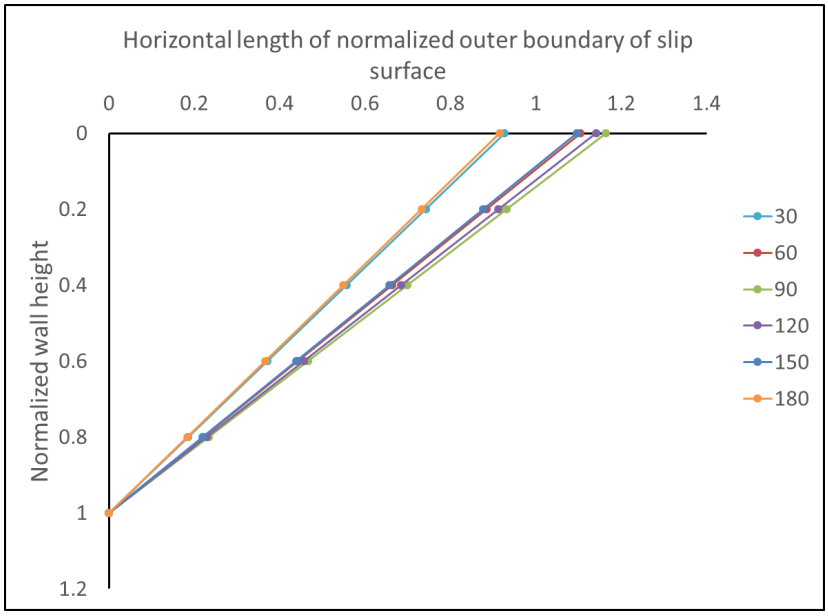

Figure B.7. Horizontal Length of Normalized Outer Boundary of Slip Surface with Changing Corner Angles at 0.15H in Soil 2.

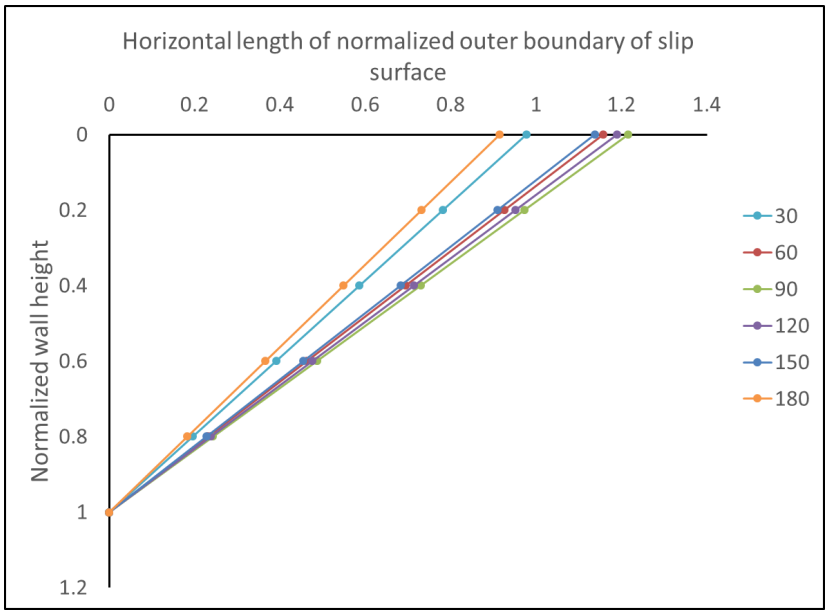

Figure B.8. Horizontal Length of Normalized Outer Boundary of Slip Surface with Changing Corner Angles at 0.35H in Soil 2.

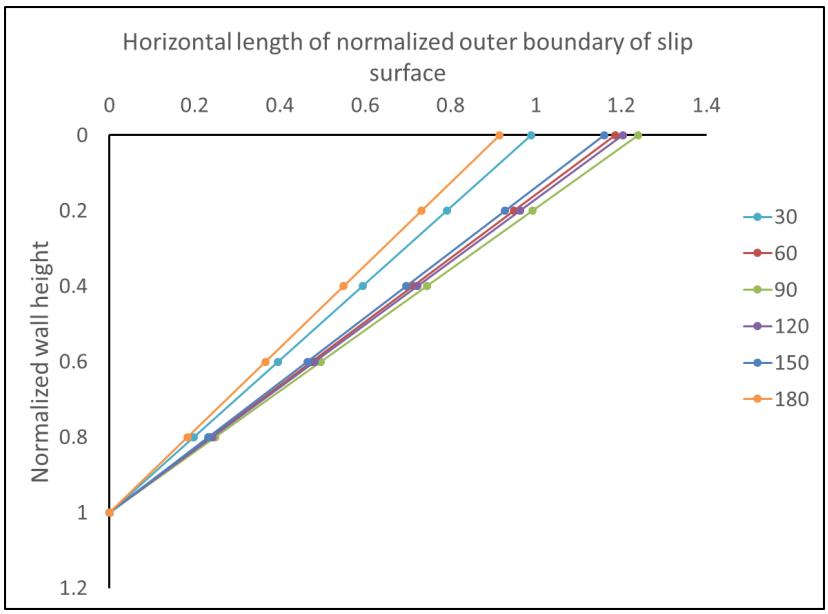

Figure B.9. Horizontal Length of Normalized Outer Boundary of Slip Surface with Changing Corner Angles at 0.5H in Soil 2.

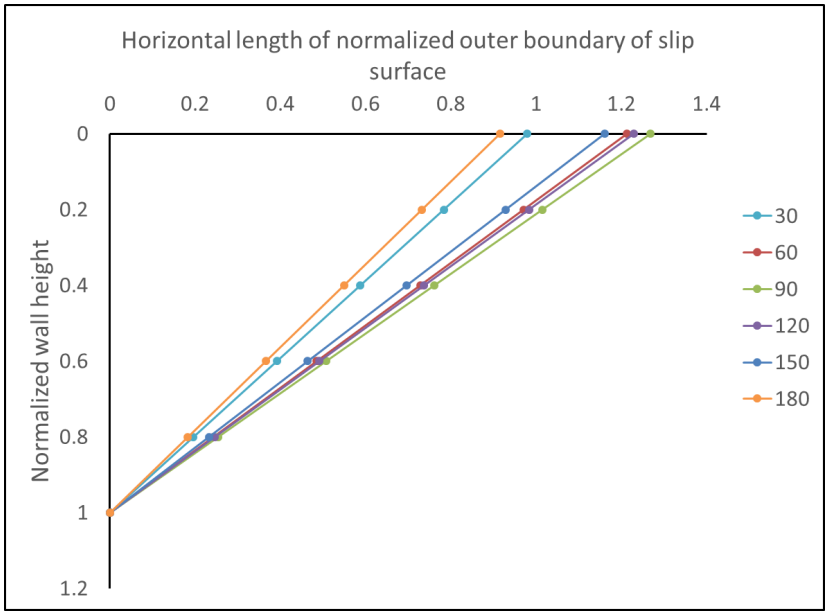

Figure B.10. Horizontal Length of Normalized Outer Boundary of Slip Surface with Changing Corner Angles at 0.75H in Soil 2.

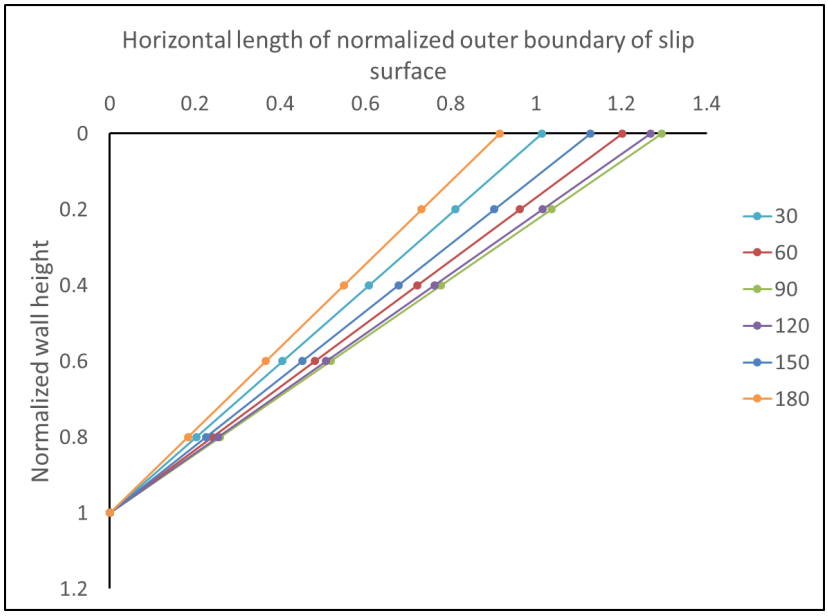

Figure B.11. Horizontal Length of Normalized Outer Boundary of Slip Surface with Changing Corner Angles at 1.5H in Soil 2.

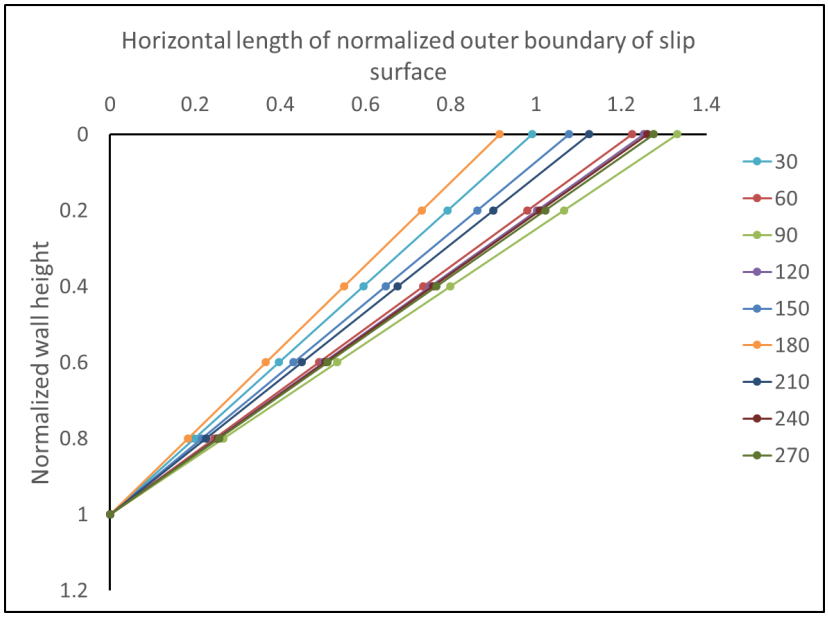

Figure B.12. Horizontal Length of Normalized Outer Boundary of Slip Surface with Changing Corner Angles at 2.5H in Soil 2.

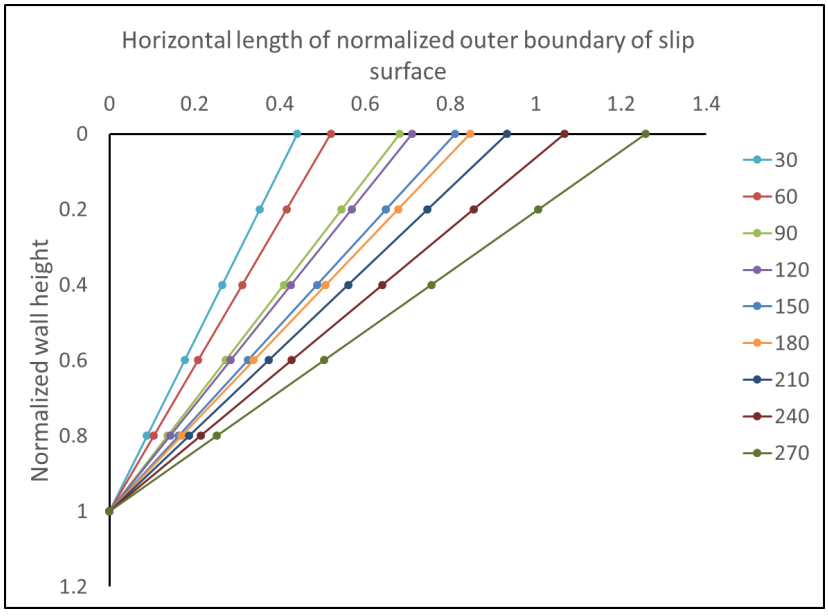

Figure B.13. Horizontal Length of Normalized Outer Boundary of Slip Surface with Changing Corner Angles at the Corner in Soil 3.

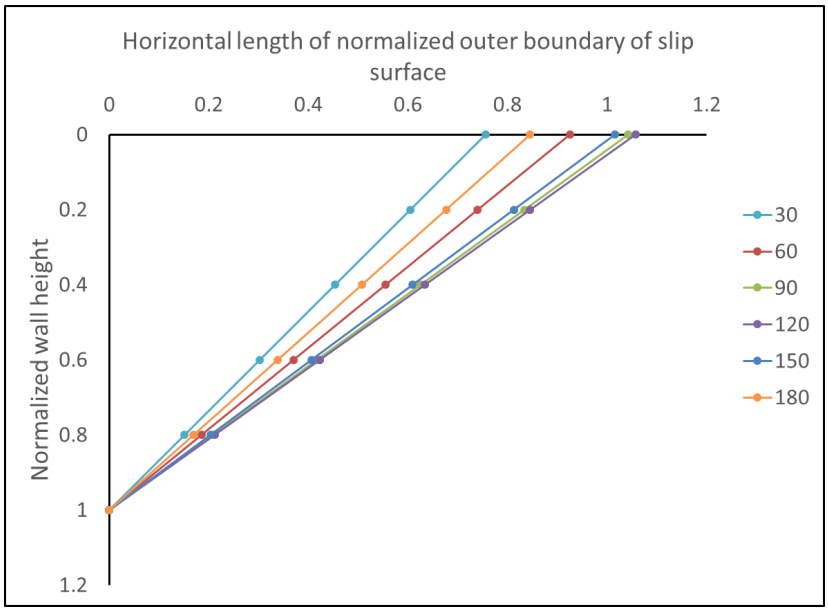

Figure B.14. Horizontal Length of Normalized Outer Boundary of Slip Surface with Changing Corner Angles at 0.005H in Soil 3.

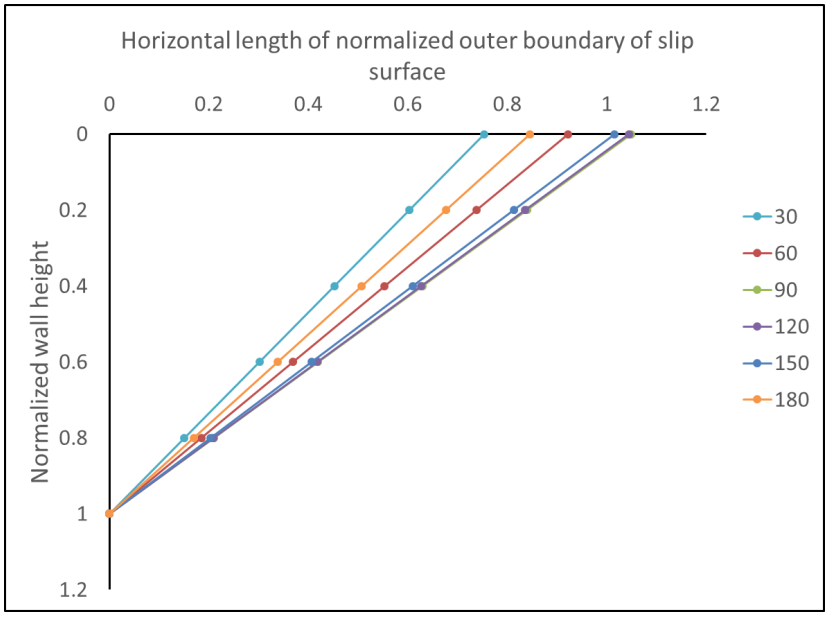

Figure B.15. Horizontal Length of Normalized Outer Boundary of Slip Surface with Changing Corner Angles at 0.015H in Soil 3.

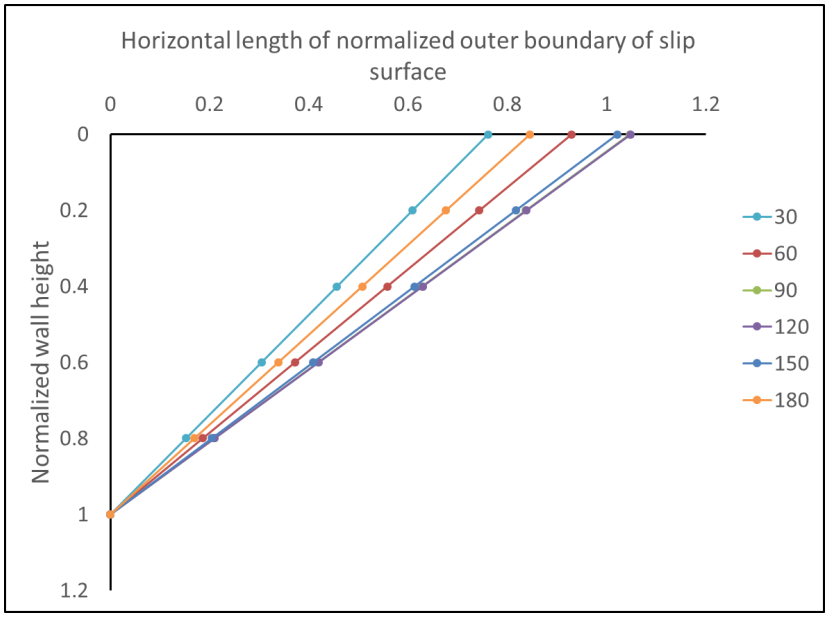

Figure B.16. Horizontal Length of Normalized Outer Boundary of Slip Surface with Changing Corner Angles at 0.025H in Soil 3.

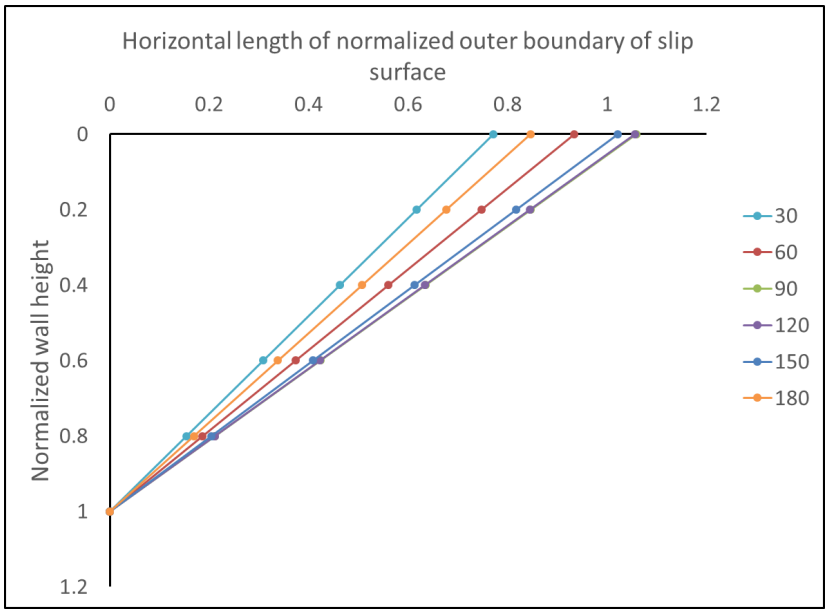

Figure B.17. Horizontal Length of Normalized Outer Boundary of Slip Surface with Changing Corner Angles at 0.04H in Soil 3.

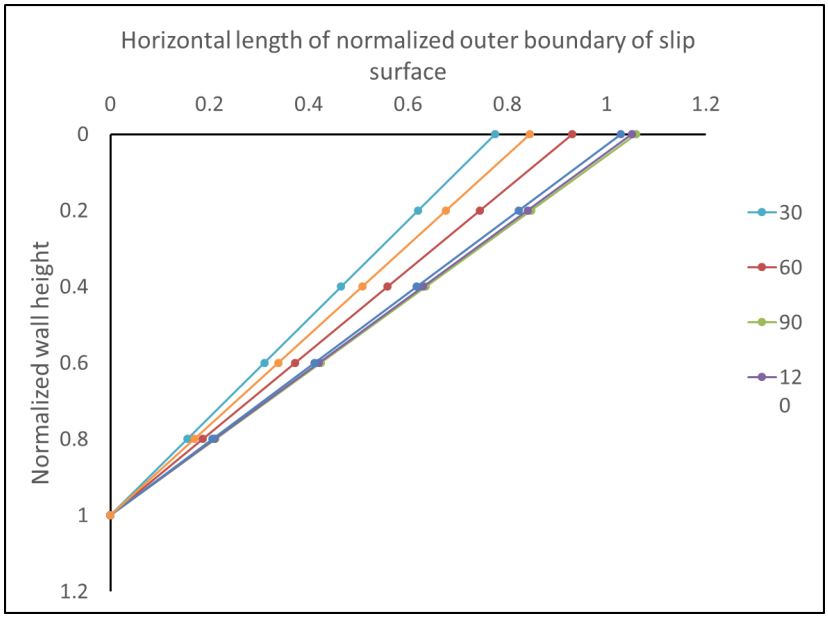

Figure B.18. Horizontal Length of Normalized Outer Boundary of Slip Surface with Changing Corner Angles at 0.05H in Soil 3.

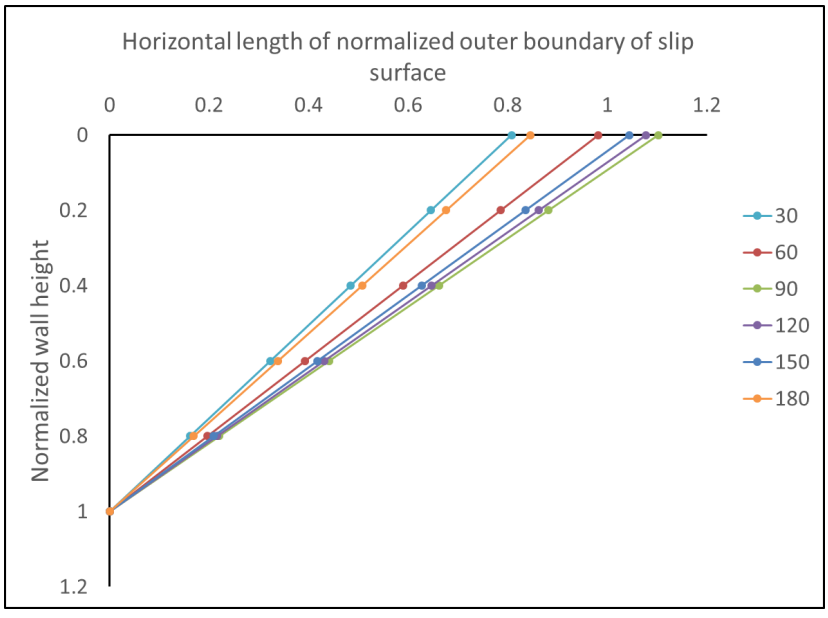

Figure B.19. Horizontal Length of Normalized Outer Boundary of Slip Surface with Changing Corner Angles at 0.15H in Soil 3.

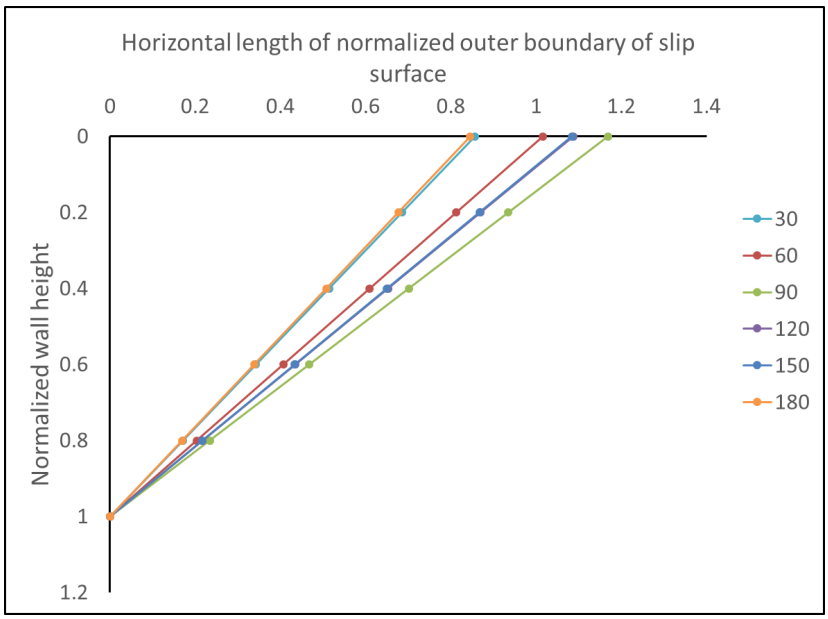

Figure B.20. Horizontal Length of Normalized Outer Boundary of Slip Surface with Changing Corner Angles at 0.35H in Soil 3.

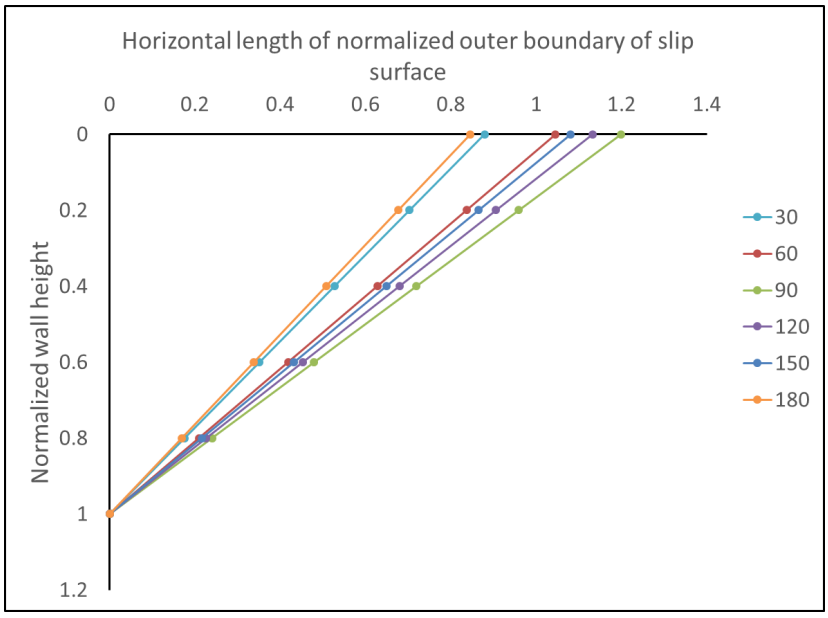

Figure B.21. Horizontal Length of Normalized Outer Boundary of Slip Surface with Changing Corner Angles at 0.5H in Soil 3.

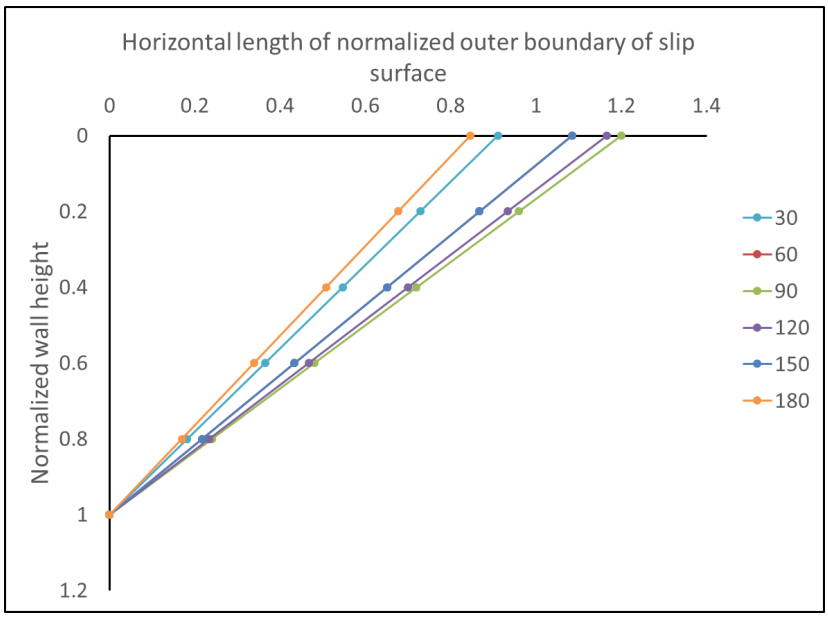

Figure B.22. Horizontal Length of Normalized Outer Boundary of Slip Surface with Changing Corner Angles at 0.75H in Soil 3.

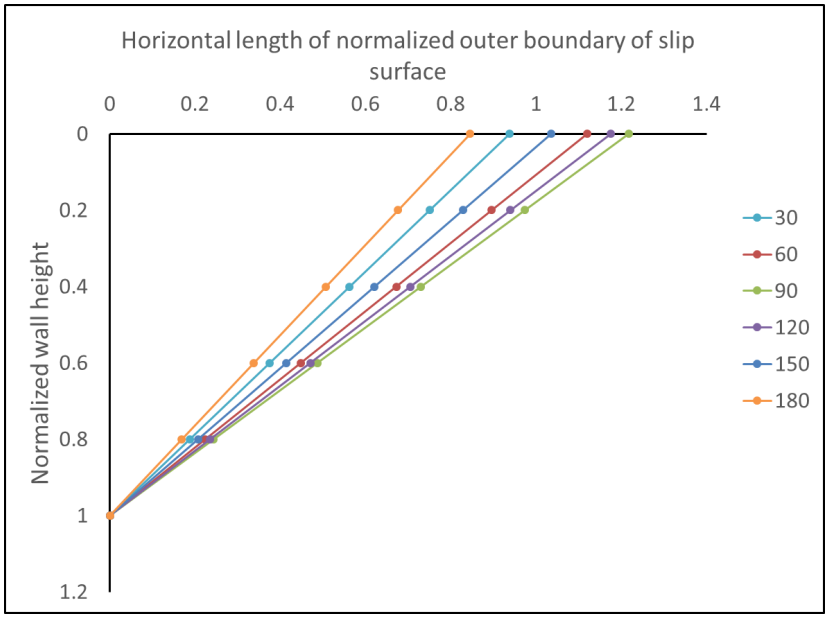

Figure B.23. Horizontal Length of Normalized Outer Boundary of Slip Surface with Changing Corner Angles at 1.5H in Soil 3.

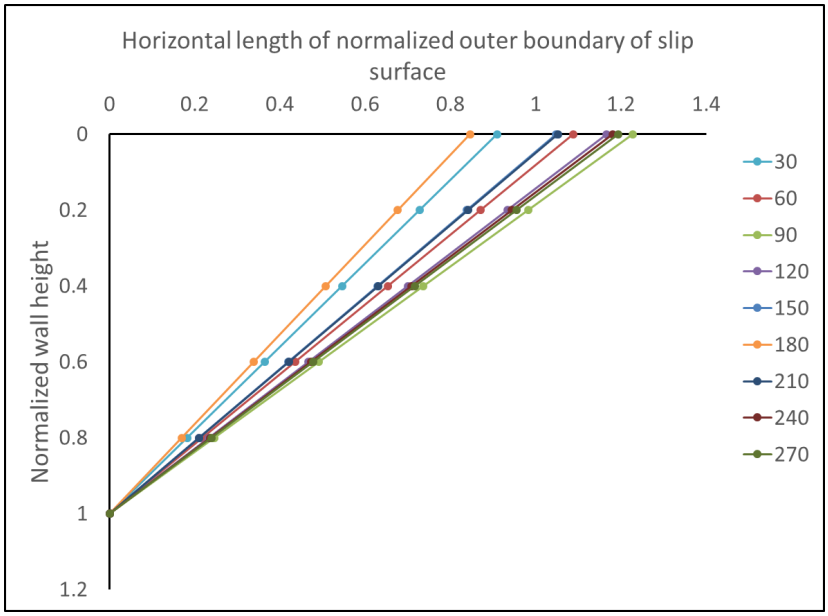

Figure B.24. Horizontal Length of Normalized Outer Boundary of Slip Surface with Changing Corner Angles at 2.5H in Soil 3.

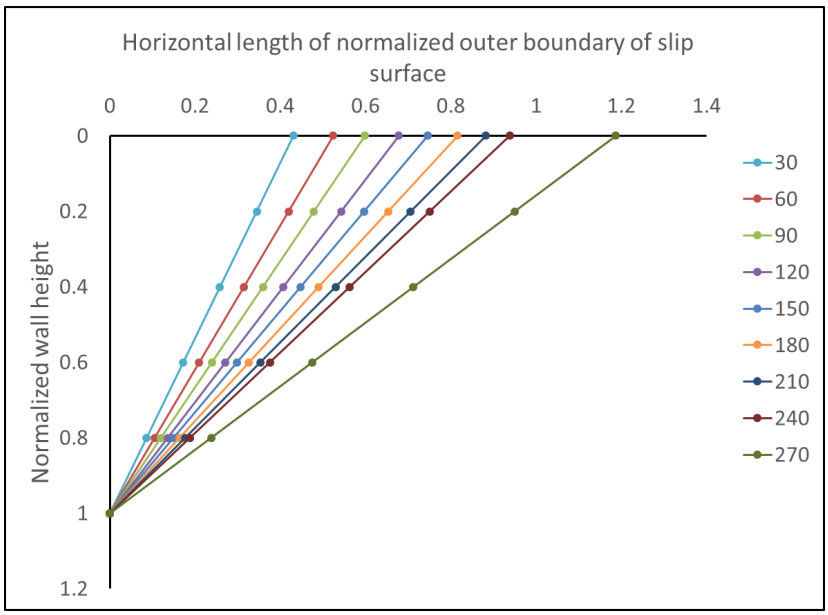

Figure B.25. Horizontal Length of Normalized Outer Boundary of Slip Surface with Changing Corner Angles at the Corner in Soil 4.

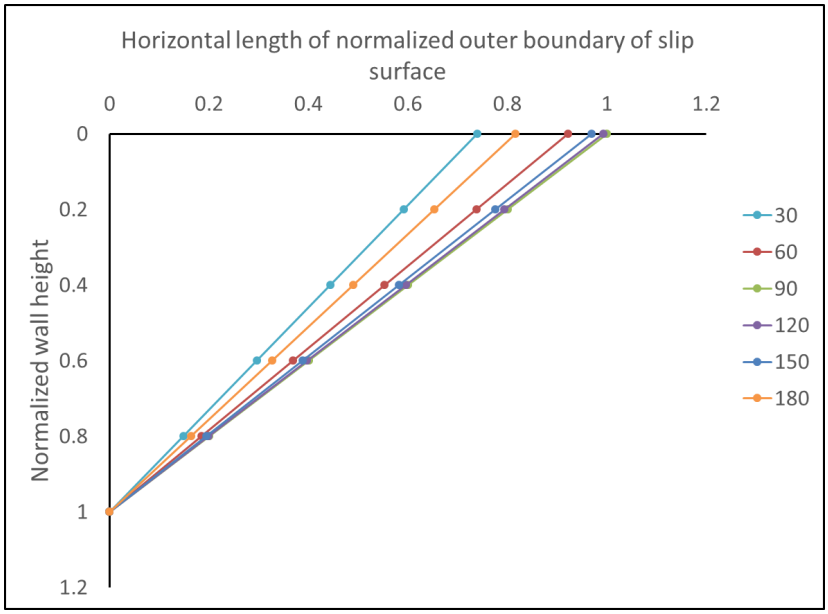

Figure B.26. Horizontal Length of Normalized Outer Boundary of Slip Surface with Changing Corner Angles at 0.005H in Soil 4.

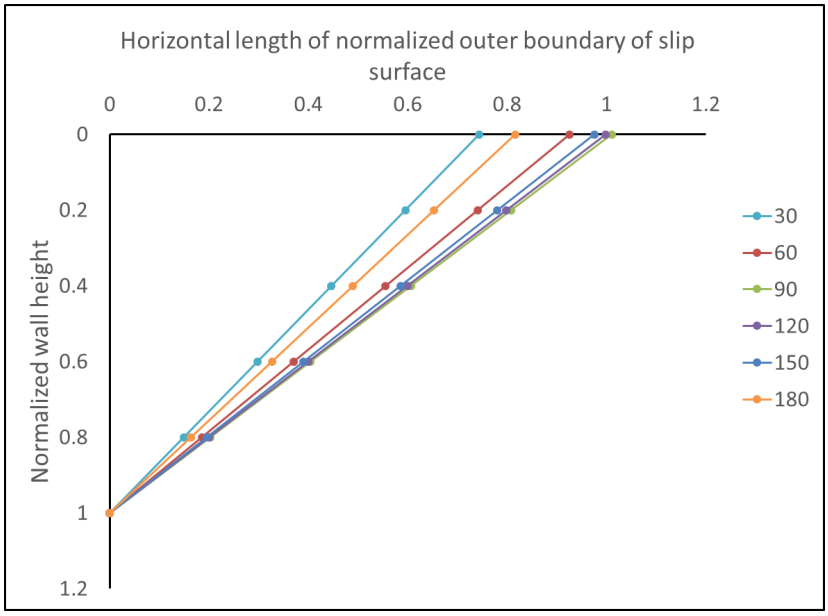

Figure B.27. Horizontal Length of Normalized Outer Boundary of Slip Surface with Changing Corner Angles at 0.015H in Soil 4.

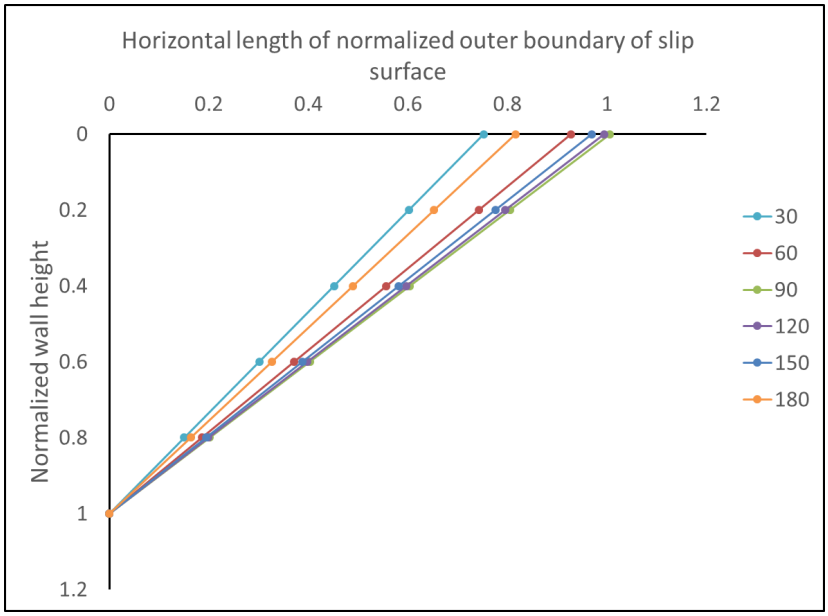

Figure B.28. Horizontal Length of Normalized Outer Boundary of Slip Surface with Changing Corner Angles at 0.025H in Soil 4.

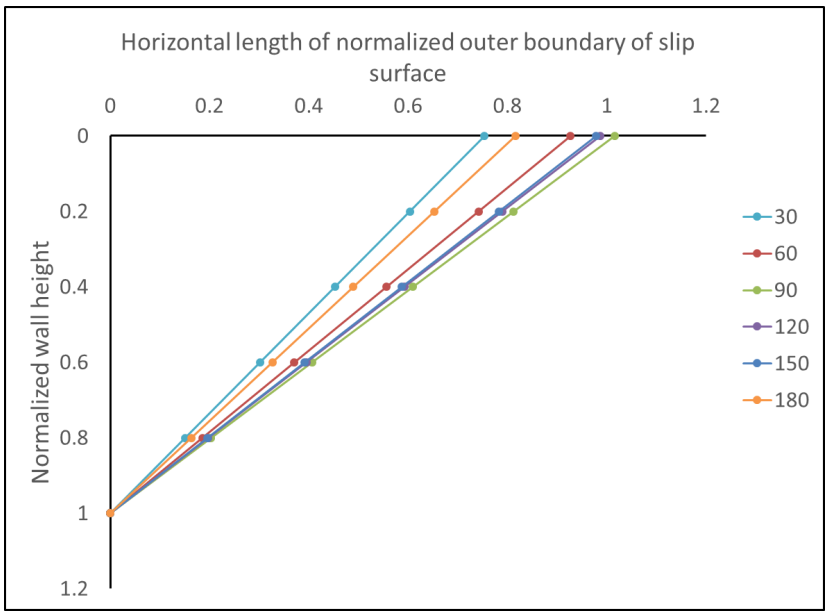

Figure B.29. Horizontal Length of Normalized Outer Boundary of Slip Surface with Changing Corner Angles at 0.04H in Soil 4.

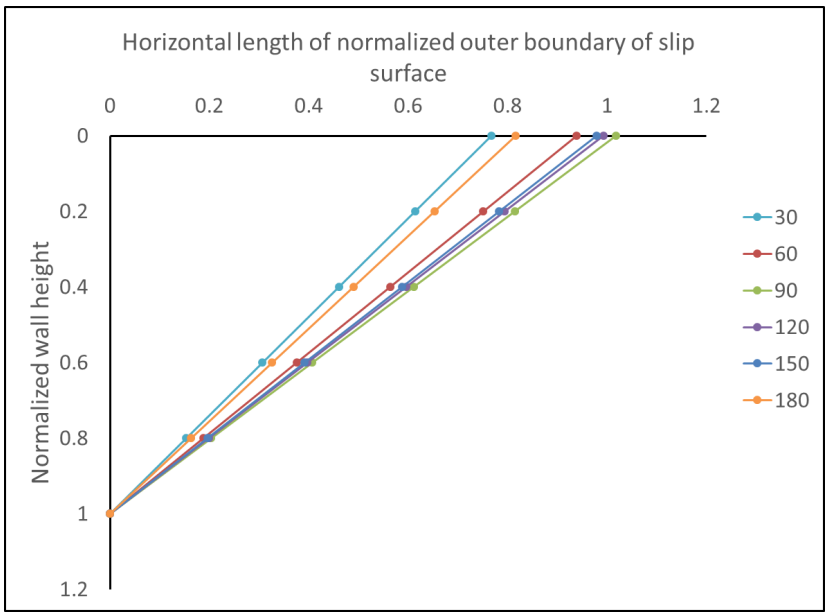

Figure B.30. Horizontal Length of Normalized Outer Boundary of Slip Surface with Changing Corner Angles at 0.05H in Soil 4.

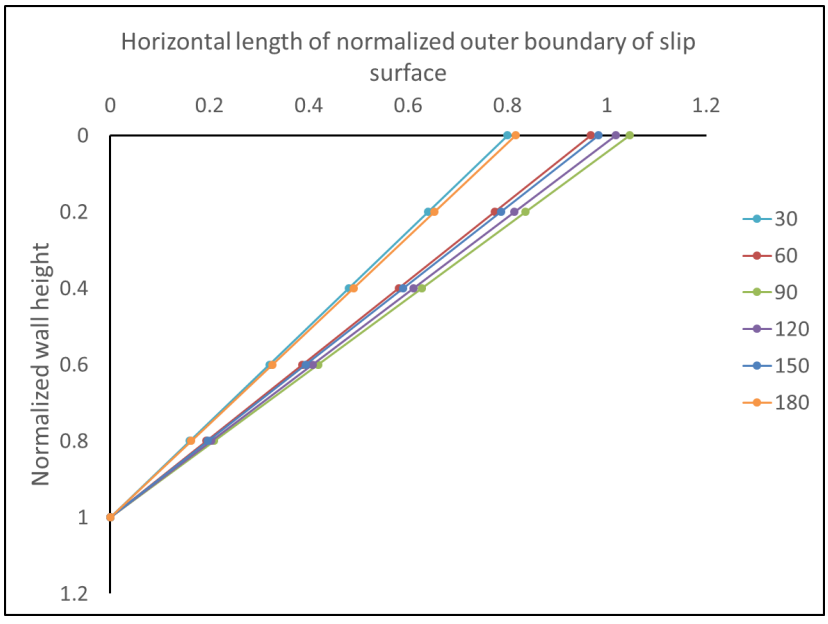

Figure B.31. Horizontal Length of Normalized Outer Boundary of Slip Surface with Changing Corner Angles at 0.15H in Soil 4.

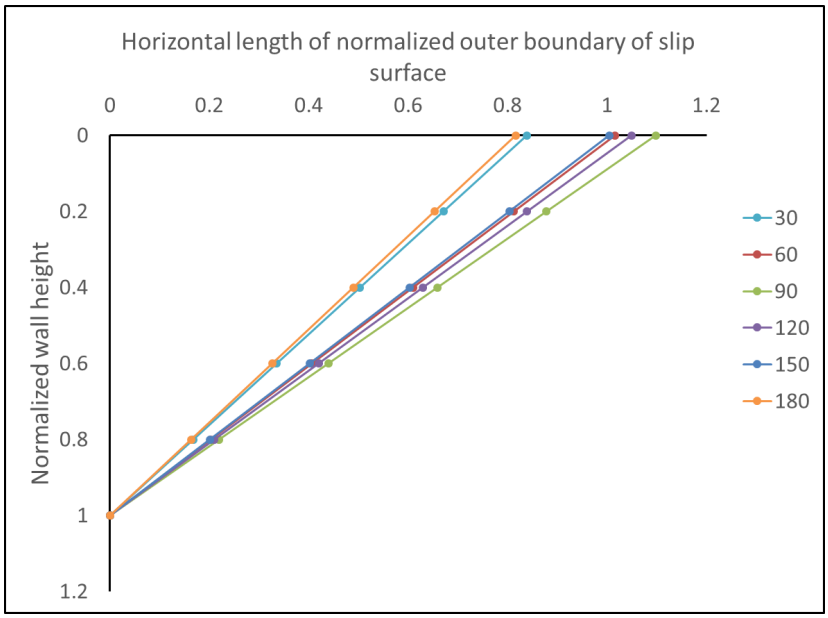

Figure B.32. Horizontal Length of Normalized Outer Boundary of Slip Surface with Changing Corner Angles at 0.35H in Soil 4.

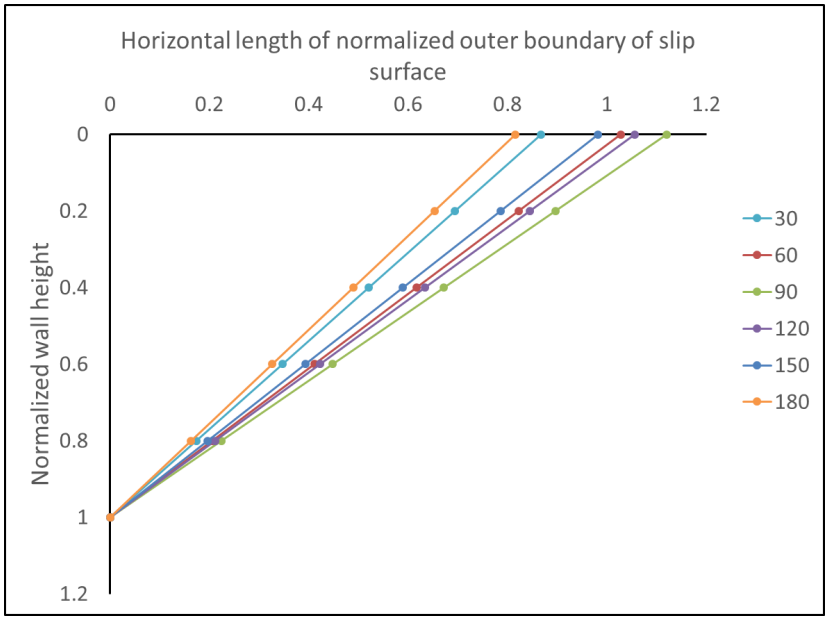

Figure B.33. Horizontal Length of Normalized Outer Boundary of Slip Surface with Changing Corner Angles at 0.5H in Soil 4.

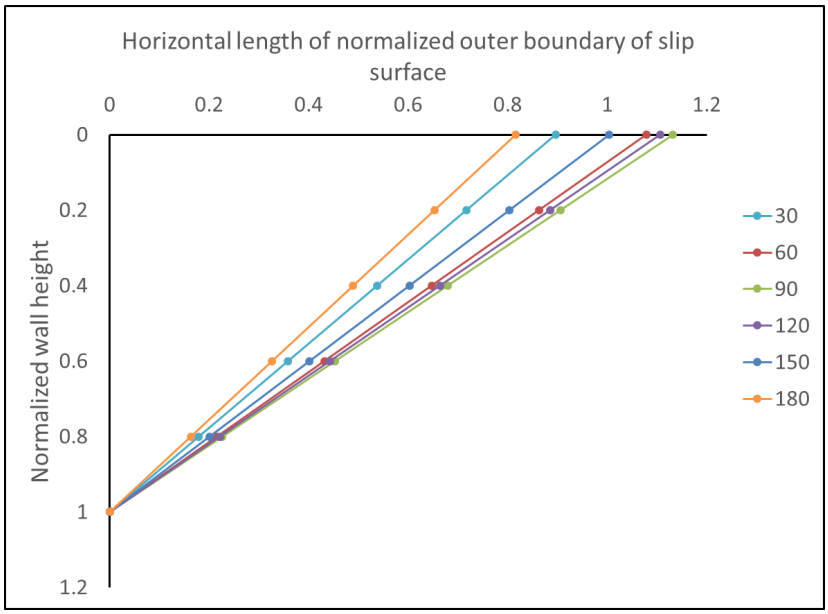

Figure B.34. Horizontal Length of Normalized Outer Boundary of Slip Surface with Changing Corner Angles at 0.75H in Soil 4.

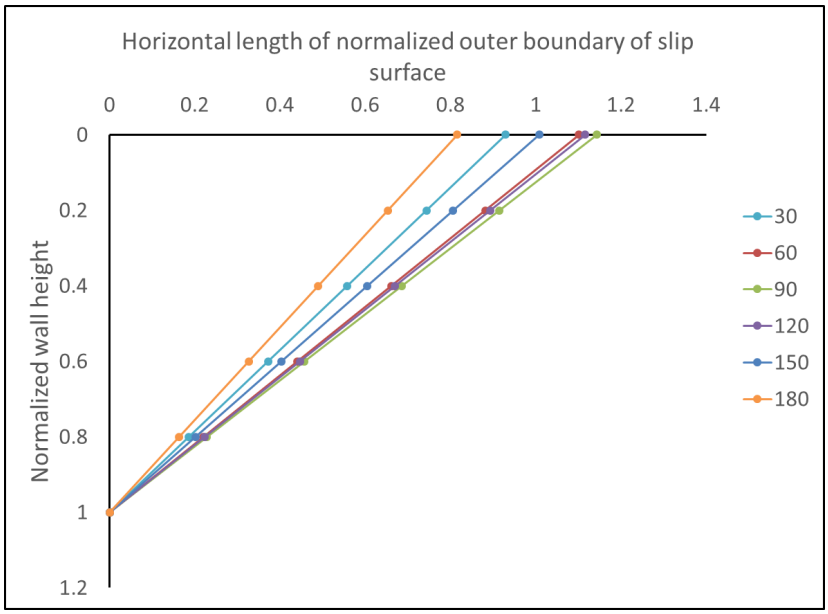

Figure B.35. Horizontal Length of Normalized Outer Boundary of Slip Surface with Changing Corner Angles at 1.5H in Soil 4.

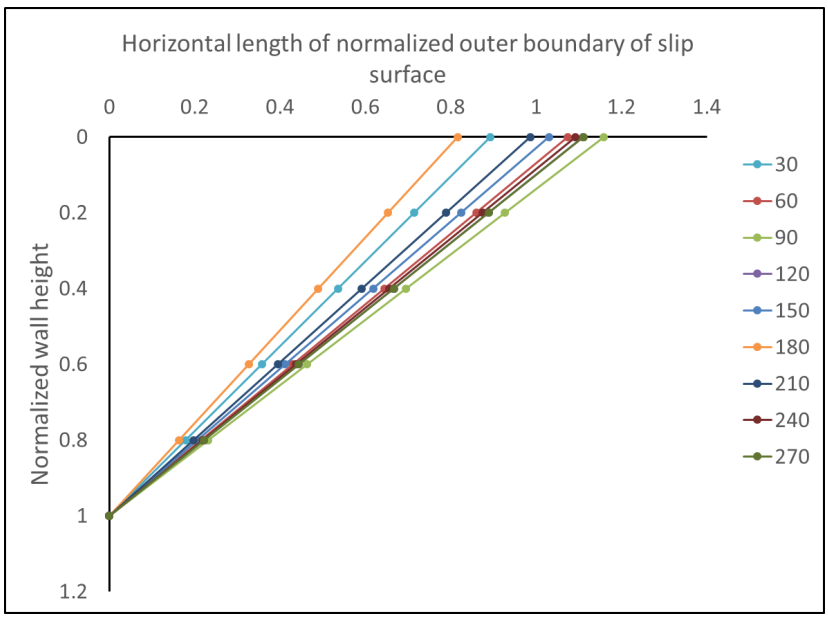

Figure B.36. Horizontal Length of Normalized Outer Boundary of Slip Surface with Changing Corner Angles at 2.5H in Soil 4.

APPENDIX C: THE CHANGE IN LENGTH OF THE DISTANCE OF THE OUTER BOUNDARY OF THE SLIP SURFACE FOR DIFFERENT CROSS SECTIONS ACCORDING TO THE CORNER ANGLE

The change in length of the distance of the outer boundary of the slip surface for different cross sections according to the corner angle for soil 2, 3 and 4 are given below

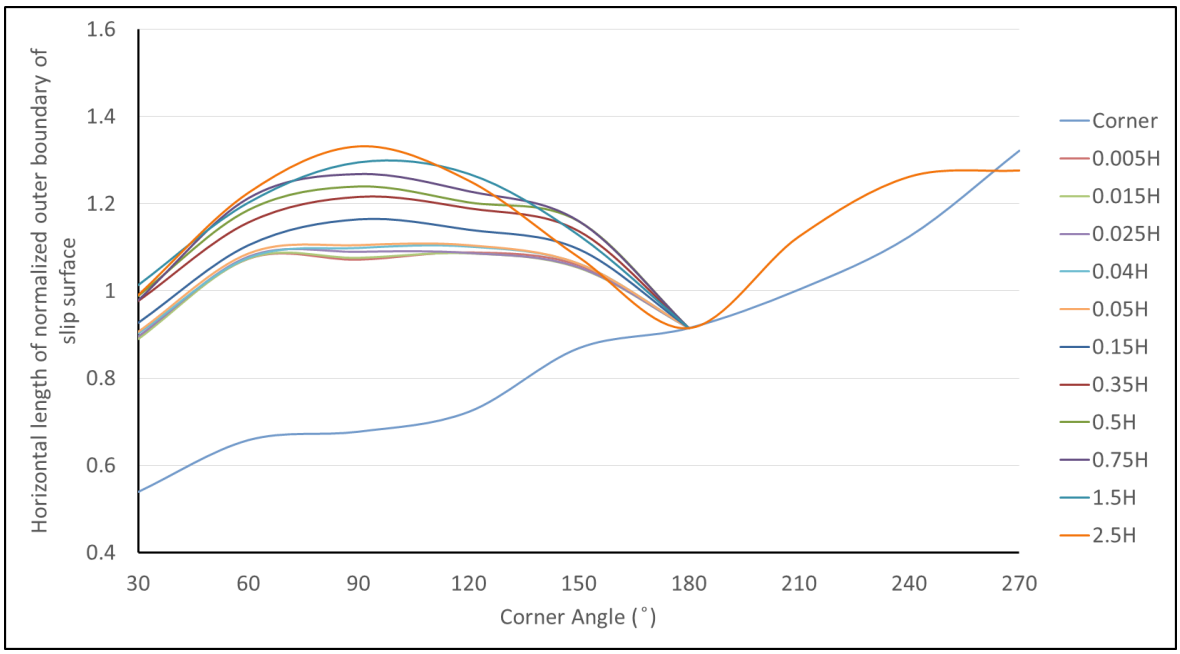

Figure C.1. The Change in Horizontal Length of the Outer Boundary of the Slip Surface for Different Cross Sections According to the Corner Angle in Soil 2.

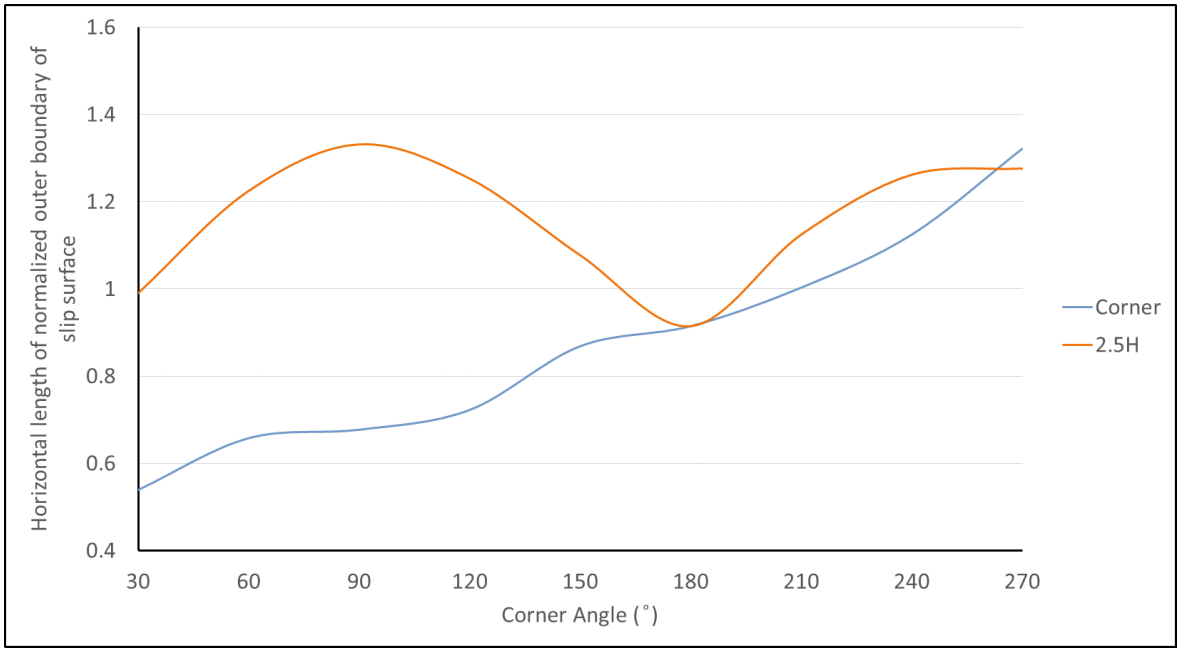

Figure C.2. The Change in Horizontal Length of the Outer Boundary of the Slip Surface at 2.5H Cross Section According to the Corner Angle in Soil 2.

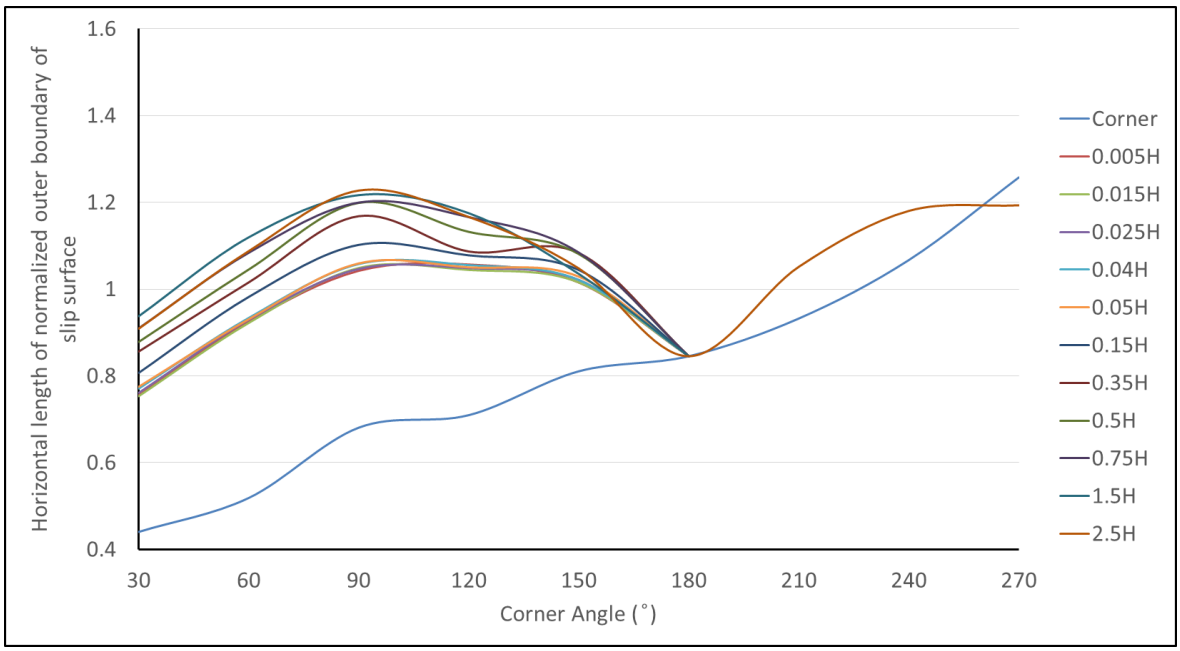

Figure C.3. The Change in Horizontal Length of the Outer Boundary of the Slip Surface for Different Cross Sections According to the Corner Angle in Soil 3.

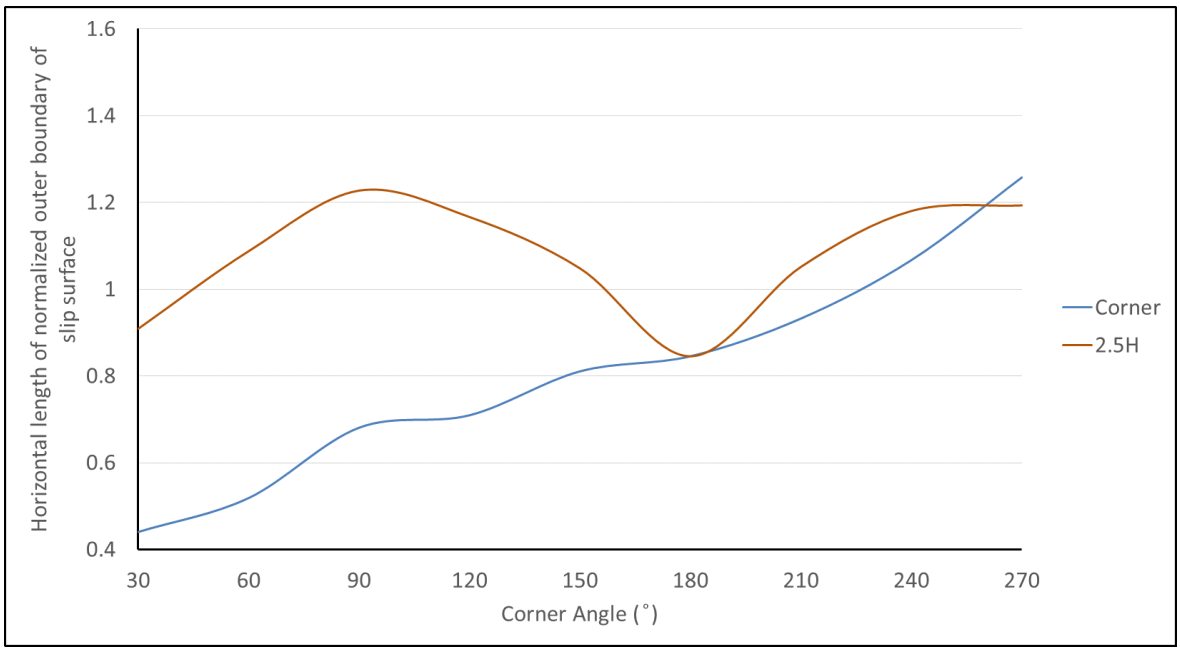

Figure C.4. The Change in Horizontal Length of the Outer Boundary of the Slip Surface at 2.5H Cross Section According to the Corner Angle in Soil 3.

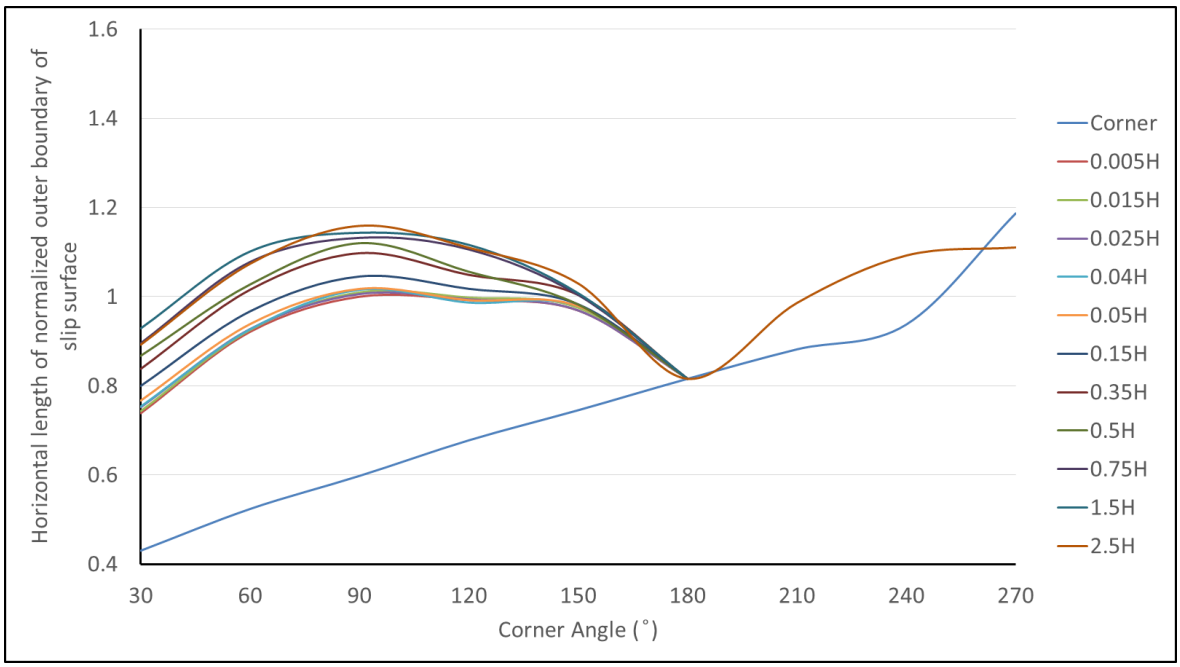

Figure C.5. The Change in Horizontal Length of the Outer Boundary of the Slip Surface for Different Cross Sections According to the Corner Angle in Soil 4.

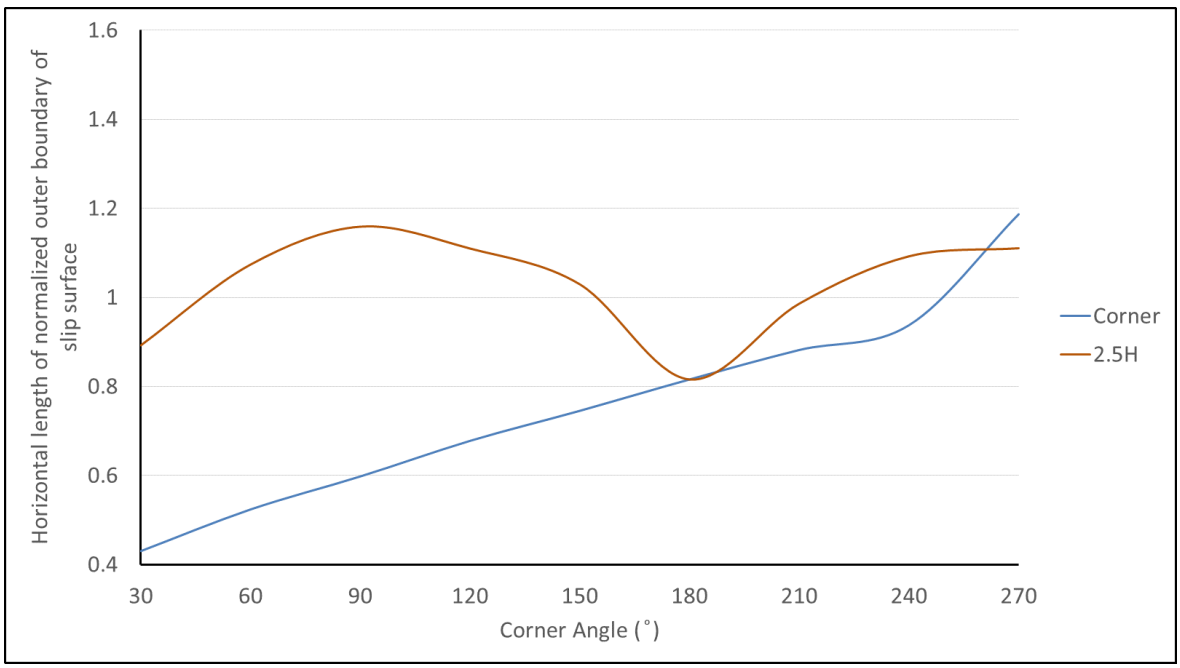

Figure C.6. The Change in Horizontal Length of the Outer Boundary of the Slip Surface at 2.5H Cross Section According to the Corner Angle in Soil 4.